Human Brain Project
Education Programme

6TH HBP STUDENT CONFERENCE ON INTERDISCIPLINARY BRAIN RESEARCH

22–25 FEBRUARY 2022

VIRTUAL EVENT

BOOK OF ABSTRACTS

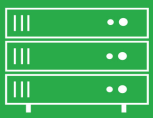

frontiers Event Abstracts

6th HBP STUDENT CONFERENCE ON INTERDISCIPLINARY BRAIN RESEARCH

ISBN: 978-2-88971-014-0
DOI: 10.3389/978-2-88971-014-0
Citation: Joana Covelo, Sandra Diaz, Alice Geminiani, Tabea Kirchner, Carmen Lupascu, Paschal Ochang, Taylan Özden, Jens Egholm Pedersen, Ingrid Reiten, Alper Yegenoglu, Alice Geminiani, Manuel Gran, Judith Kathrein, Tabea Kirchner, Paschal Ochang, Franziska Vogel. (2022). 6th HBP Student Conference on Interdisciplinary Brain Research.

February 22-25, 2022, Virtual Event

The abstracts in this collection have not been subject to any Frontiers peer review or checks, and are not endorsed by Frontiers. They are made available through the Frontiers publishing platform as a service to conference organizers and presenters. The copyright in the individual abstracts is owned by the author of each abstract or his/her employer unless otherwise stated. Each abstract, as well as the collection of abstracts, are published under a Creative Commons CC-BY 4.0 (attribution) licence (https://creativecommons.org/licenses/by/4.0/) and may thus be reproduced, translated, adapted and be the subject of derivative works provided the authors and Frontiers are attributed.

For Frontiers' terms and conditions please see https://www.frontiersin.org/legal/terms-and-conditions.

Table of Contents

8 **Welcome to the 6th HBP Student Conference on Interdisciplinary Brain Research**

10 **Preface**

11 **I Brain atlases & clinical neuroscience**

11 **Mohamed Baghdad, Niamh Brady, Irene Costantini, Giacomo Mazzamuto, Marina Scardigli, Filippo Castelli, Ludovico Silvestri, Francesco Saverio Pavone:** Reconstructing the Broca's area of the human brain using a customized dual-view light sheet for optimized imaging time and improved resolution

15 **Helena M. Ferreira, Ana Catarina Sousa, Hugo Ferreira, Sofia Santos, José Sereno, João Martins, Miguel Castelo-Branco,Joana Gonçalves:** Sex-dependent cortical excitatory/inhibitory imbalance is associated with behaviour alterations in a mouse model of autism spectrum disorder

17 **Dimitrios Georgiou, Christina Emmanouil, Georgios Vlachos, Leonidas Stefanis, Ioannis Michalopoulos:** Study on the effects of various risk factors on the onset of Parkinson's disease using machine and deep learning

22 **Marina Ivanova, Zheng Gong, Thomas Hein, Maria Herrojo Ruiz, Vadim Nikulin:** Heart-brain interactions in anxiety influence decision-making and learning

26 **Viktoriya Manyukhina, Andrey Prokofyev, Tatiana Obukhova, Tatiana Stroganova, Elena Orekhova:** Visual gamma oscillations and perceptual spatial suppression point to impaired neural inhibition in premenstrual dysphoric disorder

30 **Beatriz Martins, Miguel Castelo Branco, Joana Gonçalves, and João Martins:** Characterization of microbiome and brain NPY system alterations in a mouse model of autism spectrum disorder

32 **Svitlana Oleshko, Francesc Fernández-Albert, Matthias Heinig, Sergio Picart-Armada, Annalisa Marsico:** Integration of multi-omics data using graph neural networks to identify and contextualize biomarker genes for psychiatric disorders

36 **M. Lapo Pais, J. Martins, M. Castelo-Branco, J. Gonçalves:** *Tsc2*$^{+/-}$ mouse model: Probing clinical manifestation of epilepsy in Tuberous Sclerosis Complex

40 **II Brain simulation & brain inspired architectures**

40 **Chiara De Luca, Leonardo Tonielli, Bruno Golosio, Gianmarco Tiddia, Irene Bernava, Cristiano Capone, Davide Cipollini, Giulia De Bonis, Cosimo Lupo, Elena Pastorelli, Francesco Simula, Pier Stanislao Paolucci:** Incremental awake-NREM-REM learning cycles: Cognitive and energetic effects in a multi-area thalamo-cortical spiking model

45 **Roberta M. Lorenzi, Alice Geminiani, Claudia A.M. Gandini Wheeler-Kingshott, Fulvia Palesi, Claudia Casellato, Egidio D'Angelo:** GRL MF: Mean field model of the cerebellar granular layer

51 **Ruxandra Barbulescu, Gonçalo Mestre, Arlindo L. Oliveira, L. Miguel Silveira:** Modelling the dynamic behaviour of the *C. elegans* nervous system with machine learning techniques

56 **Panfilova, E.A., Burlakov E.O., Verkhlyutov, V.M:** Traveling waves in the resting state are initiated by the connectome

60 **Francisco P. dos Santos, Sonia Hassissene, Paul F.M.J. Verschure:** Role of excitatory-inhibitory homeostasis in the recovery of functional network properties after focal lesion: A computational account

65 **Lea Steffen, Philipp Augenstein, Stefan Ulbrich, Arne Rönnau, Rüdiger Dillmann:** Configuration aware neural path: Planning in the task space

70 **Márton Szép, Leander Lauenburg, Kevin Farkas, Xiyan Su, Chuanlong Zang, Mahmoud Akl, Florian Walter, Josip Josifovski, Alois Knoll:** Solving robotic reaching tasks in the neurorobotics platform with reinforcement learning

75 **J. Camilo Vasquez Tieck, Daniel Azanov, Jacques Kaiser, Rüdiger Dillmann:** Perception-driven control of multiple robotic arms in the Neurorobotics Platform

79 **Michiel van der Vlag, Marmaduke Woodman, Jan Fousek, Sandra Diaz-Pier, Aaron Perez Martin, Viktor Jirsa, Abigail Morrison:** RateML: A code generation tool for BrainNetwork models

85 **Ben von Hünerbein, Ismael Jaras, Laura Kriener, Jakob Jordan, Walter Senn, Mihai A. Petrovici:** Towards fully embedded biologically inspired deep learning on neuromorphic hardware

90 **III Brain organisation & theoretical neuroscience**

90 **Peter Bouss, Alessandra Stella, Günther Palm, Sonja Grün:** Surrogate techniques to evaluate significance of spike patterns

95 **Raquel Marques, Diana Tavares, António Marques, Pedro Monteiro, António Correia:** Electroencephalographic and behavioural evaluation of visual attention capacity in deaf individuals

100 **Nikita Otstavnov, Nieto Doval Carlos Murielo, Stanislav Otstavnov, Matteo Feurra:** Investigation of frontoparietal involvement to working memory functioning by transcranial direct current stimulation

105 **Sergio Plaza-Alonso, Nicolás Cano-Astorga, Javier DeFelipe, Lidia Alonso-Nanclares:** Focused Ion Bean/Scanning electron microscopy on the study of the human entorhinal cortex

111 **Meghana Gayatri Potta, Pau Vilimelis Aceituno, Benjamin F. Grewe:** Does backpropagation yield the underlying solution used by the brain?

115 **Alexis Thual, Bertrand Thirion, Stanislas Dehaene:** Deep phenotyping to build inter-subject alignments using optimal transport

119 **Nestor Timonidis, Rembrandt Bakker, Maria Carla Piastra, Maria Garcia-Amado, Mario Rubio, Francisco Clasca, Paul Tiesinga:** Finding order in thousands of fully reconstructed long-range projection neurons in the mouse brain

123 **IV Systems & cognitive neuroscience**

123 **Aleksandra Dolgoarshinnaia, Beatriz Martín-Luengo:** Reality monitoring in native and foreign language

128 **Sandra Doval, Pablo Cuesta, Ricardo Bruña, Lucía Torres Simón, Brenda Chino, Inés Abalo Rodríguez, Fernando Maestú, David López-Sanz:** Diachronic changes in oscillatory activity and its cortical generators in non-pathological development measured by MEG

134 **Claudia Sigrid Hofmann, Sonja Rossi:** Emotional prosody processing in trans women

139 **Elizaveta Ivanova, Beatriz Martín-Luengo:** Prospective metamemory monitoring: Source vs item

144 **Mica Komarnyckyj, Chris Retzler, Zhipeng Cao, Giorgio Ganis, Anna Murphy, Robert Whelan, Elsa Fouragnan:** At-risk alcohol users have disrupted valence discrimination during reward anticipation

148 **Valentina Pergher, Marc M. Van Hulle:** Effect of stimulus category on fast perceptual learning evidenced with ERP and behavioural responses

152 **Ashrafur Rahman, Mahadi Hassan Fahim, Shakil Ahmed, Mehedi Hasan Apu, Arif Anzum Shuvo, Rehnuma Tabassum Jhalak, Kazi Nishat Tasnim, Khadiza Sharmin Lopa:** M1 muscarinic acetylcholine receptor improves the memory in D-galactose induced ageing mice model

157 **Cristian Reyes, Iván Padrón, Sara Nila Yagual, Hipólito Marrero:** The effect of tDCS on the rSTS on reading speed of social sentences is modulated by personality traits

162 **Federica Robertazzi, Matteo Vissani, Guido Schillaci, Egidio Falotico:** In silico brain-inspired meta-learning framework for task-specific action suppression

169 **V Other**

169 **Claudia Bachmann, Marissa Pier Diaz, Wouter Klijn:** The Scientific Liaison Unit of EBRAINS - Our support for you!

Welcome to the 6th HBP Student Conference on Interdisciplinary Brain Research

We are excited to present the proceedings of the 6th Human Brain Project Student Conference on Interdisciplinary Brain Research, an open forum for exchange of knowledge within and across the various research fields addressed by the Human Brain Project (HBP). The conference was organized by young researchers for young researchers, as a virtual meeting for the second time now, from the 22nd to the 25th of February 2022. Reflecting the multidisciplinarity of the HBP, the abstracts from young researchers of this year's edition cover a wide range of topics: from brain organisation, theoretical and clinical neuroscience to brain simulation and brain-inspired architectures.

LIST OF ORGANISERS

Conference programme committee
Joana Covelo | August Pi i Sunyer Biomedical Research Institute
Sandra Diaz | Forschungszentrum Jülich
Alice Geminiani | University of Pavia
Tabea Kirchner | Forschungszentrum Jülich
Carmen Lupascu | Italian National Research Council
Paschal Ochang | De Montfort University
Taylan Özden | Technical University Darmstadt
Jens Egholm Pedersen | KTH Royal Institute of Technology
Ingrid Reiten | University of Oslo
Alper Yegenoglu | Forschungszentrum Jülich

Conference organisers
HBP Education Programme | Medical University Innsbruck

Proceedings editors
Alice Geminiani | University of Pavia
Manuel Gran | Medical University Innsbruck
Judith Kathrein | Medical University Innsbruck
Tabea Kirchner | Forschungszentrum Jülich
Paschal Ochang | De Montfort University
Franziska Vogel | Medical University Innsbruck

Disclaimer

The text of the abstracts is reproduced as submitted.
The opinions expressed in this publication are those of the authors and do not necessarily reflect the views of the Programme Committee, who accept no responsibility for the statements made or the accuracy of the data presented.
This project has received funding from the European Union's Horizon 2020 Framework Programme for Research and Innovation under the Specific Grant Agreement No. 945539 (Human Brain Project SGA3).

Preface

We are excited to present the proceedings of the 6th Human Brain Project Student Conference on Interdisciplinary Brain Research, an open forum for exchange of knowledge within and across the various research fields addressed by the Human Brain Project (HBP). Going virtual for the second time, from the 22nd to the 25th of February 2022, the 6th edition proved once more that also as a virtual meeting, the HBP Student Conference offers invaluable opportunities for extensive scientific discussions among fellow early career researchers and faculty. Through a variety of lectures, workshops, discussion sessions and social events, participants could learn about recent developments and tools in brain research, as well as interact with world-leading researchers and experts on career development, neuroethics and philosophy of the brain. At the heart of the conference were the invaluable contributions of all young researchers in the form of talks and posters, whose corresponding abstracts are presented in this book. The accepted abstracts cover a wide range of topics (brain atlases and clinical neuroscience, brain simulation and brain-inspired architectures, brain organisation and theoretical neuroscience, systems and cognitive neuroscience), introducing new and relevant problems, concepts and ideas, with the potential to inspire collaboration across research disciplines.

We would like to thank all authors for submitting their work to the 6th HBP Student Conference and all participants for making the conference a unique event for the future of brain research. We hope this selected set of abstracts can be of inspiration for new discussions, interactions and research opportunities for the whole scientific community.

Alice Geminiani, Tabea Kirchner & Paschal Ochang

Programme Committee Chairs of the 6th HBP Student Conference

I Brain atlases & clinical neuroscience

Reconstructing the Broca's area of the human brain using a customized dual-view light sheet for optimized imaging time and improved resolution

Mohamed Baghdad[1,3]†, Niamh Brady[1,3]*†, Irene Costantini[1,2]†, Giacomo Mazzamuto[1,2]†, Marina Scardigli[1,3]†, Filippo Castelli[1,3], Ludovico Silvestri[1,2,3], Francesco Saverio Pavone[1,2,3]

[1]European Laboratory for Non-linear Spectroscopy (LENS), University of Florence Via Nello Carrara, Sesto Fiorentino (FI), Italy

[2]National Institute of Optics, National Research Council, Fiorentino (FI), Italy

[3]Department of Physics and Astronomy, University of Florence Via G. Sansone, Sesto Fiorentino (FI), Italy

**brady@lens.unifi.it*

INTRODUCTION/MOTIVATION

Understanding the human brain's structural and functional organization is a key aspect in neuroscience. The necessity to create a detailed map of the anatomical disposition of neurons is shared among the field and would facilitate further widespread research. Previous pipelines presented shortcomings in the form of visual artefacts, long acquisitions times and poor resolution. Here, we present a new pipeline aiming to reduce these limitations by providing high-resolution 3D reconstruction of mapped neurons of the human brain, specifically the Broca's area. The pipeline obtains this volumetric information by utilising advanced Light Sheet Fluorescence Microscopy (LSFM), optimized SHORT clearing protocol [1] and a data management system. 49 slices from the human brain were cleared and labelled using four difference markers targeting nuclei, NeuN, Calretinin and Somatostatin which were then imaged at subcellular resolution, using a customized Light Sheet Microscope. This technique provides the grounds to acquire large-scale data volumes at optimized speeds to enable the analysis of a robust 3D reconstruction of tissue blocks up to the entire organ. In this study, we have constructed a whole human Broca's area of 4*4*2cm.

†these authors contributed equally to the work

METHODS

SHORT protocol: The aging tissue found in adult human organs are particularly difficult to render transparent due to the autoflorescence contributions. The optimized SHORT protocol is used to face this challenge, a procedure based on standard histological treatments and a refined clearing technique. Four neuronal markers were implemented in order to localize cells, highlight targets neurons and discriminate between the excitatory and inhibitory sub-populations of the Broca's area (Brodmann 44/45). The tissue ultrastructure of the SWITCH protocol [2], a tissue processing method enabling tissue preservation and repeated labelling, combined with the clearing capability of TDE and conventional buffers were used in each of the sequentially stained 49 slices of 450µm thickness. With the aim of optimizing contrast during imaging, hydrogen peroxide was applied as well as alkaline antigen retrieval, followed by an optimized version of the SWITCH transformation protocol and refractive index matching with 2-2'thiodiethanol (TDE) to render the sample as transparent as possible. This enhances the depth of light penetration in addition to reducing aberrations.

Custom dual-view inverted confocal light sheet fluorescence microscope (di2CLSFM): A custom built light sheet microscope, equipped with two sCMOS cameras provide two symmetric illumination and detection pathways. As shown in Figure 1, the use of an acoustic tuneable filter and appropriate band-pass filters establish a set-up that is capable of simultaneously acquiring two channels (two laser wavelengths), halving necessary acquisition time. Each slice was acquired using 4 channels in totally (405nm, 488nm, 561nm, 638nm) as a volumetric rate of 0.5cm^3/hour (47 frames per second). Two orthogonal views are leveraged, and subsequently fused computationally, to obtains almost isotropic subcellular resolution along the three optical axes.

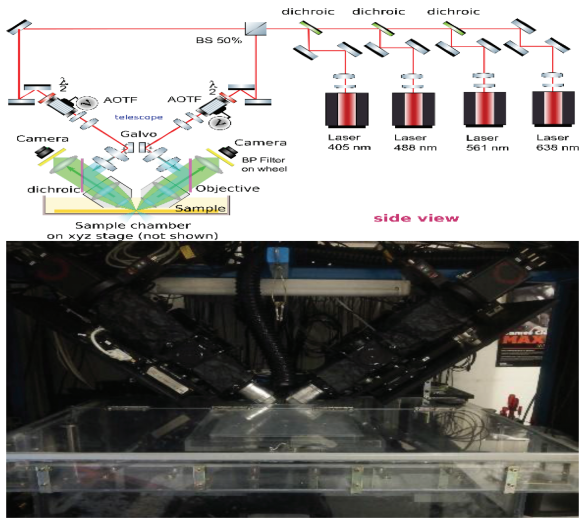

FIGURE 1: di2CLSFM optical schematic and photo of the set up. The front is a protective box, covering the chamber in which the slice is placed for imaging.

Three-dimensional reconstruction of a human hippocampus and of Broca's area: A data management system was implemented to process the large data (≈14TB/slice), combined with a machine learning technique, Convolution Neural Network (CNN) that precisely counts the neurons in 3D.

RESULTS AND DISCUSSION

Our study utilises a combination of techniques to map the neuronal architecture of the human brains. By means of specialized tissue preparation protocol, advanced light sheet fluorescence microscopy and big data analysis, we were able to analyse and to reconstruct the Broca's area of the human brain. This pipeline would not only be a useful tool in neuroscience but also for providing a tool to 3D reconstruct other tissue blocks up to the total organ for human and non-human species. This pipeline is currently being utilized to study other parts of the human brain.

All datasets acquired have been added on the DANDI platform, a platform used for publishing, sharing and processing neurophysiology data [3].

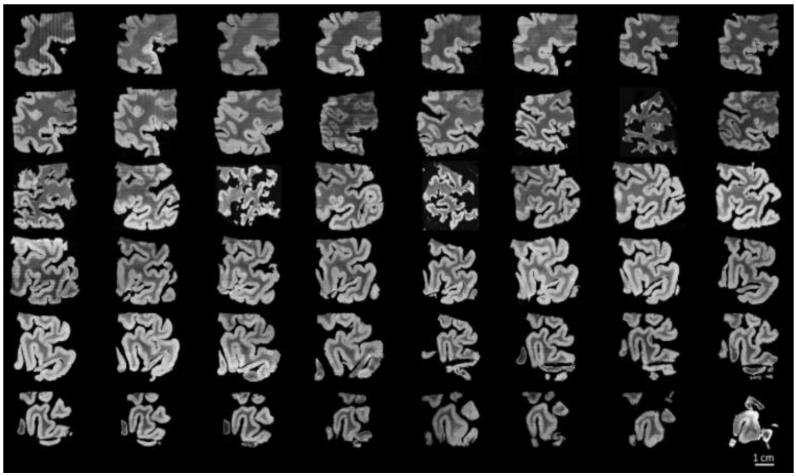

FIGURE 2: 48 slices of Broca's area imaged at a resolution of 0.56*0.56*0.3μm^3. The data is resliced and stitched together to obtain the final fused volume. The complete dataset has been uploaded on DANDI.
Source: https://gui.dandiarchive.org/#/dandiset/000026

Keywords: Light sheet fluorescence microscopy, human brain imaging, tissue clearing, Broca's area, neuron mapping

REFERENCES

[1] 3D molecular phenotyping of cleared human brain tissues with light-sheet fluorescence microscopy. Pesce et al. bioRxiv, 452829, 2021, doi: https://doi.org/10.1101/2021.07.18.452829

[2] Simple, Scalable Proteomic Imaging for High-Dimensional Profiling of Intact Systems. Murray et al. Cell, Volume 163, Issue 6, 2015, Pages 1500-1514, ISSN 0092-8674, https://doi.org/10.1016/j.cell.2015.11.025.

[3] Mazzamuta G. et al. https://dandiarchive.org/dandiset/000026/draft. U01MH117023 (Version draft) [Data set] DANDI Archive (2021).

Sex-dependent cortical excitatory/inhibitory imbalance is associated with behaviour alterations in a mouse model of autism spectrum disorder

Helena M. Ferreira[1], Ana Catarina Sousa[2], Hugo Ferreira[3,4], Sofia Santos[1], José Sereno[3,4], João Martins[3,4], Miguel Castelo-Branco[1,3,4*], Joana Gonçalves[3,4*]

[1]Faculty of Medicine, University of Coimbra, Coimbra, Portugal
[2]Faculty of Sciences and Technology, University of Coimbra, Coimbra, Portugal
[3]Coimbra Institute for Biomedical Imaging and Translational Research (CIBIT), University of Coimbra, Coimbra, Portugal
[4]Institute of Nuclear Sciences Applied to Health (ICNAS), University of Coimbra, Coimbra, Portugal
**jgoncalves@icnas.uc.pt, mcbranco@fmed.uc.pt*

INTRODUCTION/MOTIVATION

Autism spectrum disorder (ASD) is a neurodevelopmental condition characterized by deficits in social interaction, impaired communication, and repetitive behaviours. ASD has a male bias, with a 3:1 ratio of diagnosed males and females. In this sense, it is essential to study sexual dimorphisms of ASD manifestations, and understand the pathways underlying them.

METHODS

In this work, we performed *in vivo* proton magnetic resonance spectroscopy in juvenile male and female *Tsc2*$^{+/-}$ mice, a well-characterized ASD animal model carrying a mutation on the *Tsc2* gene, which causes tuberous sclerosis complex. Moreover, to find a link between metabolic profile and ASD core symptoms, we analysed behaviour and ultrasonic vocalizations during social and repetitive tasks. Behaviour was manually classified by a blind operator to sex and genotype, following a comprehensive mouse behaviour ethogram; Ultrasonic vocalizations were analysed regarding duration, frequency, amplitude and waveform.

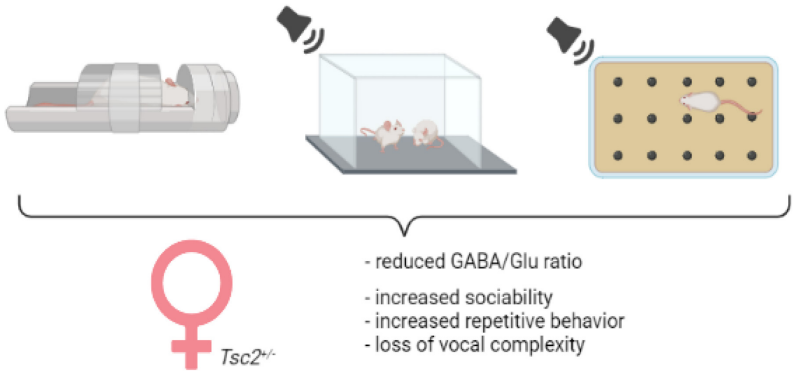

FIGURE 1: Graphical abstract of the presented work. in vivo proton magnetic resonance spectroscopy of the prefrontal cortex and hippocampus revealed reduced cortical GABA/glutamate ratio in transgenic females. Social play test and marble burying test showed an increased number of social interactions and increased repetitive/stereotyped behavior in transgenic females. Additionally, these animals also displayed deficient communication skills, with a reduced USV rate and less vocal complexity. There may be a link between the altered cortical metabolic levels and the behaviors and communication profile observed in the transgenic females.

RESULTS AND DISCUSSION

We found significant increase of glutamate (Glu) levels and decrease of gamma-aminobutyric acid (GABA) levels in the prefrontal cortex of transgenic females, in comparison to WT females (Glu: p= 0.0313; GABA: p= 0.0380). Accordingly, GABA/Glu ratio of *Tsc2*$^{+/-}$ females was decreased (p= 0.0152). No significant alterations were found in males. This data reveals the existence of an excitatory/inhibitory imbalance specific to the prefrontal cortex of transgenic females. We also observed that *Tsc2*$^{+/-}$ females have an increased sociability (p=0.0274), increased repetitive behaviour (p=0.0244) and a less complex vocal repertoire during social task. Overall, here we uncovered an association between sex-dependent altered cortical metabolic signature and abnormal behaviour and communication in autism spectrum disorder.

Keywords: Autism spectrum disorder, Hippocampus, Prefrontal cortex, Social behaviour, Repetitive/restrictive behaviour

Study on the effects of various risk factors on the onset of Parkinson's disease using machine and deep learning

Dimitrios Georgiou[1,2], Christina Emmanouil[1,3], Georgios Vlachos[1,4], Leonidas Stefanis[1,5], Ioannis Michalopoulos[1]*

[1]Biomedical Research Foundation, Academy of Athens, Athens, Greece
[2]School of Electrical and Computer Engineering, National Technical University of Athens, Athens, Greece
[3]Department of Biology, National and Kapodistrian University of Athens, Athens, Greece
[4]School of Applied Mathematical and Physical Sciences, National Technical University of Athens, Athens, Greece
[5]1st Department of Neurology, Aeginition University Hospital, National and Kapodistrian University of Athens, Medical School, Athens, Greece
**imichalop@bioacademy.gr*

INTRODUCTION/MOTIVATION

Parkinson's Disease (PD) is a progressive, neurodegenerative disorder. It affects 1% of the people over the age of 60, rising to 4% over the age of 80 [1]. The cause of the disease has not yet been clarified, with the exception of a few genes which are known to account for a small percentage of the total cases [2]. Both genetic and environmental factors are being examined as risk factors. Symptoms appear after a large number of dopaminergic neurons has died [3]. To improve the prognosis of the disease, we introduced a thorough Machine Learning (ML) approach to analyse PD data.

METHODS

1085 and 586 questionnaires from PD patients and healthy controls respectively were completed by qualified neurologists in Greek hospitals. The questionnaires contained demographic, lifestyle, pharmacological, environmental and clinical data which were stored in the Hellenic Biobank for Parkinson's Disease [4, 5] (http://biobank-informatics.bioacademy.gr), using MOLGENIS 8.6.3 [6]. The dataset contained 51 features for both patients and controls and 75 only for patients. Since this study focuses on the prognosis of the

disease, we wanted to include both patients and controls, so only those 51 features were used. After reformatting the data, we designed an ML approach to identify the factors that are associated with PD. Using Python programming language, we designed a system which compares various preprocessing and transforming steps, as well as ML classifiers:

- Imputers: Mean, Median, Most frequent, Knn, Iterative
- Scalers: Quantile, Max abs, Standard, Robust, Power, Min-max, Normalizer
- Encoders: One hot, Sum, Label, Leave one out, WOE, Target, M estimate, Helmert, James-Stein, Cat boost, GLMM
- Binners: K bins discretizer
- Undersamplers: Tomek, Condensed, Random, Edited nearest, Near miss
- Feature selectors: Select percentile
- Classifiers: Nu SVC, SVC, XGBoost, Gradient boosting, Random forest, Ridge, Logistic regression, Linear SVC, Calibrated, Adaboost, Multi-layer perceptron, Linear discriminant analysis, Stochastic gradient descent, K-nearest neighbors, Decision tree, Extra tree

For each classifier, we ran numerous experiments to identify the best combination of preprocessors and transformers. For the resulting algorithms, we tuned the most important hyperparameters using the halving gridsearch algorithm, to identify the best configurations. These were later given as input to ensemble algorithms (hard voting and soft voting), to optimise the best models. Here, we ran numerous experiments to identify the best combination of optimized classifiers for the ensemble approach, and again numerous experiments to optimize the weights of the best voting soft ensemble classifier. To prevent data leakage and overfitting, the data were split into a training and a test dataset. All experiments were performed on the training set, using 10-fold cross validation. The test set was used only once, at the end of each experiment, for evaluation. Furthermore, we compared our results with those of automated ML platforms (Auto-WEKA [7], JADBio [8], RapidMiner

[9]) using the same dataset. Finally, we introduced a deep learning (DeepL) approach for analysing the data, by converting features into embeddings, a concept used in Natural Language Processing (NLP). This approach is innovative and overcomes the problem of lack of large amount of data for neural networks and lack of interpretability, since using vectors to represent each entity removes the sparse matrices' problem of inefficient computation and shows the relationship between each entity [10]. These embeddings were given as input in a Convolutional Neural Network (CNN), the architecture and the parameters of which are still being optimised, while feature maps are being constructed to better interpret features' relationships.

RESULTS AND DISCUSSION

Based on our ML approach, the ensemble classifiers have so far achieved a Matthews Correlation Coefficient (MCC) of 0.583 and an F1 score of 0.840. As this is an ongoing project, more experiments are scheduled to run, expecting to improve these 2 metrics, and to construct new informative visualisations as well. Based on our ML approach, the factors "Family History", "Age", "Gender", "Smoking-Free Years", "Coffee Status", "Total Coffee Consumption", "Daily Average Coffee", "Smoking Years" and "Religion" played, in that order, a key role in the progression of the disease. These results confirm the literature findings that PD family history, age and male gender constitute the biggest risk factors for PD, whereas smoking and coffee consumption play a protective role. Regarding the comparison between ML platforms, all three platforms require no coding skills. JADBio stood out as the user-friendliest and most automated platform. We also used it before writing our own scripts, as a preliminary data analysis tool, in order to see if our data have the potential to be classified correctly. RapidMiner was a little more complicated, but achieved good results. Auto-WEKA requires the preprocessing to be done by the user, and overfitting was also detected. However, our custom-made Python code is more versatile and we were able to implement several extra steps, analysing in depth different transformers and models. The results are summarised in table 1.

Table 1: Results comparison

Metrics	Scores				
	Machine Learning Approach	**Deep Learning Approach**	**JADBio**	**RapidMiner**	**Auto-WEKA→ configuration tested in simple WEKA**
MCC	0.583	0.57	0.412	0.414 (not provided)	0.729 → 0.512
F1	0.840	0.840	0.678	0.812	0.820 → 0.779
ROC-AUC	0.8	0.8	0.789	0.788	0.859 → 0.753
Accuracy	0.8	0.8	0.729	0.742	0.878 → 0.778

The automated platforms also suggest hypertension, brain damage, and certain childhood prefectures and residence prefectures as risk factors. Although PD has already been studied using ML, this project studies, for the first time, the disease in Greece. As Greece includes numerous islands, genetic isolation can be observed to some degree, due to limited relocation. Genetic isolation also occurred due to the coexistence of two different religious communities (Orthodox and Catholic Christians) in some islands: Marriages between members of the two communities used to be rare. Thus, Greek populations should be studied to identify potential risk genes. One of the important advantages of our approach is that there is no size limit for the input data. We can also construct numerous visualisations to interpret the outcome of every step. In contrast with other approaches that often focus on accuracy, our main focus was to optimise MCC, since it takes into account the predictions for all classes equally. Finally, our extensive pipeline outperformed the 3 automated ML platforms, in terms of MCC, F1 ROC-AUC and accuracy scores. Last but not least we introduced the innovative concept of entity embeddings used to build a CNN model which outperforms every approach in terms of MCC.

Keywords: Parkinson's Disease, Clinical Data, Machine Learning, Classification, Python, WEKA, JADBio, RapidMiner

REFERENCES

[1] O. B. Tysnes and A. Storstein, "Epidemiology of Parkinson's disease," *J Neural Transm (Vienna),* vol. 124, no. 8, pp. 901-905, Aug 2017.

[2] C. Klein and A. Westenberger, "Genetics of Parkinson's disease," *Cold Spring Harb Perspect Med,* vol. 2, no. 1, p. a008888, Jan 2012.

[3] S. Sharma *et al.*, "Biomarkers in Parkinson's disease (recent update)," *Neurochem Int,* vol. 63, no. 3, pp. 201-29, Sep 2013.

[4] E. Angelopoulou *et al.*, "The relationship between environmental factors and different Parkinson's disease subtypes in Greece: Data analysis of the Hellenic Biobank of Parkinson's disease," *Parkinsonism Relat Disord,* vol. 67, pp. 105-112, Oct 2019.

[5] M. Bozi *et al.*, "Genetic assessment of familial and early-onset Parkinson's disease in a Greek population," *European Journal of Neurology,* vol. 21, no. 7, pp. 963-968, 2014.

[6] K. J. van der Velde *et al.*, "MOLGENIS research: advanced bioinformatics data software for non-bioinformaticians," *Bioinformatics,* vol. 35, no. 6, pp. 1076-1078, Mar 15 2019.

[7] E. Frank, M. A. Hall, and I. H. Witten, "The WEKA Workbench," Data Mining: Practical Machine Learning Tools and Techniques4th ed., 2016. [Online]. Available.

[8] I. Tsamardinos *et al.*, "Just Add Data: Automated Predictive Modeling and BioSignature Discovery," *bioRxiv,* p. 2020.05.04.075747, 2020.

[9] M. Hofmann and R. Klinkenberg, "RapidMiner: Data Mining Use Cases and Business Analytics Applications." Boca Raton: CRC Press, 2014.

[10] X. Huang *et al.*, "TabTransformer: Tabular Data Modeling Using Contextual Embeddings", *arXiv*, p 2012.06678, 2021.

Heart-brain interactions in anxiety influence decision-making and learning

Marina Ivanova[1]*, Zheng Gong[1], Thomas Hein[2], Maria Herrojo Ruiz[1,2], Vadim Nikulin[1,3]

[1]National Research University Higher School of Economics, Centre for Cognition and Decision-Making, Institute for Cognitive Neuroscience, , Moscow, Russia
[2]Department of Psychology, Goldsmith University of London, London, United Kingdom
[3]Department of Neurology, Max Planck Institute for Human Cognitive and Brain Sciences, Leipzig, Germany
**mdivanova_1@edu.hse.ru*

INTRODUCTION/MOTIVATION

Interoception is defined as sensing, integration, and regulation of internal states of an organism by the brain. Interoceptive processing plays a significant role in the functioning of a human organism, including homeostasis and allostasis, the perception of self and other, the processing of reality, learning, and decision-making. Interoceptive processing may be enhanced or disrupted in psychiatric disorders and in anxious or stressful situations. Heartbeat-evoked responses (HERs) are evoked potentials or evoked fields (in the magnetoencephalographic (MEG) setting) that occur in response to a heartbeat event (Baranauskas et al., 2017). Trait anxiety is viewed as a fairly stable characteristic in connection to personality. Experiencing state anxiety more frequently and perceiving the world as being generally unsafe and threatening are the major features of trait anxiety (Wiedemann, 2001). The amplitude of heartbeat-evoked responses time-locked to the processing of external stimuli has been shown to disrupt exteroceptive processing (Park et al., 2014). In our recent work we showed that state anxiety disrupts learning and decision making in a volatile environment, decreasing the amount to which individuals update their beliefs using feedback (Hein et al., 2021). Analysing the HER locked to the T-wave of the cardiac cycle, we aim to assess the degree to which the HER amplitude modulates trial-by-trial belief updating and learning, as a function of trait anxiety. Investigating how interoception can modulate learning in high trait anxiety, we can discover important characteristics of anxiety as a personality trait as well as a clinical condition. This knowledge can improve our understanding of mental health conditions as many of them include anxiety as a symptom, which can later used in the development of better treatments for such conditions.

METHODS

For recording brain activity, we are using magnetoencephalography (MEG) – the 306-channel magnetoencephalographic machine 'Neuromag Vector View' (Elekta Oy, Finland), located in the Moscow MEG Centre (Moscow, Russia). Along with MEG, we record ECG and electrooculogram (EOG) using the bipolar channels integrated in the system. Magnetoencephalography is characterized with the good temporal resolution similar to electroencephalography (EEG), which makes it a useful tool to investigate such things as neural evoked responses, and at the same time its spatial resolution is stronger than EEG, so it can be used for localizing the source of the signal with better precision. Our experimental task (Fig. 1) consists of three blocks: resting state, reward learning task block 1, and reward learning task block 2 Binary choice decision-making task with contingencies that change over the course of learning. Participants need to complete two blocks, each of which consists of 160 trials, and their goal is to determine which one of the two visual icons (always either a blue or an orange circle) leads to a reward (5 points). We are using the STAI-T scale (Spielberger, 1983) to measure participants' trait anxiety levels.

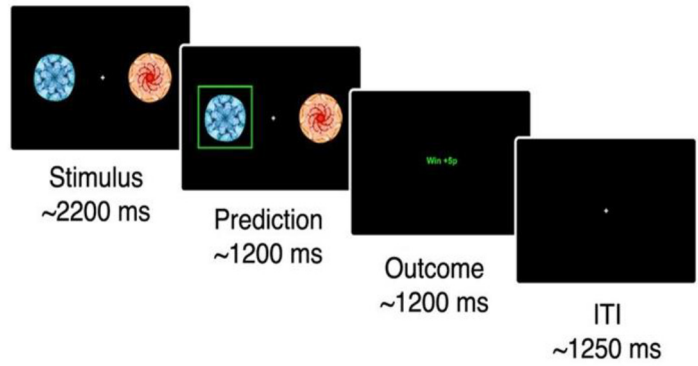

FIGURE 1: Example of a trial in the experimental task (the task had previously been applied in Hein et al., 2021).

RESULTS AND DISCUSSION

We acquired MEG, ECG, and behavioral data from 41 participant: 20 participants with high trait anxiety (STAI score: > 45) and 21 participants with low trait anxiety (STAI score: < 35). Analysis of the behavioral data revealed significant differences between the low trait anxiety and the high trait anxiety groups in model-free and model-based variables. On the one hand, the average winning rate – the percentage of winning trials – for the low trait anxiety group equals to 0.65 (SEM 0.01), while the average winning rate for the high trait anxiety group is 0.63 (SEM 0.03). These values are significantly different using permutation tests, and the p-value is 0.0186. On the other hand, preliminary analysis of the data using the Bayesian computational model that was the best model explaining the data in a previous study of the group (Hein et al., 2021) demonstrates that high trait relative to low trait anxiety leads to reduced learning through an attenuation of prediction errors updating beliefs. We have yet to complete our analysis of the HERs, however, by far, we have made an interesting

OBSERVATION

The HER amplitude is higher in both groups in lose trials than in win trials. Since we are analyzing the HER amplitude which is time-locked to the T-wave that is preceding the feedback, by the time we can observe the HER (around 150 ms after the T-wave), the feedback does not yet appear. So, the HER amplitude appears to be reacting to the outcome of the trial before the outcome is known to the participant. We also observed that most lose

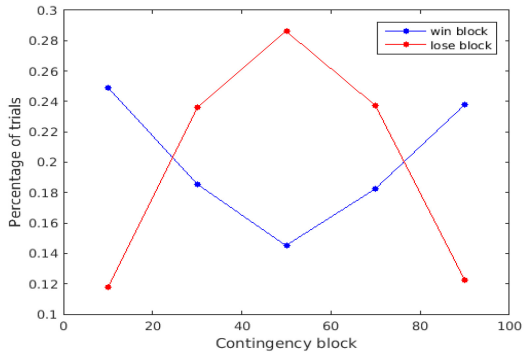

FIGURE 2: Percentage of win and lose trials depending on contingency.

trials happened during the 50/50 contingency blocks (Fig. 2), so possible explanations include some kind of processing of 'loss anticipation' occurring in participants.
The plans for further analysis in our project include the following steps:

- The behavior of both groups in the learning task to be characterized using a hierarchical Bayesian model of decision-making to link trial-to-trial HER measures to dynamic learning.

- Our aim is to focus on the trial-by-trial modulations of the HER preceding the outcome and see how the amplitude modulates with learning in the trial from the feedback information (combining analysis of the MEG HER and the trajectories of learning in a Bayesian computational model).

ACKNOWLEDGEMENTS

National Research University Higher School of Economics, Center for Neurocognitive Research (MEG Center) at the Moscow City University of Psychology and Education.

Keywords: magnetoencephalography, heartbeat-evoked response, anxiety, learning in volatile environment, reward-based learning, interoception, decision making

REFERENCES

[1] Baranauskas, M., Grabauskaitė, A., & Griškova-Bulanova, I. (2017). Brain responses and self-reported indices of interoception: Heartbeat evoked potentials are inversely associated with worrying about body sensations. *Physiology & Behavior, 180*. https://doi.org/10.1016/j.physbeh.2017.07.032

[2] Wiedemann, K. (2001). Anxiety and Anxiety Disorders. In *International Encyclopedia of the Social & Behavioral Sciences*. Elsevier. https://doi.org/10.1016/B0-08-043076-7/03760-8

[3] Park, HD., Correia, S., Ducorps, A. et al. Spontaneous fluctuations in neural responses to heartbeats predict visual detection. Nat Neurosci 17, 612–618 (2014). https://doi.org/10.1038/nn.3671

[4] Hein, T. P., de Fockert, J., & Ruiz, M. H. (2021). State anxiety biases estimates of uncertainty and impairs reward learning in volatile environments. NeuroImage, 224, 117424. https://doi.org/10.1016/j.neuroimage.2020.117424

[5] Spielberger, C.D.; Gorssuch, R.L.; Lushene, P.R.; Vagg, P.R.; Jacobs, G.A (1983). Manual for the State-Trait Anxiety Inventory. Consulting Psychologists Press

Visual gamma oscillations and perceptual spatial suppression point to impaired neural inhibition in premenstrual dysphoric disorder

Viktoriya Manyukhina[1,2]*, Andrey Prokofyev[1], Tatiana Obukhova[1], Tatiana Stroganova[1], Elena Orekhova[1]

[1]Center for Neurocognitive Research (MEG Center), Moscow State University of Psychology and Education, Moscow, Russian Federation

[2]Department of Psychology, National Research University Higher School of Economics, Moscow, Russian Federation

**mvo96@inbox.ru*

INTRODUCTION/MOTIVATION

Premenstrual dysphoric disorder (PMDD) is a depressive disorder [1] characterized by severe negative mood and physical symptoms that occur after ovulation (luteal phase) and disappear with the onset of menstruation (i.e., during the follicular phase). There is evidence that imbalance of excitatory (E) and inhibitory (I) neurotransmission caused by abnormal sensitivity of GABAergic receptors to progesterone metabolite allopregnanolone plays an important role in PMDD [2]. We hypothesised that E/I imbalance in PMDD will be evident in the cortical regions rich in GABAegric neurons, such as the primary visual cortex (V1), i.e., even beyond brain areas involved in mood control. To test this hypothesis, we used electrophysiological and psychophysical measures of inhibition efficacy in the visual cortex – visual perceptual suppression ('*spatial suppression*'; [3]) and visual *gamma response suppression index* (GRSI; [4]).

METHODS

We recruited 20 women suffering from PMDD according to the C-PASS questionnaire ([5]) and 27 age-matched control women (Age: 18-40, 28.4$\pm$5.6), who had no/mild premenstrual symptoms according to a retrospective questionnaire. The criteria for inclusion were regular menstrual cycle and absence of hormonal (e.g. contraceptive pills) or antipsychotic treatment. The participants were investigated twice: during follicular (asymptomatic) and luteal (symptomatic) phases of the menstrual cycle; the phase of the visit was balanced between visits and participants. The presence of the particular phase

(luteal/follicular) was confirmed by biochemical analysis of progesterone and estradiol concentration. During both visits, the women underwent magnetoencephalography (MEG) and psychophysical testing. MEG was recorded while the participants looked at large (18°) high-contrast circular gratings, either static or moving at one of three velocities: 'slow': 1.2°/s, 'medium': 3.6°/s, 'fast': 6.0°/s. Stimuli of this type cause reliable increase in gamma (40-90 Hz) power in the V1 – 'gamma response' (GR). The GR is generated through interaction of parvalbumin-containing inhibitory neurons and principle cells [6]. Frequency of the GR is known to increase linearly with increasing visual motion velocity, while its power demonstrates nonlinear changes: it normally increases up to 1.2-3.6°/s ('suppression transition point') and then decreases with further increase of motion velocity [4,7]. The GR attenuation at fast velocities can be explained by stronger inhibitory regulation (and lower E/I ratio) associated with strong excitatory drive [4]. To approximate the 'suppression transition point', we estimated GRSI as:

$$(Power_{STATIC}*0+Power_{SLOW}*1.2+Power_{MEDIUM}*3.6+Power_{FAST}*6.0)/(Power_{STATIC}+Power_{SLOW}+Power_{MEDIUM}+Power_{FAST}).$$

During a separate psychophysical experiment, participants detected the direction of motion of small (1°) and large (12°) high-contrast vertical gratings. The gratings moved at a constant velocity, but the duration of their presentation gradually decreased. We estimated the minimal time required to discriminate the motion direction of small ($Threshold_{SMALL}$) and large ($Threshold_{LARGE}$) grating. It has been shown previously that it usually takes people longer to discriminate motion direction of a large grating than of a small grating because of the suppression of neuronal responses caused by the activation of the inhibitory surround by large high-contrast stimuli (i.e., 'surround suppression'). Thus, the longer time required to discriminate the direction of the large grating indicates stronger inhibition in the visual cortex [8].

RESULTS AND DISCUSSION

All participants from the PMDD group reported severe premenstrual symptoms during at least two menstrual cycles. Similarly to the results of the previous study that included women with severe PMDD [9], our participants had reduced level of progesterone in the luteal phase (Mann-Whitney test, $U=168.5$, $p=0.015$) as well as an elevated estradiol/progesterone ratio in the luteal phase (Mann-Whitney test, $U=168.5$, $p=0.005$).

In both PMDD and control participants the GR frequency increased from follicular to the luteal phase ($F(1,42)=7.3$, $p=0.01$). No group differences in the GR frequency or Group x Phase interaction was found. Unlike GR frequency, GR power did not depend on the phase of the cycle, but demonstrated significant Velocity x Group interaction ($F(3,129)=3.2$, $p=0.025$): women with PMDD were characterized by stronger GR during the 'medium' and 'fast' motion conditions, but not the 'static' one, thus indicating a shift of the 'suppression transition point' to higher motion velocities. Indeed, the GRSI was significantly higher in women with PMDD than in control subjects ($F(1,42)=5.1$, $p=0.029$). Moreover, in the PMDD group the GRSI was significantly higher during luteal compared to follicular phase of the menstrual cycle ($F(1,17)=5.3$, $p=0.035$). Generally higher GRSI in PMDD than in control group suggests impaired E/I balance regulation in PMDD patients. The increase of the GRSI in women with PMDD during luteal as compared to follicular phase of the cycle suggests that E/I balance in their visual cortex is especially strongly compromised during the symptomatic phase. Despite the observed alterations, the GRSI in women with PMDD did not correlate with the symptoms severity ($GRSI_{LUTEAL}$: Spearman $R=0.014$, $p=0.95$). It is likely, that while impairment of E/I balance regulation in PMDD is widespread, the mood symptoms of PMDD are associated with E/I imbalance in specific, mood-related brain areas.

In the psychophysical experiment the reliable data were obtained from 23 controls and 13 PMDD participants. While $Threshold_{SMALL}$ did not differ between groups and phases, $Threshold_{LARGE}$ in PMDD significantly decreased during the luteal as compared to follicular phase ($F(1,11)=5.6$, $p=0.038$), suggesting reduction of neural inhibition during the symptomatic phase. For $Threshold_{LARGE}$, there was also Group x Phase interaction ($F(1,32)=5.2$, $p=0.03$): during follicular (but not luteal) phase the $Threshold_{LARGE}$ tended to be higher in the PMDD than in the control subjects ($F(1,32)=3.7$, $p=0.063$). Interestingly, the $Threshold_{LARGE}$ measured during the luteal phase correlated positively with severity of their premenstrual symptoms (Spearman $R=0.58$; $p=0.023$). These findings suggest the presence of a compensatory, possibly 'top-down' regulatory mechanism in PMDD patients that enhances neural inhibition in V1, putatively through activation of somatostatin-containing inhibitory neurons [10].

In conclusion, the results of both MEG and psychophysical studies indicate a decrease in neural inhibition in the visual cortex in women with PMDD during the luteal – symptomatic – phase of the menstrual cycle. Our results

also suggest that the regulation of E/I balance in the visual cortex in women with PMDD is atypical in both luteal and follicular phases. Although changes in E/I balance in the visual cortex are not directly related to the psychoaffective symptoms of PMDD, they may shed light on the neural mechanisms of this disorder.

Keywords: premenstrual dysphoric disorder, excitation-inhibition balance, steroid hormones, gamma oscillations, spatial suppression

REFERENCES

[1] American Psychiatric Association (2013). Diagnostic and statistical manual of mental disorders: DSM-5.

[2] Bäckström, T., Haage, D., Löfgren, M., Johansson, I. M., Strömberg, J., Nyberg, S., ... & Bengtsson, S. K. (2011). Paradoxical effects of GABA-A modulators may explain sex steroid induced negative mood symptoms in some persons. Neuroscience, 191, 46-54.

[3] Tadin, D., Lappin, J. S., Gilroy, L. A., & Blake, R. (2003). Perceptual consequences of centre–surround antagonism in visual motion processing. Nature, 424(6946), 312-315.

[4] Orekhova, E. V., Prokofyev, A. O., Nikolaeva, A. Y., Schneiderman, J. F., & Stroganova, T. A. (2020). Additive effect of contrast and velocity suggests the role of strong excitatory drive in suppression of visual gamma response. PloS one, 15(2), e0228937.

[5] Eisenlohr-Moul, T. A., Girdler, S. S., Schmalenberger, K. M., Dawson, D. N., Surana, P., Johnson, J. L., & Rubinow, D. R. (2017). Toward the reliable diagnosis of DSM-5 premenstrual dysphoric disorder: the Carolina Premenstrual Assessment Scoring System (C-PASS). American Journal of Psychiatry, 174(1), 51-59.

[6] Buzsáki, G., & Wang, X. J. (2012). Mechanisms of gamma oscillations. Annual review of neuroscience, 35, 203-225.

[7] Manyukhina, V. O., Rostovtseva, E. N., Prokofyev, A. O., Obukhova, T. S., Schneiderman, J. F., Stroganova, T. A., & Orekhova, E. V. (2021). Visual gamma oscillations predict sensory sensitivity in females as they do in males. Scientific reports, 11(1), 1-10.

[8] Tadin, D., Silvanto, J., Pascual-Leone, A., & Battelli, L. (2011). Improved motion perception and impaired spatial suppression following disruption of cortical area MT/V5. Journal of Neuroscience, 31(4), 1279-1283.

[9] Munday, M. R., Brush, M. G., & Taylor, R. W. (1981). Correlations between progesterone, oestradiol and aldosterone levels in the premenstrual syndrome. Clinical Endocrinology, 14(1), 1-9.

[10] Adesnik, H., Bruns, W., Taniguchi, H., Huang, Z. J., & Scanziani, M. (2012). A neural circuit for spatial summation in visual cortex. Nature, 490(7419), 226-231.

Characterization of microbiome and brain NPY system alterations in a mouse model of autism spectrum disorder

Beatriz Martins[1,2,3]*, Miguel Castelo Branco[2,3,4], Joana Gonçalves[2,3], João Martins[2,3]

[1]Faculty of Medicine, Doctoral Program in Health Sciences, University of Coimbra, Coimbra, Portugal
[2]Coimbra Institute for Biomedical Imaging and Translational Research (CIBIT), University of Coimbra, Coimbra, Portugal
[3]Institute of Nuclear Sciences Applied to Health (ICNAS), University of Coimbra, Coimbra, Portugal
[4]Faculty of Medicine, University of Coimbra, Coimbra, Portugal
**bmartins@fmed.uc.pt*

INTRODUCTION/MOTIVATION

Autism Spectrum Disorder (ASD) is a neurodevelopmental disorder characterized by deficits in social communication and presence of repetitive behaviors. Recent evidences suggested that microbiome may play a role in the etiology of ASD. However, the mechanisms of these effects are still poorly understood. Some evidences suggest that the gut can affect brain function through metabolite secretion, host immune response, altering the activity of the stress-associated hypothalamic–pituitary–adrenal axis and regulating the biosynthesis of active neuropeptides. Neuropeptide Y (NPY) is one of the most potent orexigenic neuropeptides found in the central and peripheral nervous systems with roles in multiple physiological processes including neuronal excitability, learning and memory and regulation of intestinal microbiota. But, it remains unclear whether behavioral disorders associated with dysbiosis of the intestinal microbiota, including ASD, are also under the control of the NPY system. The proposed work will evaluate gut microbiome relative levels and brain NPY system expression in neurofibromatosis type 1 (NF1) mice, a well-charaterized ASD animal model.

METHODS

Here, juvenile female and male NF1 mice were used. Brains were removed and brain regions, namely hippocampus and amygdala, were dissected.

Additionally, we collected stool samples directly from the colon. All samples were stored in RNA later at -80ºC until further use. mRNA from brain and colon samples were extracted using RNeasy Lipid Tissue and RNeasy PowerMicrobiome® Kit (Qiagen, Hilden Germany), respectively, according to the manufacturer's instructions. Real Time PCR (RT-PCR) on microbial samples was performed using primers for the genera *Lactobacillus*. 16S were used as a bacterial endogenous control for qRT-PCR experiment. For gene expression analysis from brain samples, primers for *npy, y1r, y2r, y5r* were used. *B2m* and *ywhaz* were used as housekeeping genes to normalize NPY mRNA changes. Importantly, all experiments used littermates as controls. Statistical analysis was performed using the Mann-Whitney test in GraphPad Prism 6.0 (GraphPad software, Inc., San Diego, CA, USA).

RESULTS AND DISCUSSION

The present study reported dysregulation of *Lactobacillus* population in the gut of NF1 mice, with a decrease in *L.Reuteri* and an increase in *L.Rumni.* In addition, we also reported changes in NPY and NPY receptors expression in amygdala and hippocampus brain regions of NF1 animal in a sex-dependent way. Indeed, NF1 males showed an increase in NPY in hippocampus and a decrease in Y_2R expression in amygdala comparing with their WT littermates. On the other hand, no changes were detected in transgenic females. This study identifed bacterial species that are sensitive to an autism-related mutation as well sex-dependent changes in brain NPY, pointing to the importance of considering the gut–brain axis in treatment of this disorder.

Keywords: neuropeptide Y, gut-brain, microbiome, NF1 mouse model, autism spectrum disorder

Integration of multi-omics data using graph neural networks to identify and contextualize biomarker genes for psychiatric disorders

Svitlana Oleshko[1,2]*, Francesc Fernández-Albert[2], Matthias Heinig[1], Sergio Picart-Armada[2], Annalisa Marsico[1]

[1]Institute of Computational Biology, Helmholtz Zentrum München, Neuherberg, Germany
[2]Global Computational Biology and Digital Sciences, Boehringer Ingelheim Pharma GmbH & Co. KG, Biberach an der Riss, Germany
**svitlana.oleshko@helmholtz-muenchen.de*

INTRODUCTION/MOTIVATION

Mental health today is a burden on a global level with various psychiatric disorders leading to a lower quality of life, a significant number of deaths and a higher pressure on healthcare systems. It is known that mental disorders influenced around 1 billion people worldwide in 2019 (point prevalence: 970,070,243) [1]. As developing more effective treatments for the most common mental disorders is of high priority for international public health, substantial research is nowadays dedicated to this issue. This includes studies where emphasis is put on biological and mechanistic understanding of the brain. For example, the PsychENCODE [2] initiative provides various molecular and genetic data generated from brain tissue and already presents some insights into the molecular mechanisms of gene regulation for psychiatric disorders such as autism spectrum disorder, bipolar disorder, and schizophrenia. These data are often referred to as multi-omics and include but are not limited to gene or protein expression read-outs, mutations, DNA methylation. In order to achieve a higher level of interpretability, we aim to develop a method based on a graph neural network which leverages prior knowledge of gene-gene associations in the form of protein-protein interaction network and multi-omics data generated from brain tissue. Methods for integration of different molecular data types such as graph neural networks for disease gene predictions have already been successfully applied in the context of cancer [3] and might be suitable to integrate heterogeneous data from the brain.

METHODS

We apply graph attention network model [4] to integrate gene expression data with protein-protein interaction data to identify candidate genes related to schizophrenia. Protein-protein interactions were retrieved from STRING database [5] and are used as a graph structure for the graph attention network model where each node corresponds to a gene. Gene expression data was extracted from PsychENCODE resource [6] in a form of a matrix where each entry represents the expression level of a particular gene in a given sample. This gene expression was pre-processed such that the final matrix contains samples that represent either control group or patients diagnosed with schizophrenia and genes that are protein-coding and have non-constant expression (the gene should have standard deviation of gene expression values across all samples higher than a certain threshold). The final gene expression matrix was used as a feature matrix for the model with each row was taken as a feature vector for respective node in the graph. After model training, we obtain prediction scores for each node/gene to identify candidate biomarker genes for schizophrenia.

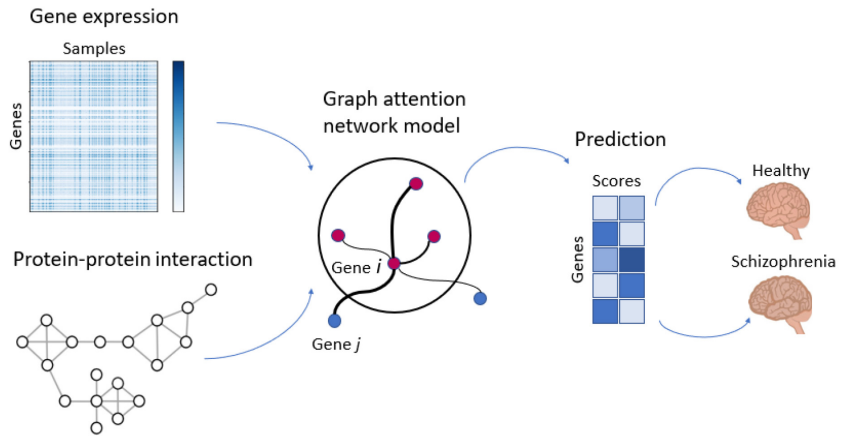

FIGURE1: Schematic overview of our method for disease state prediction using gene expression data and protein-protein interactions in a graph attention neural network model in an integrative manner.

Along with gene prediction task, we assess the value of including both tissue-agnostic and brain-specific protein-protein interaction as an additional data source and the advantages of graph neural networks as opposed to other deep learning architectures that have been used on this data so far. Brain-specific protein-protein interaction data was retrieved from the following databases: IID (Integrated Interactions Database), GIANT (Genome-wide Analysis of gene Networks in Tissues), and GTEx (Genotype-Tissue Expression). We run the model for each protein-protein interaction network individually and for each case we evaluate model performance.

RESULTS AND DISCUSSION

We compared the performance of the model with other methods for disease gene prediction such as EMOGI [3] and DeepWalk [6] as well as classifiers which do not consider network topology such as random forest and support vector machine. Based on different metrics we calculated, the model on average outperforms other machine learning architectures that can be used on this data. However, according to all model performance metrics, we do not have an advantage from having brain-specific protein-protein interactions over tissue-agnostic protein-protein interactions when using these networks as a prior knowledge of gene-gene associations.

The result of prediction task is a list of genes that are candidate biomarker genes for schizophrenia which we put into a context using gene set enrichment analysis. Moreover, we achieve a higher level of interpretability by directly utilizing the attention weights which are additionally learned during model training. Those attention weights mean the importance of expression values of one gene for disease state prediction made for another node. They provide us with new insights on gene relations and allow us to visualize the new graphs that our model has learned. Therefore, by exploiting attentional weights, we benefit in terms of model explainability and overcome the problem of low reliability of protein-protein interaction networks.

Further, we will extend the method to allow the inclusion of other molecular data types such as ChIP-Seq (chromatin immunoprecipitation sequencing), DNA methylation, and genotype data in an integrative manner. The approach should not only allow for integration of multiple data types into the model, but we will implement an interpretation framework for model explanation. Then, the framework will be used to identify and contextualize biomarker

genes for other psychiatric disorders such as bipolar disorder and autism spectrum disorder.

ACKNOWLEDGEMENTS

The present contribution is supported by the Helmholtz Association under the joint research school "Munich School for Data Science - MUDS".

Keywords: multi-omics data integration, predictive modelling, graph neural network, protein-protein interaction, gene expression

REFERENCES

[1] Global Burden of Disease Collaborative Network. Global Burden of Disease Study 2019 (GBD 2019) results. Accessed: 25/06/2021. Available from: http://ghdx.healthdata.org/gbd-results-tool

[2] Akbarian, S., Liu, C., Knowles, J. et al. The PsychENCODE project. Nature Neuroscience 18, 1707–1712 (2015). https://doi.org/10.1038/nn.4156

[3] Schulte-Sasse, R., Budach, S., Hnisz, D., Marsico, A. Integration of multiomics data with graph convolutional networks to identify new cancer genes and their associated molecular mechanisms. Nat Mach Intell 3, 513–526 (2021). https://doi.org/10.1038/s42256-021-00325-y

[4] Veličković, P., Cucurull, G., Casanova, A., Romero, A., Liò, P., Bengio, Y. Graph Attention Networks. arXiv (2018). https://arxiv.org/abs/1710.10903

[5] Szklarczyk, D., Gable, A. L., Lyon, D., Junge, A., Wyder, S., Huerta-Cepas, J., Simonovic, M., Doncheva, N. T., Morris, J. H., Bork, P., Jensen, L. J., von Mering, C. STRING v11: protein–protein association networks with increased coverage, supporting functional discovery in genome-wide experimental datasets, Nucleic Acids Research, Volume 47, Issue D1, 08 January 2019, Pages D607–D613. https://doi.org/10.1093/nar/gky1131

[6] *PsychENCODE Integrative Analysis*, http://resource.psychencode.org/

[7] Perozzi, B., Al-Rfou, R. & Skiena, S. DeepWalk: online learning of social representations. In Proc. 20th ACM SIGKDD International Conference on Knowledge Discovery and Data Mining 701–710 (ACM, 2014). https://doi.org/10.1145/2623330.2623732

Tsc2$^{+/-}$ mouse model: Probing clinical manifestation of epilepsy in Tuberous Sclerosis Complex

M. Lapo Pais[1,2,3]*, J. Martins[2,3], M. Castelo-Branco[2,3,4], J. Gonçalves[2,3]

[1]Faculty of Sciences and Technology, University of Coimbra, Doctoral Program in Biomedical Engineering, Coimbra, Portugal
[2]Coimbra Institute for Biomedical Imaging and Translational Research (CIBIT), University of Coimbra, Coimbra, Portugal
[3]Institute of Nuclear Sciences Applied to Health (ICNAS), University of Coimbra, Coimbra, Portugal
[4]Faculty of Medicine, University of Coimbra, Coimbra, Portugal
**marianalapopais@gmail.com*

INTRODUCTION/MOTIVATION

Tuberous Sclerosis Complex (TSC) is a rare genetic disorder characterized by severe epilepsy, cerebral hamartomas and intellectual disability [1]. Epilepsy is the most common neurological complication in TSC and up to 80–90% of individuals with TSC develop epilepsy at some point in their lifetime [2,3]. Further studies are needed to understand and better characterize the mechanisms behind this comorbidity in TSC. Similarly to the human condition, Tsc2$^{+/-}$ mice display hyperactivation of the mammalian target of rapamycin (mTOR) pathway, which theoretically causes a propensity to exhibit increased epileptic activity [5,6]; however, there is little evidence in the literature supporting this assumption. We aim to determine whether Tsc2$^{+/-}$ mice have altered susceptibility to seizures and explore how sex, age and time of day influence Tsc2-related seizure severity and locomotor activity.

METHODS

We assessed seizure susceptibility and progression in a *Tsc2*$^{+/-}$ mouse model using the chemical convulsant kainic acid (KA), a potent agonist of the AMPA/kainate class of glutamate receptors [7]. Both male and female animals at late adolescent and adult age were evaluated during non-active and active periods (zeitgeber time (ZT) 6 and 18, respectively).

The animals were recorded for 20 minutes under control conditions (saline, i.p.) and for 100 minutes after KA administration (20mg/kg, i.p.). Seizure severity was determined by integrating individual scores per mouse during a 4-minute timeframe 15 minutes after KA administration according to a modified Racine scale as previous described by *E. Akyuz et. al* [8]. Locomotor behaviour was monitored during the same timeframe using related metrics extracted from top-video recordings using *ezTrack*, an open-source video analysis pipeline for the investigation of animal behaviour [9]. The metrics under study included: distance travelled over time (cm), percentage of time in which the animals were not moving (%) and the percentage of animals exhibiting exploratory behaviour (%) - characterized by the movement of the animal to the centre of the field.

RESULTS AND DISCUSSION

Tsc2$^{+/-}$ mice displayed an increased susceptibility in both ages and at both time periods (Ordinary One-Way ANOVA test, $p<0.0001$). Moreover, transgenic and Wild Type (WT) mice were differently affected by age: *Tsc2*$^{+/-}$ mice exhibited a constant and severe susceptibility not dependent on age (Kruskal-Wallis test, $p= 0.8$); while WT mice exhibited an increased susceptibility at earlier stages of development that significantly decreased on adult age (Kruskal-Wallis test, $p<0.0001$). Furthermore, susceptibility to seizures was sex-dependent, with females being more susceptible in both ages (Kruskal-Wallis test, $p<0.001$) (**Figure 1**). Regardless of mice activity levels, analysis on the respective motion tracks revealed that WT mice showed increased exploratory behaviour (44.44% WT showed exploratory behaviour at ZT6 and

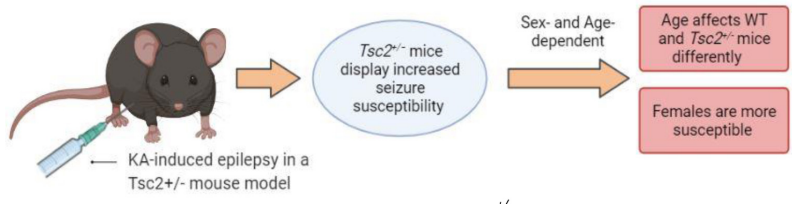

FIGURE 1: Graphical overview of the most relevant results of this work: *Tsc2*$^{+/-}$ mice display increased seizure susceptibility that is sex- and age- dependent. Created using Biorender (https://biorender.com/).

ZT18) while *Tsc2*$^{+/-}$ mostly preferred to remain in the same location or move closer to the walls of the field (18.75% *Tsc2*$^{+/-}$ showed exploratory behaviour at ZT6 and 22.22% at ZT18) (**Figure 2**). All animals exhibited overall reduced movement during the night-time period (Kruskal-Wallis test, $P<0.05$). With this work we demonstrated for the first time that *Tsc2*$^{+/-}$ mice display an increased susceptibility following KA administration, supporting the use of this model in future TSC-related epilepsy research. Furthermore, we showed that KA-induced epilepsy is sex- and age- dependent and that mice activity is affected by daytime period.

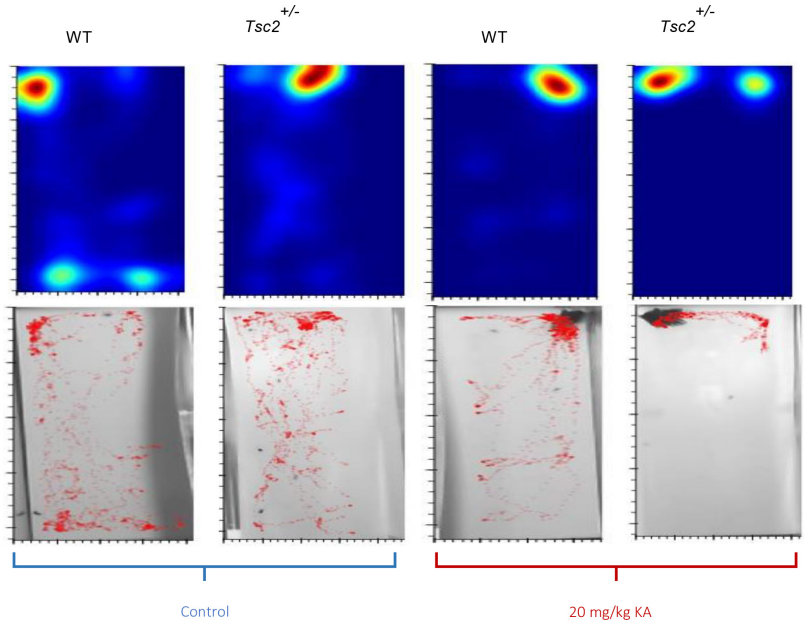

FIGURE 2: Representative heatmaps and motion trace of Wild Type (WT) and transgenic *Tsc2*$^{+/-}$ mice: under control conditions and after KA-induced epilepsy (4-minutes time frame).

ACKNOWLEDGEMENTS

This work was supported by PhD Fellow 2020.06582. BD from FCT and Strategic Plan UIDP/04950/2020, COMPETE and FEDER funds, FCT, Portugal, ICNAS-P.

Keywords: Tuberous Sclerosis Complex, Epilepsy, *Tsc2*$^{+/-}$ mouse model

REFERENCES

[1] B. Zhang, J. Zou, L. Han, B. Beeler, J.L. Friedman, E. Griffin, Y.S. Piao, N.R. Rensing, M. Wong, The specificity and role of microglia in epileptogenesis in mouse models of tuberous sclerosis complex, Epilepsia. 59 (2018) 1796–1806. https://doi.org/10.1111/epi.14526.

[2] M. Mizuguchi, M. Ohsawa, H. Kashii, A. Sato, Brain Symptoms of Tuberous Sclerosis Complex: Pathogenesis and Treatment, Int. J. Mol. Sci. 22 (2021) 6677. https://doi.org/10.3390/IJMS22136677.

[3] M.B. Connolly, G. Hendson, P. Steinbok, Tuberous sclerosis complex: A review of the management of epilepsy with emphasis on surgical aspects, Child's Nerv. Syst. 22 (2006) 896–908. https://doi.org/10.1007/s00381-006-0130-7.

[4] I.E. Overwater, K. Bindels-De Heus, A.B. Rietman, L.W. Ten Hoopen, Y. Vergouwe, H.A. Moll, M.C.Y. De Wit, Epilepsy in children with tuberous sclerosis complex: Chance of remission and response to antiepileptic drugs, Epilepsia. 56 (2015) 1239–1245. https://doi.org/10.1111/epi.13050.

[5] The Jackson Laboratory, (n.d.). https://www.jax.org/strain/004686 (accessed August 6, 2021).

[6] D. Ehninger, S. Han, C. Shilyansky, Y. Zhou, W. Li, D.J. Kwiatkowski, V. Ramesh, A.J. Silva, Reversal of learning deficits in a Tsc2 $^{+/-}$ mouse model of tuberous sclerosis, 14 (2008) 843–848. https://doi.org/10.1038/nm1788.

[7] C. JT, Neurotoxic action of kainic acid, J. Neurochem. 41 (1983) 1–11. https://doi.org/10.1111/J.1471-4159.1983.TB11808.X.

[8] E. AKYÜZ, Pentilentetrazol Epilepsi Modelinde Racine Skorlama Sistemine Yeni Bir Bakış, Harran Üniversitesi Tıp Fakültesi Derg. 17 (2020) 306–310. https://doi.org/10.35440/hutfd.763232.

[9] Z.T. Pennington, Z. Dong, Y. Feng, L.M. Vetere, L. Page-Harley, T. Shuman, D.J. Cai, ezTrack: An open-source video analysis pipeline for the investigation of animal behavior, Sci. Reports 2019 91. 9 (2019) 1–11. https://doi.org/10.1038/s41598-019-56408-9.

II Brain simulation & brain inspired architectures

Incremental awake-NREM-REM learning cycles: Cognitive and energetic effects in a multi-area thalamo-cortical spiking model

Chiara De Luca[1,2]*, Leonardo Tonielli[2], Bruno Golosio[3,4], Gianmarco Tiddia[3,4], Irene Bernava[2], Cristiano Capone[2], Davide Cipollini[5], Giulia De Bonis[2], Cosimo Lupo[2], Elena Pastorelli[2], Francesco Simula[2], Pier Stanislao Paolucci[2]

[1]PhD Behavioural Neuroscience, Sapienza University of Rome, Rome, Italy
[2]Sezione di Roma1, Istituto Nazionale di Fisica Nucleare (INFN), Rome, Italy
[3]Sezione di Cagliari, Istituto Nazionale di Fisica Nucleare (INFN), Cagliari, Italy
[4]Dipartimento di Fisica, Università di Cagliari, Cagliari, Italy
[5]Bernoulli Institute for Mathematics, University of Groningen, Computer Science and Artificial Intelligence, University of Groningen, Groningen, The Netherlands
**chiara.deluca@roma1.infn.it*

INTRODUCTION/MOTIVATION

The alternation of wakefulness and sleep supports the brain energetic and cognitive efficiency in a large variety of high-level functions: among them, the capability of fast incremental learning from a few noisy examples, as well as the ability to associate similar memories in autonomously-created categories, to combine contextual hints with sensory perceptions and to maintain the metabolic cost of brain functions within a budget notwithstanding the progressive increment in knowledge and performance. Sleep is known to be essential for a performance, but the mechanisms underlying its role in supporting learning and energetic management are still to be clarified. This work leverages the recent experimentally driven hypotheses of apical isolation and apical drive [1][2] principles to induce in a model some of the favourable energetic and cognitive effects associated to NREM and REM sleep, reconciling the experimental observation of [11][12]. Also, we follow the apical amplification [3] concept to combine context and perception during training during awake learning. This way, we added REM to the brain states accessible to the thalamo-cortical spiking model [4][5] that demonstrated the effects of incremental awake-NREM learning cycles. Specifically, we investigate both the effects of sleep on the internal synaptic structure of the network and

on its neural activity in a two-area model. We demonstrate complementary homeostatic and associative effects of slow-wave and dreaming-like phases of sleep on cortico-cortical synapses and we show the consequent beneficial energetic consumption effects while keeping the sleep-induced cognitive effects.

METHODS

In this work, we improved to REM simulation the data-driven thalamo-cortical spiking model [4][5] that was already able to carry out cognitive tasks (such as object recognition or decision-making), while expressing realistic brain dynamics in different states (AWAKE and NREM) through the modulation of adaptation, synaptic asymmetry and inhibitory conductance parameters. Specifically, we implemented a multi-area thalamo-cortical spiking model in NEST[6] made of adaptive exponential conductance based excitatory and inhibitory neurons: the thalamic layer projects into the cortical layer through symmetric top-down synaptic connections. The cortical layer, in turn, is organized into two areas recurrently and reciprocally connected, as depicted in Figure 1A. During the awake phase, a visual input [7] is encoded into the thalamic layer and projected to the cortical one: each area in the cortex has access to a different portion of the visual input with a region of overlapping. Plastic synapses are updated in the training and sleeping phase through a STDP (Spike-timing-dependent plasticity) synaptic rule. The training of the network is implemented with a combination of lateral contextual and perceptual signals to correctly sculpt the synaptic weight encoding for the learnt examples, analogously as in [4], in accordance with an Apical Amplification situation [3]. The training protocol is unsupervised, meaning that no information concerning the perception class is provided to the cortex. During the classification phase, on the other hand, the network is provided with a perceptual signal only. In the sleeping phase, the network is not exposed to any perceptual signal and is stimulated by a random lateral signal. During REM sleep the network adaptation is decreased with respect to the awake state [10] while all cortico-cortical connections are active and plastic, in particular those connecting the two areas, implementing an Apical Drive-like situation [1,2]. To emulate the NREM sleep, on the other hand, the adaptation is increased [10] and inter-area cortico-cortical connections are cut, in accordance with the Apical Isolation principle [1,2].

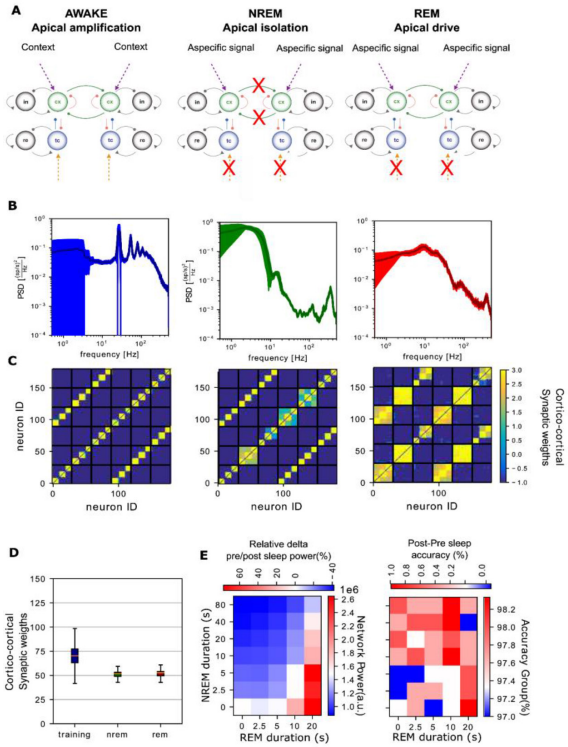

FIGURE 1: Awake-NREM-REM cycle effects. **A**) Network structure: two-area thalamo-cortical model with interconnected cortical populations in awake, nrem and rem phases (Apical Amplification [3], Apical Isolation and Apical Drive principles [1,2]) **B**) Network's Power Spectral Density (PSD) in awake (left), NREM (center), REM (right) stages. Results are comparable with what experimentally observed[9]. **C**) Associative effects of sleep on the cortico-cortical synaptic structure of a network trained over 3 examples per 3 categories. Awake (Left): each subgroup of cortical neurons is orthogonal to the others; NREM stages (center) intra-area connections between groups of neurons responding to similar perceptions are strengthened, while stronger synapses are subjected to homeostatic depression (accordingly with the "shy hypothesis" [12] and selective reinforcement [11]); REM (right) inter-area connections between groups trained over similar perceptual stimuli are strengthened. **D**) Homeostatic effects of sleep: box-plots describing the cortico-cortical synaptic weights distribution after the training (blue), NREM (green) and REM (red) phases. **E**) Effects and Calibration of NREM and REM cycles duration. (Left) Network power consumption during a classification task and relative difference ($\Delta_{post\text{-}pre}$) compared to the pre-sleeping phase. (Right) Post-sleep classification accuracy, and relative improvement compared to pre-sleep, versus NREM and REM duration after a training over 3 examples per 3 categories.

RESULTS AND DISCUSSION

We show the beneficial effects of sleep on both classification performances and energy consumption; to show the beneficial effects of sleep on the network cognitive tasks, we tested the classification performances when classifying the MNIST [7] dataset after a balanced training over 3 examples belonging to 10 classes. First, we calibrated the NREM and REM stages duration, as shown in Figure 1D: the optimal combination is at 40s of NREM and 10s of REM duration, corresponding to a reduction of 22% in the network power consumption and an improvement of 1% in classification accuracy (in agreement with experimental data [8,11]). The power spectra of the network activity in awake classification, NREM and REM stages (shown in Figure 1B) are comparable with what is expected by experimental biological recordings [9]. In Figure 1C and D, we respectively show the associative and homeostatic effect of sleep on cortical synapses. Indeed, as depicted in Figure 1C, cortical groups trained over different examples belonging to the same class (i.e. described by similar perceptual signals) are grouped together in each area during the NREM phase whereas groups of neurons belonging to different cortical areas are associated during the REM phase. This association is implemented by cortico-thalamo-cortical activation loops mediated by inhibitory neurons causing different groups of cortical neurons to respond to similar perceptual stimuli with a contemporaneous up-state in the sleeping phase. Figure 1D, on the other hand, demonstrates the homeostatic effect of sleep on cortico-cortical synapses leading to a general reduction of synaptic weight distributions during the sleeping phase.

ACKNOWLEDGEMENTS

This work has been supported by the European Union Horizon 2020 Research and Innovation program under the FET Flagship Human Brain Project (grant agreement SGA3 n. 945539) and by the INFN APE Parallel/Distributed Computing laboratory. D. Cipollini contributed to this work during his master thesis research project at La Sapienza University of Rome.

Keywords: Awake-NREM-REM cycles, Spiking Models, Classification task, Thalamo-cortical network, Apical Amplification-Drive-Isolation

REFERENCES

[1] Aru, J., Suzuki, M., Larkum, M.E. (2020) "Cellular Mechanisms of Conscious Processing", *Trends in Cognitive Sciences* 24(10) https://doi.org/10.1016/j.tics.2020.07.006

[2] Aru, J. Siclari, F., Phillips, W.A., Storm, J.F. (2020) "Apical drive - A cellular mechanism of dreaming?" *Neuroscience and Biobehavioral Reviews,* 119 p.440-445 https://doi.org/10.1016/j.neubiorev.2020.09.018

[3] Larkum, M. (2013) "A cellular mechanism for cortical associations: an organizing principle for the cerebral cortex" *Trends in neuroscience,* 36(3) https://doi.org/10.1016/j.tins.2012.11.006

[4] Golosio, B., De Luca, C., Capone, C., Pastorelli E, Stegel G, Tiddia G, et al. (2021) "Thalamo-cortical spiking model of incremental learning combining perception, context and NREM-sleep", *PLoS Comput Biol* 17(6): e1009045. https://doi.org/10.1371/journal.pcbi.1009045

[5] Capone, C., Pastorelli, E., Golosio, B. et al. Sleep-like slow oscillations improve visual classification through synaptic homeostasis and memory association in a thalamo-cortical model. Sci Rep 9, 8990 (2019). https://doi.org/10.1038/s41598-019-45525-0

[6] Fardet, T. et al. Vennemo, Stine Brekke, Mitchell, Jessica, Mørk, Håkon, Graber, Steffen, Hahne, Jan, Spreizer, Sebastian, Deepu, Rajalekshmi, Trensch, Guido, Weidel, Philipp, Jordan, Jakob, Eppler, Jochen Martin, Terhorst, Dennis, Morrison, Abigail, Linssen, Charl, Antonietti, Alberto, Dai, Kael, Serenko, Alexey, Cai, Binghuang, ... Plesser, Hans Ekkehard. (2021). NEST 2.20.2 (2.20.2). Zenodo. https://doi.org/10.5281/zenodo.5242954

[7] Y. LeCun, L. Bottou, Y. Bengio, and P. Haffner. "Gradient-based learning applied to document recognition." Proceedings of the IEEE, 86(11):2278-2324, November 1998. [on-line version]

[8] H.R. Colten, B.M. Altevogt. "Sleep Disorders and Sleep Deprivation: An Unmet Public Health Problem" Institute of Medicine (US) Committee on Sleep Medicine and Research. Washington (DC): National Academies Press (US) (2006) 10.17226/11617

[9] González, J. et al. (2019) "Decreased electrocortical temporal complexity distinguishes sleep from wakefulness." *Scientific Reports* 9: 18457 https://doi.org/10.1038/s41598-019-54788-6

[10] Krishnan, G.P. et al. "Cellular and neurochemical basis of sleep stages in the thalamocortical network." eLife 2016;5:e18607 10.7554/eLife.18607

[11] B. O. Watson et al. "Network Homeostasis and State Dynamics of Neocortical Sleep." https://doi.org/10.1016/j.neuron.2016.03.036

[12] Giulio Tononi, Chiara Cirelli. Sleep and the Price of Plasticity: From Synaptic and Cellular Homeostasis to Memory Consolidation and Integration. Neuron, 2014; 81 (1): 12 DOI: 10.1016/j.neuron.2013.12.025

GRL MF: Mean field model of the cerebellar granular layer

Roberta M. Lorenzi[1]*, Alice Geminiani[1], Claudia A.M. Gandini Wheeler-Kingshott[1,2,3], Fulvia Palesi[1], Claudia Casellato[1], Egidio D'Angelo[1,3]

[1]Department of Brain and Behavioural Sciences, University of Pavia, Pavia, Italy
[2]Department of Neuroinflammation, Queen Square MS Centre, UCL Institute of Neurology, London, United Kingdom
[3]Brain Connectivity Center IRCCS Mondino Foundation, Pavia, Italy
**robertamaria.lorenzi01@universitadipavia.it*

INTRODUCTION

Simulation of the brain activity is a stimulating challenge that is addressed at different scales. Models of brain function are currently being developed, including both at micro and macroscale, to increase regional fidelity and to lead to more accurate whole-brain dynamics. Mean Field(MF) is a widespread formalism that provides a computational advantageous representation of the neuronal population dynamics, oversimplifying the physiological properties of an entire neuronal circuit through ad-hoc transfer functions(Boustani and Destexhe,2009; Zerlaut et al.,2016, 2018). The MF models developed so far are tailored to the cerebral cortex but may not be effective to capture other brain regional dynamics, e.g. the cerebellar cortex, due to their specific structural organization. Here, we aim to develop an advanced MF model of the cerebellar circuit considering its complex neuronal features, multi-layer organization, local connectivity deriving from the quasi-crystalline geometry(D'Angelo et al.,2016). Specifically, we present a MF model of the granular layer(GRL MF), the cerebellar input stage, retaining the salient properties of its neuronal populations, Golgi cells(GoC) and Granule cells(GrC). Our model will be used to provide theoretical insight on the cerebellar input stage and represents the promising first brick for the development of a whole-cerebellar advanced MF model.

METHODS

The design of the GRL MF model started from an accurate and extensive knowledge of the GrC and GoC structural and functional properties within the cerebellar microcircuit. Population-specific Transfer Functions(TF) allow translating spiking patterns into time-continuous global outputs. A semi-analytical TF fitting was inspired to that already validated for the implementation of MF models of isocortical circuits made of excitatory and inhibitory neurons (Carlu et al.,2020). We expanded this framework introducing topological parameters that modelled the biological properties of GrCs and GoCs so enabling a physiological interpretation of the network output. The granular layer detailed reconstruction(placement and connectivity), generated by a scaffold model approach, was used to set realistic probability for each connection type(K). Quantal synaptic conductance and synaptic time decays(Q,τ) are set relying on detailed synaptic model (Casali et al.,2019; De Schepper et al.,2021) The reference functional target was the neuronal spiking activity that emerged in network simulations(in-vivo conditions) using E-GLIF single-point neurons optimized for each population (Geminiani et al., 2018, 2019). The population frequencies were extracted from simulation results using the Brain Scaffold Builder framework (De Schepper et al.,2021) interfacing with the NEST simulator.

TF equations were adapted to model the alpha synapses consistently with the E-GLIF models in the network.

The GoC TF was computed maintaining the excitatory contribution from mossy fibres and GrC separately, enabling it to investigate the specific contribution of the two excitatory synapses to the granular layer dynamics. Furthermore, for each population we defined the eligible frequency ranges combinations of its presynaptic populations, to fit the TF on the plausible granular layer working frequencies. The GRL MF model equations were written with population inter-dependent transfer functions, and the model prediction was tested for different driving inputs coming from mossy fibres(ν_{drive}). The MF time constant(T) was fixed to 20ms(Di Volo et al.,2019).

RESULTS AND DISCUSSION

The MF formalism proposed here for the first time is a bottom-up approach tailored on the biological properties of the granular layer of the

cerebellar cortex. We exploit all the advantages of the MF versatile formalism, which provides an established pipeline to reduce spiking networks activity to realistic average models of neuronal population dynamics.

In the fitting procedures to define the GrC and GoC TFs, we included fine-tuned parameters to maintain a strong physiological reference. The numerical templates(2D for GrC population and 3D for GoC population) and the output of the fitting(analytical TFs) are reported in Figure 1.

First order GRL MF model equations are reported in Figure 2–Panel A, with the granular layer network included in the context of the cerebellar cortex. GrC and GoC dynamics were simulated with the GRL MF based on the nested TFs. We reported the output for two different input patterns (Panel B and C), which correspond to in-vivo recordings of the Granular Layer response to different sensorial stimuli (Svensson et al.,1997).

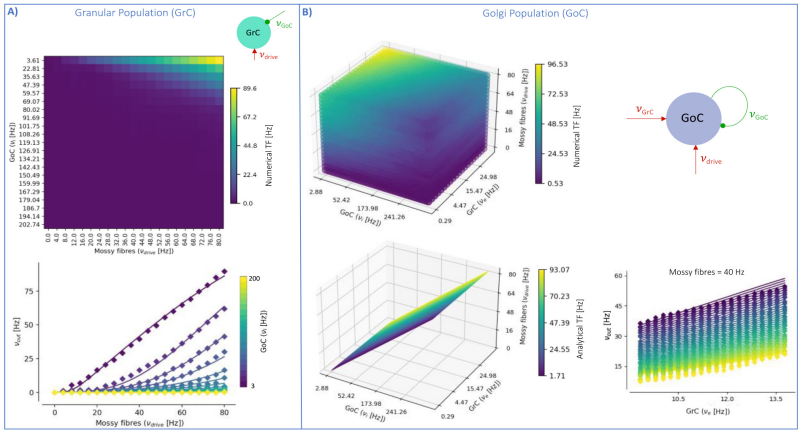

FIGURE 1: TF Fitting Procedure: from the numerical template to the analytical expression. Panel A refers to the GrC population, with its 2 synaptic inputs; the upper part shows the numerical template used as input for the fitting of the TF analytical expression; fitting outcomes(lines) against numerical template(dots) are reported at the bottom. Panel B refers to the GoC population, with its 3 synaptic inputs; the upper part shows the numerical template(left) and connections(right). Numerical values used for the fitting are extracted from the actual interdependent working frequencies(ν_{drive}, ν_{I}, and ν_{E}) come out with BSB-NEST simulations(bottom left). On the right, the result of the fitting(lines) compared with the numerical template(dots) is reported for mossy input=40Hz.

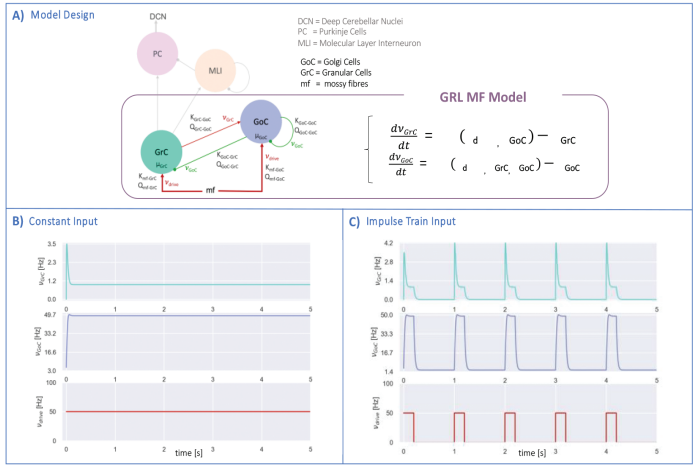

FIGURE 2: GRL MF network design and model prediction. Panel A shows the cerebellar cortex network where K_c and Q_c are the mean convergence and the quantal synaptic conductance for the connection c, and ν_p is the output firing rate of the population p. Granular layer design and corresponding MF equations with nested TFs are reported in the purple box, with T=20ms. Panel B and C report the GrC and GoC activities predicted by the GRL MF model for a constant input at mossy fibres of 50Hz and an impulse train at mossy fibres(amplitude=50Hz, length=200ms). Simulations last 5s.

Currently, we are comparing the GRL MF output with the Local Field Potential(LFP) recorded with extracellular electrophysiological experiments(HD-MEA) to validate the population activities generated by the GRL MF with biological recordings on the same spatial scale. Once the GRL MF validation is completed, we will move up to the Molecular Layer to extend our formalism to all the cerebellar neuronal populations. Then we will expand our formalism to the second order to include covariance terms. Finally, this cerebellar-specific MF will be integrated in a whole-brain framework, The Virtual Brain(TVB), to investigate the impact of complex cerebellar responses into whole-brain dynamics. Indeed, the cerebellar impact on whole-brain activity simulated with TVB has been preliminarily demonstrated (Sanz-Leon et al.,2013; Palesi et al.,2020) by including specific cerebellar nodes.

ACKNOWLEDGEMENTS

We thank Robin De Schepper for useful discussions about the Brain Scaffold Builder framework (De Schepper et al., 2021)) https://github.com/dbbs-lab/bsb.

Keywords: cerebellum, granular layer, modelling, mean field, transfer function

REFERENCES

[1] Boustani, S. El, and Destexhe, A. (2009). A master equation formalism for macroscopic modeling of asynchronous irregular activity states. *Neural Comput.* 21, 46–100. doi:10.1162/neco.2009.02-08-710.

[2] Carlu, M., Chehab, O., Dalla Porta, X. L., Depannemaecker, D., Héricé, X. C., Jedynak, M., et al. (2020). A mean-field approach to the dynamics of networks of complex neurons, from nonlinear Integrate-and-Fire to Hodgkin-Huxley models. *J. Neurophysiol.* 123, 1042–1051. doi:10.1152/JN.00399.2019.

[3] Casali, S., Marenzi, E., Medini, C., Casellato, C., and D'Angelo, E. (2019). Reconstruction and simulation of a scaffold model of the cerebellar network. *Front. Neuroinform.* 13, 1–19. doi:10.3389/fninf.2019.00037.

[4] D'Angelo, E., Antonietti, A., Casali, S., Casellato, C., Garrido, J. A., Luque, N. R., et al. (2016). Modeling the cerebellar microcircuit: New strategies for a long-standing issue. *Front. Cell. Neurosci.* 10, 1–29. doi:10.3389/fncel.2016.00176.

[5] De Schepper, R., Geminiani, A., Masoli, S., Rizza, M. F., Antonietti, A., Casellato, C., et al. (2021). Scaffold modelling captures the structure-function-dynamics relationship in brain microcircuits. *bioRxiv*, 2021.07.30.454314. doi:https://doi.org/10.1101/2021.07.30.454314.

[6] Di Volo, M., Romagnoni, A., Capone, C., and Destexhe, A. (2019). Biologically Realistic Mean-Field Models of Conductance-Based Networks of Spiking Neurons with Adaptation. *Neural* 31, 653–680. doi:10.1162/neco_a_01173.

[7] Geminiani, A., Casellato, C., D'Angelo, E., and Pedrocchi, A. (2019). Complex Electroresponsive Dynamics in Olivocerebellar Neurons Represented With Extended-Generalized Leaky Integrate and Fire Models. *Front. Comput. Neurosci.* 13, 1–12. doi:10.3389/fncom.2019.00035.

[8] Geminiani, A., Casellato, C., Locatelli, F., Prestori, F., Pedrocchi, A., and D'Angelo, E. (2018). Complex dynamics in simplified neuronal models: Reproducing golgi cell electroresponsiveness. *Front. Neuroinform.* 12, 1–19. doi:10.3389/fninf.2018.00088.

[9] Palesi, F., Lorenzi, R. M., Casellato, C., Ritter, P., Jirsa, V., Gandini Wheeler-Kingshott, C. A. M., et al. (2020). The Importance of Cerebellar Connectivity on Simulated Brain Dynamics. *Front. Cell. Neurosci.* 14, 1–11. doi:10.3389/fncel.2020.00240.

[10] Sanz Leon, P., Knock, S. A., Woodman, M. M., Domide, L., Mersmann, J., Mcintosh, A. R., et al. (2013). The virtual brain: A simulator of primate brain network dynamics. *Front. Neuroinform.* 7. doi:10.3389/fninf.2013.00010.

[11] Svensson, P., Ivarsson, M., and Hesslow, G. (1997). Effect of varying the intensity and train frequency of forelimb and cerebellar mossy fiber conditioned stimuli on the latency of conditioned eye- blink responses in decerebrate ferrets. *Learn. Mem.* 4, 105–115. doi:10.1101/lm.4.1.105.

[12] Zerlaut, Y., Chemla, S., Chavane, F., and Destexhe, A. (2018). Modeling mesoscopic cortical dynamics using a mean-field model of conductance-based networks of adaptive exponential integrate-and-fire neurons. *J. Comput. Neurosci.* 44, 45–61. doi:10.1007/s10827-017-0668-2.

[13] Zerlaut, Y., Teleńczuk, B., Deleuze, C., Bal, T., Ouanounou, G., and Destexhe, A. (2016). Heterogeneous firing rate response of mouse layer V pyramidal neurons in the fluctuation-driven regime. *J. Physiol.* 594, 3791–3808. doi:10.1113/JP272317.

Modelling the dynamic behaviour of the *C. elegans* nervous system with machine learning techniques

Ruxandra Barbulescu[1]*, Gonçalo Mestre[1,2]*, Arlindo L. Oliveira[1,2], L. Miguel Silveira[1,2]

[1]INESC-ID, Universidade de Lisboa, Lisboa, Portugal
[2]IST Técnico Lisboa, Universidade de Lisboa, Lisboa, Portugal
**ruxi@inesc-id.pt, goncalo.mestre@tecnico.ulisboa.pt*

INTRODUCTION / MOTIVATION

The study of the human brain is probably one of the greatest challenges in the field of neuroscience due to the inner complexity of the human nervous system. While ongoing developments in experimental neuroscience are increasing the availability of novel recordings and reconstructions, innovative modelling methods and flexible simulation environments are being developed to capture their complex behaviour. Moreover, studying smaller and simpler organisms, such as the nematode Caenorhabditis Elegans (*C. elegans*), is useful in bringing insight into the dynamics of more complex neuronal structures. *C. elegans* is a nematode (roundworm) of about 1 mm in length with a small nervous system consisting of less than 1000 cells across all sexes and around 15000 connections [1, 2]. Due to its relative simplicity, the nervous system of *C. elegans* is almost completely described, generating detailed connectomes of geometrically distributed neurons and synapses. These detailed descriptions may lead to complicated models, implying more computationally demanding, potentially intractable simulations of the dynamic behaviour. This increased complexity is a side effect of the detailed modelling of the internal structure whereas often one is only interested in the peripheral input-output behaviour.

METHODS

We propose a methodology for generating completely data-driven black-box models of the neuronal behaviour of organisms using only peripheral information of the system. We start from synthetic data, extracted from a high-fidelity model of *C. elegans*, which comprises the complete connectome

of the adult hermaphrodite, with 302 multi-compartmental neurons and 6702 synapses. We simulate two behavioural scenarios in the NEURON simulator [3], the Forward Crawling Motion (FCM) and the Nictation (NIC), with scenario-specific neurons stimulated according to the behaviour being replicated. In the FCM scenario four specific neurons are stimulated and the output is observed in sixteen neurons known to show a strong response in this behaviour. The Nictation behaviour, when the worm stands on its tail and waves its head in three dimensions, is reproduced by stimulating six different neurons and evaluating the response of twelve motor neurons associated with head muscles. Each scenario simulated produces a dataset with the input currents used for stimulation and the voltage variations in time of the output neurons. By using different signals for the input currents, we are able to generate 40 diverse examples for each dataset. We further create completely equation-free data-driven models assuming no prior knowledge of the original system's structure and equations, using sequential neural networks trained on this data. For each scenario, we use 20 examples to train the neural networks models, 10 for validation and 10 for testing.

The models are generated using Recurrent Neural Networks (RNNs), first proposed in their simplest form in the 1980s to model sequential data [4, 5, 6]. Later, maintaining the same structure of the network, to better model long term dependencies, the Long Short-Term Memory (LSTM) unit was introduced [7, 8], with three gates used to remember past data and filter input and output information. In 2014 the Gated Recurrent Unit (GRU), consisting only of two gates with the same functions, was suggested to reduce the complexity of the LSTM unit [9]. These three different architectures are commonly used to model sequential data in tasks such as predicting energy demands, process monitoring or even machine translation.

RESULTS AND DISCUSSION

The three different flavours of Recurrent Neural Networks were trained on each of the two datasets, then tested and compared in terms of their properties and ability to model the *C. elegans* system response to diverse stimuli. The LSTM and GRU units proved able to accurately reproduce the system's response in both scenarios, producing significantly superior results when compared to the simple RNN unit. In Figure 1 we show the Root Mean Square Error (RMSE) over the number of epochs for the FCM scenario, computed in

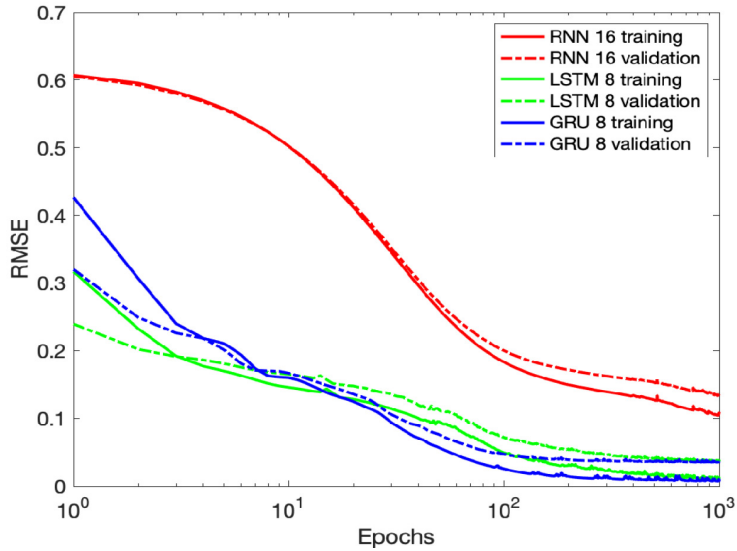

FIGURE 1: Average training and validation RMSE out of ten simulations, with recurrent layers of size 16 (RNN) and 8 (LSTM and GRU).

the interest of fairness for the RNN with 16 units in the recurrent layer (404 parameters) and LSTM and GRU with 8 units in the recurrent layer (452 and 348 parameters). Examples of the predicted output voltage of the LSTM and GRU units on previously unseen data even with a modest recurrent layer of 8 neurons are shown in Figure 2. The examples shown are selected randomly from the test set, the prediction behaves quite similarly for the rest. Due to its simplicity, the GRU is preferable and was able to reproduce the original model's responses with an acceptable RMSE even with a hidden size as small as 4 units.

The LSTM and GRU units were further trained to produce a single model using both datasets, each unit generating a model able to predict the system's response on both the FCM and the NIC behaviours with low RMSE. These models were tested for previously unseen data, proving able to produce promising results with a small recurrent layer of eight neurons (as already done for each of the behaviours individually). The results show that it is

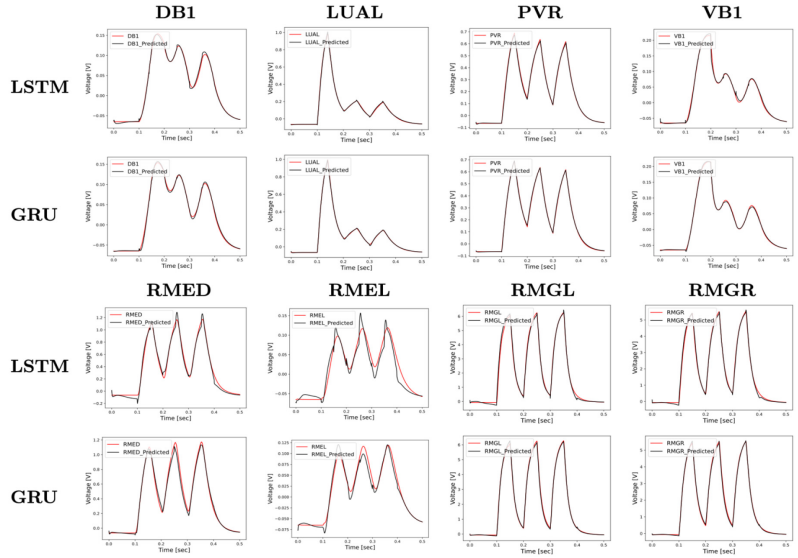

FIGURE 2: Real and predicted output voltages corresponding to 4 selected neurons (columns) and 2 examples selected randomly from the test set (top two and bottom two lines), for each dataset. The red lines show the real time series and the black lines the voltage predicted with LSTM and GRU. Each column corresponds to one neuron: DB1, LUAL, PVR and VB1 for the FCM scenario and RMED, RMEL, RMGL and RMGR for the NIC behaviour.

feasible to develop Recurrent Neural Network models able to infer input-output behaviours of real biological systems, even in the absence of a detailed level of connectivity.

ACKNOWLEDGEMENTS

This work was partially supported by Portuguese national funds through FCT, Fundação para a Ciência e a Tecnologia, under project UIDB/50021/2020 as well as project PTDC/EEI-EEE/31140/2017.

Keywords: data-driven models, RNNs, LSTMs, GRUs, *C. elegans*, time series regression, black-box

REFERENCES

[1] S. J. Cook, T. A. Jarrell, C. A. Brittin, Y. Wang, A. E. Bloniarz, M. A. Yakovlev, K. C. Nguyen, L. T.-H. Tang, E. A. Bayer, J. S. Duerr et al., "Whole-animal connectomes of both Caenorhabditis elegans sexes," Nature, vol. 571, no. 7763, pp. 63–71, 2019.

[2] C. A. Brittin, S. J. Cook, D. H. Hall, S. W. Emmons, and N. Cohen, "Beyond the connectome: A map of a brain architecture derived from whole-brain volumetric reconstructions," bioRxiv, 2020.

[3] N. T. Carnevale and M. L. Hines, The NEURON book, Cambridge University Press, 2006

[4] D. E. Rumelhart, G. E. Hinton, and R. J. Williams, "Learning representations by back-propagating errors," Nature, vol. 323, pp. 533–536, 1986.

[5] P. J. Werbos, "Generalization of backpropagation with application to a recurrent gas market model," Neural Networks, vol. 1, no. 4, pp. 339–356, 1988. [Online]. Available: https://www.sciencedirect.com/science/article/pii/089360808890007X

[6] J. L. Elman, "Finding structure in time," Cognitive Science, vol. 14, no. 2, pp. 179–211, 1990. [Online]. Available: https://onlinelibrary.wiley.com/doi/abs/10.1207/s15516709cog1402_1

[7] S. Hochreiter and J. Schmidhuber, "Long Short-Term Memory," Neural Computation, vol. 9, no. 8, pp. 1735–1780, 11 1997. [Online]. Available: https://doi.org/10.1162/neco.1997.9.8.1735

[8] F. Gers, J. Schmidhuber, and F. Cummins, "Learning to forget: continual prediction with lstm," in 1999 Ninth International Conference on Artificial Neural Networks ICANN 99. (Conf. Publ. No. 470), vol. 2, 1999, pp. 850–855 vol.2.

[9] K. Cho, B. van Merrienboer, Ç. Gülçehre, F. Bougares, H. Schwenk, and Y. Bengio, "Learning phrase representations using RNN encoder-decoder for statistical machine translation," CoRR, vol. abs/1406.1078, 2014. [Online]. Available: http://arxiv.org/abs/1406.1078

Traveling waves in the resting state are initiated by the connectome

Panfilova, E.A.[1]*, Burlakov E.O.[2], Verkhlyutov, V.M.[3]*

[1]Faculty of Biomedicine, Pirogov Russian National Research Medical University, Moscow, Russia
[2]Laboratory of Mathematical Methods of Research of Optimum Operated Systems, V. A. Trapeznikov Institute of Control Sciences of RAS, Moscow, Russia
[3]Human Higher Nervous Activity Lab, Institute of Higher Nervous Activity and Neurophysiology of RAS, Moscow, Russia
**likzola@gmail.com; verkhliutov@mail.ru*

INTRODUCTION/MOTIVATION

There are two points of view on the large-scale spatial dynamics of spontaneous and evoked EEG and MEG activity. The intra-cortical hypothesis assumes the propagation of traveling waves [1] in the cortex on a meso-scale due to intra-cortical axons (velocity < 1.0 m/s, 0.2 m/s characteristic speed). This propagation results in rotating electric dipoles that are projected onto the scalp, giving rise to the large-scale wave dynamics. The other point of view (namely, cortico-cortical hypothesis) assumes the propagation of large-scale waves due to cortico-cortical axons (velocity > 1.0 m/s, 6 m/s characteristic speed) [2]. The latter wave speed is observed in EEG, MEG and ECoG, but is not confirmed by direct recording (using intracortical microelectrodes or Utah arrays). Previously, we tested the validity of the above two approaches and showed a significantly higher-level correlation of the MEG experimental data by the results obtained using the meso-scale model [3]. However, a close look at the meso-scale model showed that the initiation of traveling waves could be related to the structure of the connectome.

METHODS

For the MEG analysis, we used one healthy right-handed subject. The registration was carried out with a 306-channel MEG. The MEG recording had been carrying out for 9 minutes in the state of quiet wakefulness with closed eyes. A high-resolution structural MRI of the head was obtained using 3T tomograph. Based on the MRI data, a model of individual surfaces of the head and brain with the resolution of about 300 000 vertices was built. Each vertex was assigned to be an epicenter, for which the distributions of the current density in the form of radial traveling waves with propagation velocities of 0.2 m/s

(distances of 2 cm) and an average frequency of 11 Hz were calculated. We used radial traveling waves for simulation, since they are typically observed in recordings by microelectrodes and by optical methods in animals [1], and also by the Utah multielectrode arrays in humans [5]. The forward MEG problem was solved using the BEM separately for each hemisphere in the Brainstorm software environment. The model MEGs were compared with the experimental data by calculating two-dimensional correlation each time shifting the analysis window by 2 ms. The technique is described in detail in our previous works [4].

RESULTS

As an example, we demonstrate a reconstructed traveling wave of the alpha rhythm with an epicenter located in the central part of the retinotopic projection at $r>0.7$, $p<0.001$ the border of fields V1 and V2 (highlighted in purple and green, respectively) at rest with the eyes closed (Fig. 1A, B). Analysis of the 9-minute of MEG segment made it possible to identify a multitude of epicenters of such waves in the calcarine and parieto-occipital sulci (in the primary and secondary fields of the visual cortex). The epicenters were located chaotically, but strictly in the fields V1 and V2 of the cortex at $r> 0.8$, $p <0.005$ (Fig. 1C).

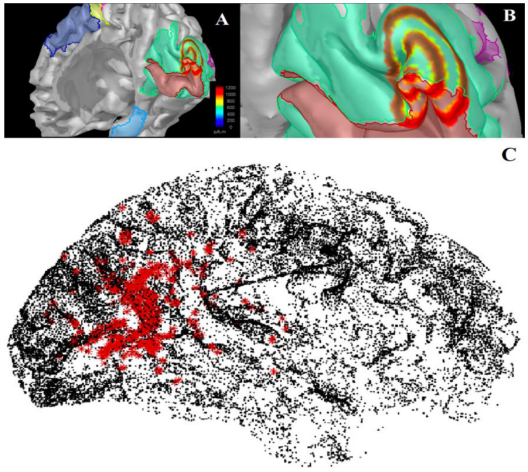

FIGURE 1: Single traveling wave of alpha rhythm in the right hemisphere. The red color codes the local field potentials-LFP (**A**). An enlarged view of the occipital lobe, the radial wave is distorted by the complex surface of the hemisphere (**B**). Spatial distribution of the epicenters of traveling waves (red stars) prevailing in the left hemisphere during 9 min of the MEG recording (**C**).

CONCLUSION

Our previous study comparing two traveling wave models showed an unexpected effect of jumps in the epicenters of the traveling wave [3]. These results are in good agreement with the data on the dynamics of traveling waves in the human brain [5]. Alpha waves are specific to the visual cortex, and we previously considered their epicenters to be relatively stable [6]. The new result shows that, like saccades, when viewing images, there are changes in the position of the traveling waves epicenters in the visual cortex. The scale of traveling waves propagation we confirmed is comparable to the spatial dimension of the resting state networks, and we can assume the role of traveling waves in the local synchronization of such networks. Macroscale traveling waves are explained by the spatial dynamics of mesoscale cortical waves due to intracortical interactions. In turn, the role of connections between the visual cortex and the thalamus, which are part of the connectome, in the emergence of the alpha rhythm is well known [7]. In addition, these waves can be originated by cortico-cortical connections that are elements of the connectome. Thus, we assume that cortical traveling waves of the alpha rhythm are initiated by the connectome [8] and, of course, should be considered as one of the important elements of large-scale brain models.

ACKNOWLEDGEMENTS

We would like to thank the management and staff of the Moscow MEG Center for the opportunity for registration.

The reported study was funded by RFBR, project number 20-015-00475.

Keywords: cortex traveling wave, connectome, intra-cortical hypothesis, MEG

REFERENCES

[1] Muller, et al. Cortical travelling waves: mechanisms and computational principles (2018) https://doi.org/10.1038/nrn.2018.20

[2] Hindriks, et al. Intra-cortical propagation of EEG alpha oscillations (2014) https://doi.org/10.1016/j.neuroimage.2014.08.027

[3] Verkhlyutov, et al. Comparison of Simulated Macro- and Mesoscopic Cortical Traveling Waves with MEG Data (2021) https://doi.org/10.1007/978-3-030-71637-0_81

[4] Verkhlyutov, et al. Towards localization of radial traveling waves in the evoked and spontaneous MEG: A solution based on the intra-cortical propagation hypothesis (2018) https://doi.org/10.1016/j.procs.2018.11.073

[5] Martinet, et al. Human seizures couple across spatial scales through travelling wave dynamics (2017) https://doi.org/10.1038/ncomms14896

[6] Verkhlyutov, A model of the dipole structure of the alpha rhythm source in the human visual cortex (1996) https://ihna.ru/files/member/verkhlyutov/art/1996ModelAlphaRhithm.pdf

[7] Halgren, et al. The generation and propagation of the human alpha rhythm (2019) https://doi.org/10.1073/pnas.1913092116

[8] Breakspear, Dynamic models of large-scale brain activity (2017) https://doi.org/10.1038/nn.4497

Role of excitatory-inhibitory homeostasis in the recovery of functional network properties after focal lesion: A computational account

Francisco P. dos Santos[1,2,3]*, Sonia Hassissene[4], Paul F.M.J. Verschure[2,5]

[1]Eodyne Systems SL, Barcelona, Spain
[2]Laboratory of Synthetic, Perceptive, Emotive and Cognitive Systems (SPECS), Institute for Bioengineering of Catalonia (IBEC), Barcelona, Spain
[3]Department of Information and Communication Technologies, Universitat Pompeu Fabra (UPF), Barcelona, Spain
[4]Polytech Marseille, Université d'Aix-Marseille, Marseille, France
[5]Catalan Institution for Research and Advanced Studies (ICREA), Barcelona, Spain
**f.pascoadossantos@gmail.com*

INTRODUCTION/MOTIVATION

In stroke, localized lesions lead to an acute loss of excitation to distant cortical regions and to significant disruptions in functional connectivity (FC), spreading beyond lesion vicinity, a phenomenon known as diaschisis [1]. During recovery, FC network properties are often recovered to nearly healthy levels through functional reorganization [2], [3]. However, it is not clear how the brain orchestrates this process globally, given the localized nature of lesions. Further, the process of recovery is accompanied by widespread changes in excitability [4], [5] that closely resemble synaptic scaling [6]. Therefore, we propose that local excitatory-inhibitory (EI) homeostasis, occurring through synaptic scaling, may play an essential role in the recovery of global network properties of stroke patients. We aim to understand how to tie the local and global scales in stroke recovery, essential for improving the prediction of future deficits and informing targeted rehabilitation techniques that maximize the potential of recovery.

METHODS

To model large-scale cortical activity, we used a network of nodes constrained by human structural connectivity data, simulating the activity of individual regions with Wilson-Cowan coupled EI populations (Fig. 1A). Homeostatic

plasticity was implemented through a plasticity rule that adjusts the weight of local inhibitory connections according to presynaptic activity and the deviation of postsynaptic activity from a target, as in synaptic scaling (Fig. 1B). Lesions were simulated by removing all the connections to and from a single node and model activity was extracted pre-lesion (T0), post-lesion (T1) and post-lesion after stabilization of inhibitory weights (T2) (Fig. 1C). Lesion effects were measured through changes in FC graph properties representing

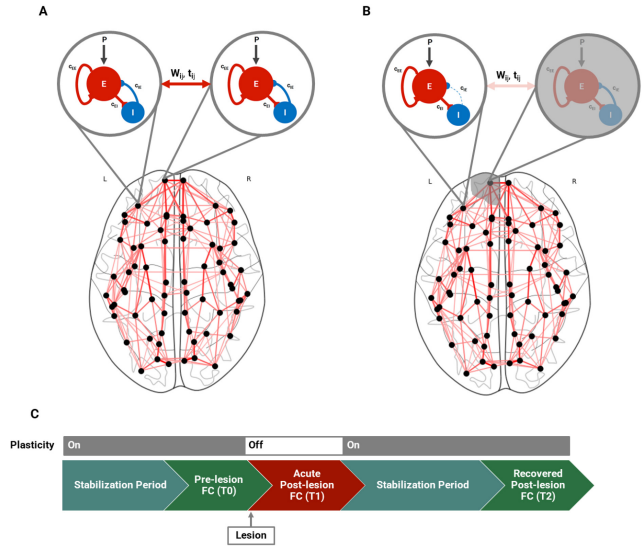

FIGURE 1: Modeling approach and simulation protocol. (**A**) Schematic of model for healthy brain. Cortical regions are represented by nodes in a network, where the weights and delays of connections are informed by human diffusion tensor imaging. Individual nodes consist of coupled excitatory and inhibitory neural masses, receiving excitatory input from other nodes in the network and an intrinsic input P. (**B**) Schematic of lesioned brain. After removal of one node in the network, simulating a lesion in the cortical gray matter, areas previously connected to it experience a loss in excitation. In response, homeostatic plasticity decreases the strength of local inhibition (dashed blue line from I to E) in order to bring the firing rate of E to a target value. (**C**) Diagram of simulation protocol. Networks are initialized and simulations are run until the local inhibitory weights, subject to plasticity, stabilize and 120s of activity were extracted to compute pre-lesion FC. After lesion application, plasticity is turned off and acute post-lesion FC is extracted, after which plasticity is turned back on, until the local inhibition is stabilized again and the network adapts to the lesion, when 120s of activity are extracted to represented recovered post-lesion FC.

segregation (average clustering coefficient, CC) and integration (global efficiency, GE), and FC distance (FCD). Changes in excitability were quantified by differences in local inhibitory-to-excitatory weights between T1/T2 and T0, representing changes in GABAergic transmission.

RESULTS AND DISCUSSION

As in previous literature [2], [3], results showed increased CC (0.162 ± 0.041, $p < 0.001$) and decreased GE (-0.068 ± 0.067, $p < 0.001$) at T1, indicating more segregation and less integration between cortical areas. Both metrics were globally recovered towards baseline levels at T2 ($p < 0.001$ for both) through the action of local EI homeostatic mechanisms (Fig. 2A,B). Furthermore, while FCD at T1 was strongly dependent on the strength of the lesion node ($\rho = 0.85$), correlations at T2 were weaker ($\rho = 0.33$), indicating a lesser dependence of recovery on the properties of lesioned areas, being more reliant on the ability of the brain to restore balance, indicating an important role of EI homeostasis in stroke recovery. The connectivity within and between resting-state networks was also evaluated at T2, showing a complex pattern of widespread reorganization (e.g. decreased internal connectivity in default mode network). Furthermore, changes in excitability in individual regions could be moderately predicted from structural connectivity of said regions with lesioned nodes ($\rho = 0.47$) and, similarly to previous research [5], the magnitude of changes decreased with distance from the lesion in individual simulations (Fig. 2D). Looking at variations in excitability across simulations (Fig. 2C)., we observed significant widespread increases (56 regions out of 68), fitting results from rodent models [5] and human patients [4]. Surprisingly, a tendency to experience decreases in excitability in particular cortical areas, mainly the superior frontal gyrus, temporal pole and cuneus, could be responsible for the increased propensity of patients to develop late-onset symptoms (e.g. depression) [7], previously linked to decreased excitability in the same regions.

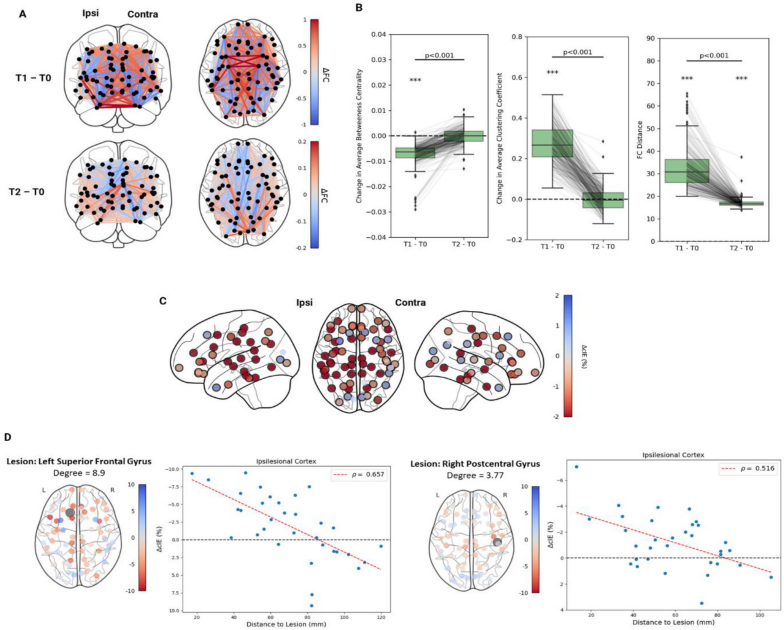

FIGURE 2: Changes in connectivity and excitability post-lesion and after recovery. (**A**) Visualization of changes in FC, from baseline, averaged over lesions for T1 and T2. **(B**) Changes in graph properties of functional connectivity at T1 and T2. Betweenness centrality was significantly reduced at T1 (T1 vs T0, p<0.001), being recovered towards baseline levels at T2 (T1 vs T2, p<0.001). A similar process occurred for clustering coefficients, although with an increase at T1 (T1 vs T0, p<0.001; T2 vs T1, p<0.001). Although the difference between T2 and baseline is still significant (T2 vs T0, p<0.001), there was a significant recovery when compared to T1 (T1 vs T2, p<0.001). (**C**) Variation in local excitability at T2, quantified by changes in the strength of local inhibition, averaged over lesions. Dark contours represent significant changes (p<0.05). (**D**) Examples of correlation between variation in excitability and distance for individual simulations of lesions in high and low degree nodes. Note that, for both lesions, the change in local inhibitory weights is positively correlated with distance, such that nodes closer to the lesion have greater decreases in inhibition, and thus greater increases in excitability. In all figures, ipsi and contra represent the ipsilesional and contralesional sides.

Keywords: stroke, functional connectivity, cortical reorganization, diaschisis, excitatory-inhibitory balance, homeostatic plasticity, large-scale modeling

REFERENCES

[1] E. Carrera and G. Tononi, "Diaschisis: past, present, future," *Brain*, vol. 137, no. 9, pp. 2408–2422, Sep. 2014, doi: 10.1093/brain/awu101.

[2] G. R. Philips, J. J. Daly, and J. C. Príncipe, "Topographical measures of functional connectivity as biomarkers for post-stroke motor recovery," *J. NeuroEngineering Rehabil.*, vol. 14, no. 1, p. 67, Jul. 2017, doi: 10.1186/s12984-017-0277-3.

[3] J. S. Siegel *et al.*, "Re-emergence of modular brain networks in stroke recovery," *Cortex*, vol. 101, pp. 44–59, Apr. 2018, doi: 10.1016/j.cortex.2017.12.019.

[4] Y. K. Kim, E. J. Yang, K. Cho, J. Y. Lim, and N.-J. Paik, "Functional Recovery After Ischemic Stroke Is Associated With Reduced GABAergic Inhibition in the Cerebral Cortex: A GABA PET Study," *Neurorehabil. Neural Repair*, vol. 28, no. 6, pp. 576–583, Jul. 2014, doi: 10.1177/1545968313520411.

[5] T. Neumann-Haefelin and O. W. Witte, "Periinfarct and Remote Excitability Changes after Transient Middle Cerebral Artery Occlusion," *J. Cereb. Blood Flow Metab.*, vol. 20, no. 1, pp. 45–52, Jan. 2000, doi: 10.1097/00004647-200001000-00008.

[6] G. Turrigiano, "Too Many Cooks? Intrinsic and Synaptic Homeostatic Mechanisms in Cortical Circuit Refinement," *Annu. Rev. Neurosci.*, vol. 34, no. 1, pp. 89–103, Jul. 2011, doi: 10.1146/annurev-neuro-060909-153238.

[7] C. E. Page and L. Coutellier, "Prefrontal excitatory/inhibitory balance in stress and emotional disorders: Evidence for over-inhibition," *Neurosci. Biobehav. Rev.*, vol. 105, pp. 39–51, Oct. 2019, doi: 10.1016/j.neubiorev.2019.07.024.

Configuration aware neural path planning in the task space

Lea Steffen*, Philipp Augenstein, Stefan Ulbrich, Arne Rönnau, Rüdiger Dillmann

Interactive Diagnosis and Service Systems (IDS), Intelligent Systems and Production Engineering (ISPE), FZI Research Center for Information Technology, Karlsruhe, Germany
**steffen@fzi.de*

INTRODUCTION/MOTIVATION

Robots working in manufacturing must be adaptive, due to the dynamic manufacturing processes. They need to be able to spontaneously adapt to their environment and avoid obstacles online, which requires a fast and flexible planning algorithm, to enable Human-robot collaboration. However, the complexity for such a calculation increases significantly for high degree-of-freedom (DOF) robots. Inspired by the excellent sense of orientation of mammals, researchers [1], imitated the presumed virtual map made from so-called place cells in the hippocampus, using Spiking Neural Networks (SNNs). In [1] and [2] a neural Wavefront Algorithm (WFA), realizing path planning as a breadth-first search, is executed on a grid of place cells represented by an SNN. Due to learning via Spike Timing Dependent Plasticity (STDP), synapses on a path between target and start position are strengthened. The 2D approach for mobile robots introduced in [1] got expanded to 3D by [2] which both have shown to be executable in reasonable time. However, robotic path planning must not only deal with a single point, as which the TCP can be understood as the focus of a task, but all joints regarding collision avoidance and energy efficient paths must be considered primarily. The goal of this work is to design a collision-free path planner for industrial robot arms with 6 DOF. Due to the demanding time requirement of the required online planning, a SNN based path finding technique based on the mechanics of place cells is used. A planning that takes place exclusively in the configuration space of the robot is discarded to avoid the complexities of a high dimensional search space.

METHODS

To represent the 6D configuration space (C-space) of an industrial robot with 6 DOF two separate neural networks are created as visualized in Figure 1. The first represents the elbow of the robot and depicts a map in its 2D C-space, depending on the first two relevant robot joints. The second symbolizes the TCP's task space in 3D.

Hebbian learning, a common paradigm of synaptic plasticity, embodies two factors, the income of pre-synaptic and the creation of post-synaptic spikes. However, Hebbian learning merely makes a synapse receptive, a third factor is needed to transform synaptic plasticity into learning in form of weight change [3] The so called three-factor rule influences synaptic plasticity with a neuromodulator.

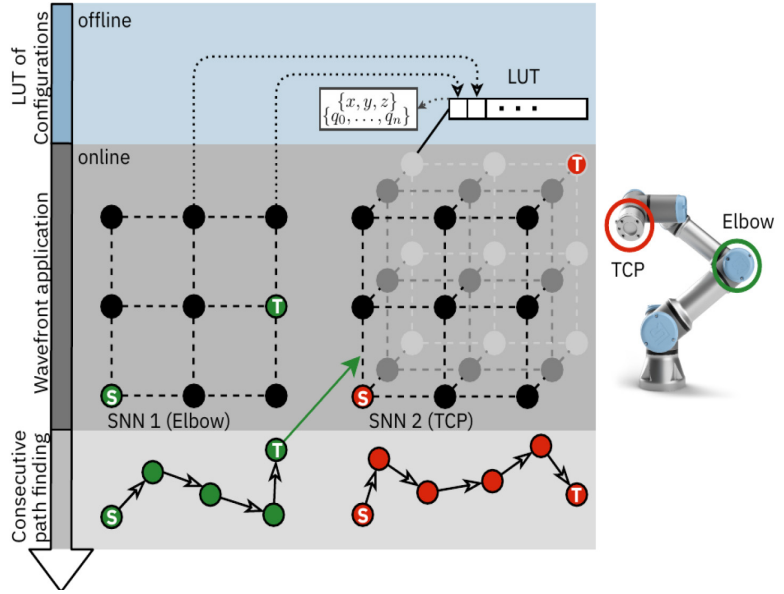

FIGURE 1: The elbow's SNN is a 2D C-space while the TCP moves in the 3D task space. The planner is divided into creating a LUT with all necessary information offline and secondly, applying the WFA with subsequent path finding online.

Path planning in a high dimensional C-space holds computationally intensive elements. First of all, the calculation of the inverse kinematic (IK) to get an appropriate configuration for a large number of positions. But also finding all reachable points in the complementary voxel grid is too complex to be done online while the robot is moving. Therefore, the approach is separated into two parts. The first part takes place purely offline and consists of the majority of all necessary complex computations, which are then stored in a LUT. Thereby the position in the Cartesian and the C-space as well as the weighted connections of all neurons in both networks are calculated and stored. During the actual online planning, it is then only necessary to plan between these known points. The LUT, represents the neuromodulator of the three-factor rule for our learning process. The planner's second stage, the WFA, is performed online after using the previously saved information to create the two SNNs that are simulated with Nengo [4].

During the online planning, firstly a WFA is initiated in SNN 1 (elbow). Subsequently, the synapses of the SNN2 (TCP) are adapted before a second WFA is applied within that network. The synaptic adaptations between the two consecutive neural WFA guarantee valid movement options later on. In Figure 2 it is visualized which network combinations generate unfeasible trajectories and are thus deleted. As the WFA alters the synaptic weights by STDP, for each node a synaptic vector can be calculated. These vectors are considered forces propelling an agent through the network.

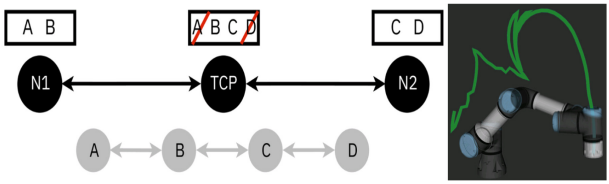

FIGURE 2: At the left, the central black circle represents the TCP's initial voxel. It can reach the elbow points A to D. As its neighbors (N1, N2) are only able to reach two of the four elbow voxel some connections are deleted. At the right, the green line shows the traversed points by the TCP in the 3D task space.

RESULTS AND DISCUSSION

The resulting robot motion is simulated using the MoveIt framework, with ROS2. For all experiments a simulated UR3 e-series robot shown in Figure 1 & 2 is used. It was shown that two WFA in two SNN can be applied for motion planning of a 6 DOF robot. The performance results of a separated analysis of the on- and offline parts show that creating a LUT in a time-uncritical environment was very helpful. The time required to calculate the IK and create and link the two networks takes hours, depending on the size of both networks which contradicts the requirements to be fast and flexible. However, this effort is only required once per robot and workspace and can then be used to significantly reduce the time required for the online calculation of a path.

Generally, the results, as visualized in Figure 2, show that collision-free paths cannot be guaranteed. The coverage of the 6D C-space in 3D is not sufficient, why some configurations do not exist in the networks. This results in planning tasks being traversed very extensively and also configurations with a large 6D distance for two points adjacent to each other in the Cartesian task space. To overcome this distance, linear interpolation is currently used. Nevertheless, there is great potential in splitting into two networks of manageable dimensions. Also precomputing and storing potential network connections in a LUT, can circumvent the problematics of 6D planning in general. As one weakness is the implementation of the link between the two SNNs, future work focusses on improving the C-space's mapping to the task space of the TCP. Finally, the SNN simulation will be applied on neuromorphic hardware.

ACKNOWLEDGEMENTS

The research leading to this paper received funding from the EuropeanUnion's Horizon 2020 Framework Program for Research and Innovation under the Specific Grant Agreement No. 945539 (HumanBrain Project SGA3).

Keywords: Neural Wavefront algorithm, robotic motion control, Synaptic plasticity, brain inspired controllers

REFERENCES

[1] F. Ponulak und J. . J. Hopfield, ¨Rapid, parallel path planning by propagating wavefronts of spiking neural activity," *Frontiers in Computational Neuroscience,* 2013.

[2] L. Steffen, R. Kübler da Silva, S. Ulbrich , J. C. Vasquez Tieck, A. Rönnau und R. Dillmann, "Networks of Place Cells for Representing 3D Environments and Path Planning," *BioRob,* 2020.

[3] W. Gerstner, M. Lehmann, V. Liakoni, D. Corneil und J. Brea, "Eligibility Traces and Plasticity on Behavioral Time Scales: Experimental Support of NeoHebbian Three-Factor Learning Rules," *Frontiers in Neural Circuits,* 2018.

[4] T. Bekolay, J. Bergstra, E. Hunsberger, T. DeWolf, T. C. Stewart, D. Rasmussen, X. Choo, A. R. Voelker und C. Eliasmith, "Nengo: a Python tool for building large-scale functional brain models," *Frontiers in Neuroinformatics,* 2014.

Solving robotic reaching tasks in the neurorobotics platform with reinforcement learning

Márton Szép, Leander Lauenburg, Kevin Farkas, Xiyan Su, Chuanlong Zang, Mahmoud Akl, Florian Walter, Josip Josifovski*, Alois Knoll

Department of Informatics, Chair of Robotics, Artificial Intelligence and Real-time Systems, Technical University of Munich, Munich, Germany
**marton.szep@tum.de; leander.lauenburg@tum.de; kevin.farkas@tum.de; tim.su@tum.de; chuanlong.zang@tum.de; mahmoud.akl@tum.de; florian.walter@tum.de; josip.josifovski@tum.de; alois.knoll@tum.de*

INTRODUCTION/MOTIVATION

Psychological theories and experiments on animal learning through conditioning and reward mechanisms have strongly influenced reinforcement learning (RL) for artificial agents [1]. By merging these psychological insights with neuroscience and robotics, RL enables new perspectives on multiple scientific fields. To facilitate this kind of interdisciplinary research, we tackle a robotic reaching task with RL using a 6-degrees-of-freedom HoLLiE robot arm [2] simulated in the Neurorobotics Platform (NRP) (Fig. 1) [3]. The goal of the reaching task is to find a valid motion trajectory for a robot's end effector to reach a predefined target position in 3D space by maximizing a reward function.

Our main contributions are a self-contained simulation-based RL environment in the NRP for rapid prototyping and scalable RL experiments using docker, and a comprehensive study comparing different state-of-the-art RL algorithms, using different state representations, network architectures, learning mechanisms and reward types, under different levels of difficulty of the reaching task. Both the environment and code are available online .

METHODS

The simulation environment is shown in Fig. 1. The agent completes the reaching task in an episode by moving the end effector, from its initial pose within a predefined proximity of the target position using a single movement, based on the ground truth (GT) target position or the image data. A camera

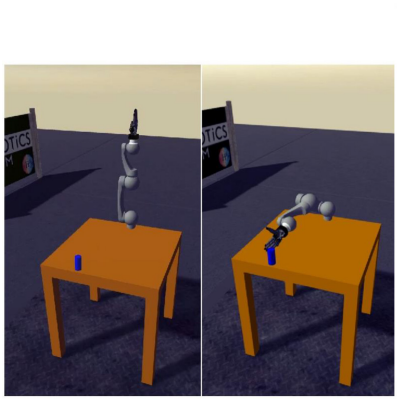

(a) Initial and final pose

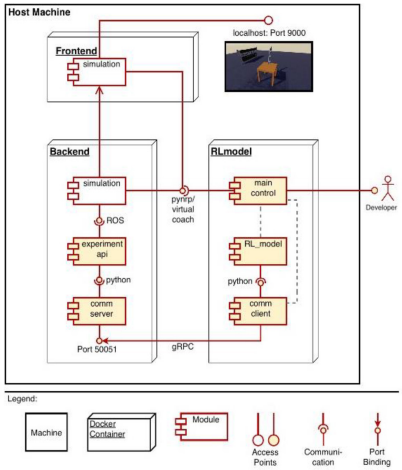

(b) Software Architecture

FIGURE 1: (**a**) Initial pose (left) and final pose (right) in a reaching episode. The blue cylinder represents the target (initialized randomly). (**b**) shows the core components of the designed setup. The 3d-boxes represent the docker containers of the NRP (frontend and a backend) and of the RL algorithms. The communication channel between the RL and NRP containers is based on gRPC [6].

looks down at the table from above when learning from image data. The agent's decisions are based on a state space vector which includes the end effector position, joint angles, and GT cylinder position or image information. Our experiments investigate sparse and dense reward functions and action space variations with three, four, or six active joints. The sparse reward function only rewards the task completion (overstepping a proximity threshold). The dense reward function encourages movements in the right direction. We compared two model-free, actor-critic architecture-based algorithms: Twin Delayed Deep Deterministic Policy Gradient (TD3) [4] and Soft Actor Critic (SAC) [5]. A video demonstration showing the setup and some of the experiment results is available .

When **learning from GT** data, the agent's task is to find an approximation for the inverse kinematics – which set of joint angles correspond to a given end effector location in the Cartesian space. We distinguished between models trained with TD3 and SAC, incorporation or exclusion of hindsight experience replay (HER) [7], dense or sparse reward functions, and the number of

actuated joints (Table 1). HER improves learning efficiency by reinterpreting unsuccessful experiences in achieving a particular goal into successful ones by adapting the goal to the result of the chosen action.

When **learning from images,** we can either extract the GT data, extract a latent space representation, or directly feed the images as input to the agents. The GT extraction benefits from reusing the previously trained models and reducing computational time since processing high-dimensional data is expensive. On the downside, such a pre-processing step is rigid and shows poor cross-domain generalization. To predict the position of the cylinder, we implemented a classical computer vision (CV) and a CNN-based approach. The former isolates the cylinder by subtracting an averaged image mask, applying a threshold, and transforming the extracted image coordinates to simulation coordinates. The latter uses a shallow model with two output logits that we pre-trained on CIFAR10 [8]. The latent space approach aims to derive a low-dimensional representation that encodes the most meaningful features of the image, including the cylinder position. However, the small variation in our data makes it difficult to train such a model, motivating the use of transfer learning in further work.

We trained all models using threshold scheduling as a curriculum learning approach. In this process, all models started with an initial threshold of 20 cm. The threshold was then progressively reduced whenever the model reached a specified performance level.

RESULTS AND DISCUSSION

Table 1 contains the evaluation results of our different model configurations. When learning from GT, our best performing three-joint and four-joint TD3 models use dense rewards and HER. The four-joint model is the most successful TD3 model, with an average distance to the target of 2.4 cm. Interestingly, the six-joint agent cannot compete with the four-joint agent. This reflects how complexity increases exponentially with the state space dimensionality.

Regarding the SAC models, the most successful three- and four-joint configuration used sparse rewards and no HER. In turn, the less constrained six-joint SAC model benefited from HER (Table 1). The fact that HER led to a drop in performance for the first two cases was unexpected and stood in direct contrast to the three- and four-joint TD3 models. It indicates that our

Table 1: Evaluation of the RL algorithms. The threshold is the minimum proximity of the robot end effector to the target in order to consider an episode successful. The actuated joints show which joints could be used by the agent to solve the reaching task.

	Actuated Joints	Reward Type	HER	Average Distance (m)	Success Rate (–)						Training length [b]
					20 cm[a]	*15 cm*[a]	*10 cm*[a]	*7 cm*[a]	*5 cm*[a]	*3 cm*[a]	
TD3	1–3	dense	no	0.057	0.999	0.978	0.872	N/A	0.542	N/A	10000
	1–3	dense	yes	0.052	0.998	0.985	0.890	N/A	0.658	N/A	10000
	1–3	sparse	no	0.074	0.981	0.907	0.799	N/A	0.381	N/A	10000
	1–3	sparse	yes	0.062	1.000	0.975	0.849	N/A	0.472	N/A	10000
	1–3, 5	**dense**	**yes**	**0.024**	N/A	N/A	**0.982**	**0.958**	**0.924**	**0.766**	**30000**
	1–6	dense	yes	0.046	N/A	N/A	0.866	0.806	0.744	0.534	60000
	1–3, 5[c]	dense	yes	0.061	N/A	N/A	0.940	0.790	0.540	0.312	30000
	1–3, 5[d]	dense	yes	0.056	N/A	N/A	0.918	0.800	0.630	0.320	30000
SAC	1–3	dense	no	0.070	0.986	0.936	0.758	N/A	0.454	N/A	5000
	1–3	dense	yes	0.091	0.988	0.884	0.568	N/A	0.252	N/A	5000
	1–3	sparse	no	0.054	0.988	0.940	0.868	N/A	0.646	N/A	5000
	1–3	sparse	yes	0.109	0.866	0.788	0.612	N/A	0.342	N/A	5000
	1–3, 5	dense	no	0.047	1.000	0.984	0.948	N/A	0.760	N/A	4000
	1–3, 5	dense	yes	0.086	1.000	0.992	0.840	N/A	0.688	N/A	4500
	1–3, 5	sparse	no	0.029	N/A	N/A	0.966	0.932	0.866	0.600	4000
	1–3, 5	sparse	yes	0.042	N/A	N/A	0.924	0.864	0.742	0.376	4500
	1–6	**sparse**	**yes**	**0.021**	N/A	N/A	**0.998**	**0.978**	**0.932**	**0.816**	**18000**

[a]Evaluation threshold.
[b]The length of the training process is given in the number of episodes.
[c]Learning from images: manual extraction
[d]Learning from images: CNN extraction

constrained action spaces already ensure a high enough sampling efficiency for SAC. Despite relatively short training time compared to the TD3 models, the six-joint SAC model reached an average distance of 2.1 cm and thus represents our overall best model.

When learning from images, we used our best performing TD3 model with the manual and CNN extraction pipeline, respectively (Table 1 below dashed line). Both methods extracted the target position with an average error of ~2 cm. Overall, the CNN extraction method showed slightly better performance with an average distance of 5.6 cm.

In future work, we want to approach the same task using RL and Spiking Neural Networks and compare their performance to the Artificial Neural Network models used here.

ACKNOWLEDGEMENTS

This project has received funding from the European Union's Horizon 2020 Framework Programme for Research and Innovation under the Specific Grant Agreement No. 945539 (Human Brain Project SGA3). Further, we want to

thank TUM for providing us with considerable computational resources via the Leibniz-Rechenzentrum.

Keywords: reinforcement learning, robotics, neurorobotics platform, simulation, kinematics, deep learning

REFERENCES

[1] R. S. Sutton and A. G. Barto, Reinforcement learning: An introduction MIT press, 2018. [Online]. Available: http://www.incompleteideas.net/book/the-book-2nd.html

[2] A. Hermann, J. Sun, Z. Xue, S. W. Ruehl, J. Oberländer, A. Roennau, J. M. Zöllner, and R. Dillmann, "Hardware and software architecture of the bimanual mobile manipulation robot hollie and its actuated upper body," in 2013 IEEE/ASME International Conference on Advanced Intelligent Mechatronics. IEEE, 2013, pp. 286–292.

[3] E. Falotico, L. Vannucci, A. Ambrosano, U. Albanese, S. Ulbrich, J. C. Vasquez Tieck, G. Hinkel, J. Kaiser, I. Peric, O. Denninger, N. Cauli, M. Kirtay, A. Roennau, G. Klinker, A. Von Arnim, L. Guyot, D. Peppicelli, P. Martnez-Caada, E. Ros, P. Maier, S. Weber, M. Huber, D. Plecher, F. Rhrbein, S. Deser, A. Roitberg, P. van der Smagt, R. Dillman, P. Levi, C. Laschi, A. C. Knoll, and M.-O. Gewaltig, "Connecting artificial brains to robots in a comprehensive simulation framework: The neurorobotics platform," Frontiers in Neurorobotics, vol. 11, p. 2, 2017. [Online]. Available: https://www.frontiersin.org/article/10.3389/fnbot.2017.00002

[4] S. Fujimoto, H. Hoof, and D. Meger, "Addressing function approximation error in actor-critic methods," in International Conference on Machine Learning. PMLR, 2018, pp. 1587–1596.

[5] T. Haarnoja, A. Zhou, P. Abbeel, and S. Levine, "Soft Actor-Critic: Off-Policy Maximum Entropy Deep Reinforcement Learning with a Stochastic Actor," University of California Berkeley, Tech. Rep., 2018.

[6] M. Marculescu, C. Tiller, J. Tattermusch, and Y. Tibrewal, "gRPC,"2015. [Online]. Available: https://github.com/grpc/grpc

[7] M. Andrychowicz, F. Wolski, A. Ray, J. Schneider, R. Fong, P. Welinder, B. McGrew, J. Tobin, P. Abbeel, and W. Zaremba, "Hindsight experience replay," arXiv preprint arXiv:1707.01495, 2017.

[8] Krizhevsky, A., & Hinton, G. (2009). Learning multiple layers of features from tiny images.

Perception-driven control of multiple robotic arms in the Neurorobotics Platform

J. Camilo Vasquez Tieck*, Daniel Azanov, Jacques Kaiser, Rüdiger Dillmann

Applied technical cognitive systems, FZI Research Center for Information Technology, Karlsruhe, Germany
**tieck@fzi.de*

INTRODUCTION/MOTIVATION

Reaching a target is one of the most important tasks in robotics — object interaction, manipulation and grasping tasks require moving the arm to specific targets [1]. However, there are many models of industrial robotic arms. They have different kinematics and hardware components. The robotic arms usually have different controllers depending on the manufacturer. In addition, each application developer will add different sensors for their setup.

This is problematic because there is no unified and understandable way of controlling multiple robots, which makes it difficult to port controllers between systems. In this work, we show how the same control strategy can be used with four different robot arms in the Neurorobotics Platform (NRP) [2][3]. This work extends the work presented in [4][5] of motor control for target reaching using motor primitives with spiking neural networks (SNN) [6]. The same SNN is used for all robots, but the motor primitives are trained with corresponding trajectories for each robot. This approach is model free and does not require the calculation of the inverse kinematics or the validation of the configurations.

METHODS

In [4][5] an SNN for target reaching was presented (see Fig. 1). To model the motion in 3D, the work in [4][5] uses three motor primitives for the arm – left-right, up-down and far-near. The motions of the three motor primitives are combined using an error signal from the desired target. This method resembles characteristics of visual-servoing [7], but instead of using visual feedback, we use the ground truth position of the target in simulation. In this work we extend the work from [4][5] to control four different robotic arms.

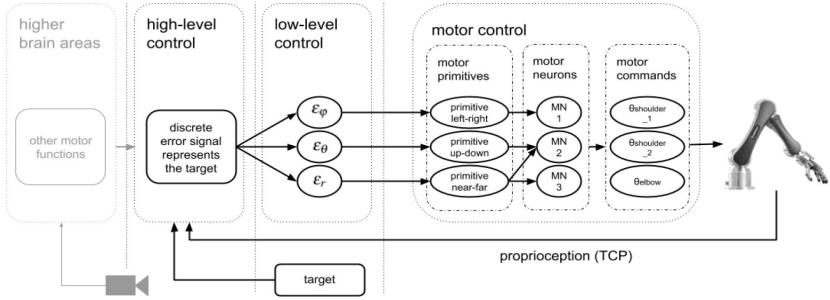

FIGURE 1: Detail of the SNN with all layers and populations in the closed-loop scenario (adapted from [4]).

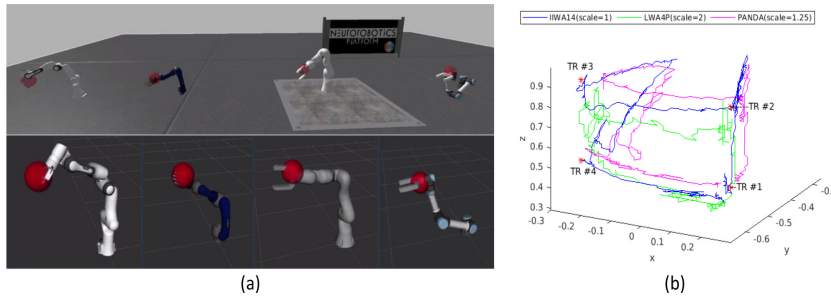

FIGURE 2: Arm control for multiple robots using SNNs. (**a**) NRP experiment with four robotic arms -- Kuka IIWA14, Schunk LWA4P, Panda and UR5e. (**b**) Rectangular movement experiment. The target points are red dots labeled "TR # 1-3".

The first step is to integrate the SNN for one robot implemented using Nengo [8] in the NRP. Then we define an experiment with four robotic arms in simulation – Kuka IIWA14, Schunk LWA4P, Panda and UR5e (see Fig. 2a). We extend the brain simulation of the NRP to use multiple brains, one for each robot. Which allows the use of an instance of the SNN for target reaching for each robot. Each of the SNNs is trained with three example trajectories of each robot – one for each primitive. We add transfer functions between each robot and each brain. We also added a state machine that generates targets for all the robots. The targets are represented as spheres, where the

center is the target, and the radius is the allowed error (see Fig. 2a). Each brain gets the corresponding feedback about its target. When the target changes the SNN of each robot generates control commands for each arm to reach the targets.

RESULTS AND DISCUSSION

As a benchmark task we defined an experiment where the state machine generates targets in the corners of a rectangle, so that the robots perform a trajectory across the edges of a hypothetical rectangle. Although, the SNNs for each robot have the same topology, the primitives are defined individually for each robot. This means that it is possible that different robots have different configurations for the same target as shown in Fig. 2a. The resulting trajectories are shown in Fig. 2b. The robots are different, with different sizes, and so the trajectories are not of the same size, and thus they are scaled accordingly. The similarity in the appearance of the motion can be observed. The target points for the rectangle are shown as red dots in Fig. 2b. The experiment shows that the SNN control strategy can be used to control different robots. Still, as it can be seen in the trajectories in Fig. 2b, there are control problems on the system as in [4][5]. This is happening because the raw spiking output of the network is being used for the control. This can be solved by using a low-level controller to smooth the control signal. This work presents an opportunity for porting a flexible control architecture with SNN to neuromorphic hardware such as SpiNNaker [9] or Loihi [10] and use it to control the real robots. The proposed experiment can be used as a benchmark for other control approaches with SNN and highlights the use of the NRP for this purpose.

ACKNOWLEDGMENT

This research has received funding from the European Union's Horizon 2020 Framework Programme for Research and Innovation under the Specific Grant Agreement No. 785907 (Human Brain Project SGA2) and No. 945539 (Human Brain Project SGA3).

Keywords: arm control, motor primitives, spiking neural networks, neurorobotics platform, multiple robots

REFERENCES

[1] J.-C. Latombe, *Robot motion planning*. Springer Science & Business Media, 2012.

[2] E. Falotico *et al.*, "Connecting artificial brains to robots in a comprehensive simulation framework: the Neurorobotics Platform," *Front. Neurorobotics*, vol. 11, no. JAN, 2017, doi: 10.3389/fnbot.2017.00002.

[3] J. C. V. Tieck *et al.*, "The neurorobotics platform for teaching – embodiment experiments with spiking neural networks and virtual robots," presented at the 2019 IEEE International conference on cyborg and bionic systems (CBS), 2019. doi: 10.1109/CBS46900.2019.9114395.

[4] J. C. V. Tieck, L. Steffen, J. Kaiser, D. Reichard, A. Roennau, and R. Dillmann, "Combining motor primitives for perception driven target reaching with spiking neurons," *Cogn. Inform. Nat. Intell. IJCINI*, vol. 13, no. 1, p. 12, 2019, doi: 10.4018/IJCINI.2019010101.

[5] J. C. V. Tieck, L. Steffen, J. Kaiser, D. Reichard, A. Roennau, and R. Dillmann, "Controlling a robot arm for target reaching without planning using spiking neurons," in *2018 IEEE 17th international conference on cognitive informatics & cognitive computing (ICCI* CC)*, 2018, pp. 111–116. doi: 10.1109/ICCI-CC.2018.8482049.

[6] W. Maass, "Networks of spiking neurons: The third generation of neural network models," *Neural Netw.*, vol. 10, no. 9, pp. 1659–1671, 1997, doi: 10.1016/S0893-6080(97)00011-7.

[7] F. Chaumette, S. Hutchinson, and P. Corke, "Visual servoing," in *Springer handbook of robotics*, Springer, 2016, pp. 841–866.

[8] T. Bekolay *et al.*, "Nengo: a Python tool for building large-scale functional brain models," *Front. Neuroinformatics*, vol. 7, no. 48, pp. 1–13, 2014, doi: 10.3389/fninf.2013.00048.

[9] S. B. Furber *et al.*, "Overview of the SpiNNaker System Architecture," *IEEE Trans. Comput.*, vol. 62, no. 12, pp. 2454–2467, 2013, doi: 10.1109/TC.2012.142.

[10] M. Davies *et al.*, "Loihi: A Neuromorphic Manycore Processor with On-Chip Learning," *IEEE Micro*, vol. 38, no. 1, pp. 82–99, 2018, doi: 10.1109/MM.2018.112130359.

RateML: A code generation tool for BrainNetwork models

Michiel van der Vlag[1]*†, Marmaduke Woodman[2]†, Jan Fousek[2], Sandra Diaz-Pier[1], Aaron Perez Martin[1], Viktor Jirsa[2] , Abigail Morrison[1,3]

[1]Forschungszentrum Jülich, Jülich Super Computingcenter (JSC), Jülich, Germany
[2]Institut de Neurosciences des Systèmes, Aix Marseille Universite, Marseille, France
[3]Institute of Neuroscience and Medicine (INM-6) & Institute for Advanced Simulation(IAS-6) & JARA-Institute Brain
**m.van.der.vlag@fz-juelich.de*

INTRODUCTION/MOTIVATION

Simulation frameworks in computational neuroscience support the interdisciplinary study of the relationships between structure and dynamics in the brain integrating knowledge from different disciplines and reproducing functional features at multiple scales. These virtual spaces where researchers can model the brain, generate hypotheses and perform multiple experiments have become an essential tool to understand the brain in states of health and disease, as well as during development and aging [2]. Emerging computing infrastructures support the development and execution of such frameworks and allow for the simulation of detailed models. These models take into account a variety of features and variables related to the function of neurons, networks and brain regions.

The Virtual Brain enables simulation of the whole brain with advanced mathematical models in combination with emprical data such as Electroencephalography, Magnetoencephalography and Magnetic Resonance Imaging [3].

Translating the mathematical and abstract descriptions of brain models into efficient code is a task which requires speciallized knowledge and experience. Whole brain simulations can also be tuned to fit the parameters of specific subjects [5] using experimental measurements from individual brain structures and dynamics [6]. This process is computationally intensive and requires scientists to explore vast combinations of parameters in their models.

†these authors contributed equally to the work

In order to ease the translation from differential equations to executable code and make computational infrastructure accessible to scientists with different backgrounds, we have designed a modelling framework which combines a domain specific language with an automatic code generator; called RateML. This allows us to detach modelling from software implementation, a technique which is becoming ever more common in computational neuroscience [7].

NestML [17], i.e., is a modelling tool which targets the description of point neuron models and synapses. NeuroML [18], which is used by Arbor [14], enables users to define single cells and network of these cells. Another modeling tool is NineML [15] which focuses on neworks of point neurons. RateML focuses on modeling the dynamic variable of mesoscopic brain activity, identical to the models used by the TVB simulator. A modeling tool for TVB and TVB on HPC does not exist in this fashion.

METHODS

RateML builds on top of a domain specific language called 'Low Entropy Model Specification' (LEMS) [8], the language is not extended and can be used natively. With RateML users can formulate the differential equations which describe their models using an XML representation which is later used to produce Python and CUDA [9] code. With the CUDA code, end users can utilize the parallelization power of Graphic Processing Units (GPUs) in order to explore wide ranges of values for parameters specified in their models.

RateML is part of the main TVB repository[1]. Documentation as well as blank model from which you can get started can be found in this repository. Next to this many existing TVB models have already been ported to RateML.

To use RateML and for instance generate a Python model which can be simulated with the TVB simulator, the user can start by opening the blank model from the repository and complete the *ComponentType derivatives*. This *ComponentType*, shown in Figure 1, has elements with which the behaviour of the users model can be defined. It consists of the elements: *Constant*, *Exposure*, *StateVariables* and *TimeDerivatives*. *Constant*s are use to define the unmutable intrinsic chracteristics of the model. The *Exposure* is used to

[1]https://github.com/the-virtual-brain/tvb-root.git

```
<ComponentType name="derivatives">

    <Constant name="omega" value="60.0 * 2.0 * 3.1415927 / 1e3"
    dimension=""
    description="base line frequency Kuramoto oscillator [rad/ms]"/>

    <Exposure name="theta" dimension="" />

    <Dynamics>
        <StateVariable name="theta" dimension="0.0, 1.0"
        exposure="0.0, numpy.pi * 2.0"/>
        <TimeDerivative variable="dV" value="omega + c_pop0"/>
    </Dynamics>
</ComponentType>
```

FIGURE 1: XML derivatives definition for Python Kuramoto model.

define the to be monitored variable of the simulation, the *StateVariable* and *TimeDerivative* make up the dynamic behaviour of the model.

When the user is finished, she can run at the command line:

python XML2model.py --model kuramoto --language python

To generate a TVB model which will be familiarized by the her TVB installation directly. The user can immediately make a simulation with the generated model. She never has to see the resulting model file or has to worry about the performance of the underlying code; this has all been abstracted from the modeling effort.

The example in Figure 1 is for the Python backend. For the CUDA backend, two extra ComponentTypes have to be defined, namely for the *coupling* and *noise*. In the repository the user will find many example and Jupyter notebooks on how to generate the CUDA models.

RESULTS

We have implemented the RateML framework which is currently available as part of The Virtual Brain distribution. We have benchmarked simulations using three well known and widely used neuraml mass models from TVB: the Kuramoto [10], WongWang [11] and Epileptor [12].

The simulations used for the benchmarking were executed for 40,000 simulation steps, with a time step of 0.1 ms and using a deterministic Euler integration scheme. The number of parameters was increased in order to observe the changes in the execution time and memory usage by the different models. Figure 2 shows the results of the benchmarking, indicating how RateML is able to produce code which exploits the whole capacity of a GPU to enable explorations of thousands of parameters in parallel. All simulations were executed in the Booster partition of the JUWELS supercomputer in the Julich Supercomputing Centre. Each node in the JUWELS booster has 4 A100GPUs with 40 GB of memory.

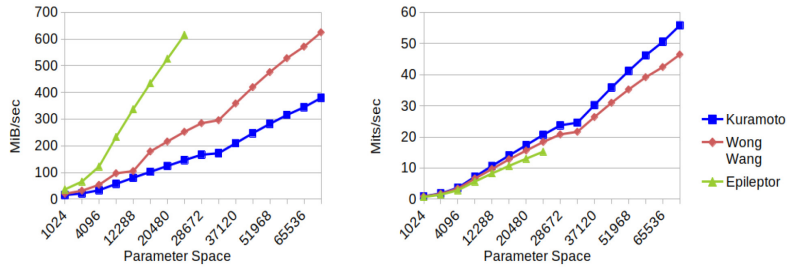

FIGURE 2: Memory bandwidth consumption and model iterations per second for three TVB CUDAmodels when scaling the parameter space. Results indicate linear scaling when increasing the parameter space and that the application is memory bound.

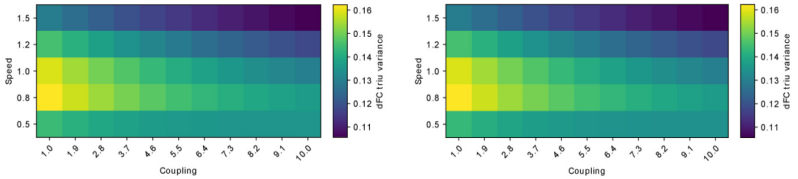

FIGURE 3: CPU & GPU parameter sweep validation for 68 nodes, 40k simulation steps, varying the global_speed and global_coupling parameter (van der Vlag et al. 2021 (in preparation).

To validate the RateML generated models, we used an existing experiment as a scaffold. The Montbrió [14] model was used in a study on the role which neuronal cascades play in the causation of whole-brain dynamics at rest [13]. RateML was used to input their models charactaristics and produce a CUDA model and driver to mimick their results. This CUDA model was then compared against the TVB results for 5x10 of different parameter combinations. Figure 3 shows the results when comparing the CUDA and the TVB results. The error is smaller than *13.4e-5*t*, in relation to the timestep, proving that the generated model is suited and accurate to use for such experiments.

DISCUSSION

In conclusion, RateML offers the neuroscience community with a new tool to automatically generate code from abstract model representations, enabling easy computing with Python as well as access to the full power of GPUs for parameter exploration. RateML allows the modeling of brain neural models and Neural Mass Models in a simple way, detaching the optimized implementations from the modeling and simulation infrastructure. RateML supports the investigation and generation of new models to study the links between structure and function in the brain enabling also a thorough investigation of the link between specific model parameters and the dynamics produced.

Keywords: brain network models, simulation, high performance computing, automatic code generation, domain specific language

REFERENCES

[1] [Dataset] Peyser, A., Diaz Pier, S., Klijn, W., Morrison, A., and Triesch, J. (2019). Linking experimental and computational connectomics

[2] Einevoll, G. T., Destexhe, A., Diesmann, M., Grün, S., Jirsa, V., de Kamps, M., et al. (2019). The scientific case for brain simulations. Neuron 102, 735744388

[3] Lynn, C. W. and Bassett, D. S. (2019). The physics of brain network structure, function and control. Nature Reviews Physics 1, 318332

[4] Sanzleon, P., Knock, S. A., Woodman, M. M., Domide, L., Mersmann, J., Mcintosh, A. R., et al. (2013). The virtual brain: A simulator of primate brain network dynamics. Frontiers in Neuroinformatics 7. doi:10.3389/fninf.2013.00010

[5] Falcon, M. I., Jirsa, V., and Solodkin, A. (2016). A new neuroinformatics approach to personalized medicine in neurology: The virtual brain. Current opinion in neurology 29, 429 Furber,

S. B., Lester, D. R., Plana, L. A., Garside, J. D., Painkras, E., Temple, S., et al. (2012). Overview of the spinnaker system architecture. IEEE Transactions on Computers 62, 24542467

[6] Deco, G., McIntosh, A. R., Shen, K., Hutchison, R. M., Menon, R. S., Everling, S., et al. (2014). Identification of optimal structural connectivity using functional connectivity and neural modeling. Journal of Neuroscience 34, 79107916386

[7] Blundell, I., Brette, R., Cleland, T. A., Close, T. G., Coca, D., Davison, A. P., et al. (2018). Code Generation in Computational Neuroscience: A Review of Tools and Techniques. Frontiers in Neuroinformatics 12, 68. doi:10.3389/fninf.2018.00068

[8] Vella, M., Cannon, R. C., Crook, S., Davison, A. P., Ganapathy, G., Robinson, H. P. C., et al. (2014). libNeuroML and PyLEMS: using Python to combine procedural and declarative modeling approaches in computational neuroscience. Frontiers in Neuroinformatics 8, 38. doi:10.3389/fninf.2014.00038

[9] [Dataset] NVIDIA, Vingelmann, P., and Fitzek, F. H. (2020). Cuda, release: 10.2.89

[10] Kuramoto, Y. (1975). International symposium on mathematical problems in theoretical physics. Lecture notes in Physics 30, 420

[11] Wong, K.-F. and Wang, X.-J. (2006). A recurrent network mechanism of time integration in perceptual decisions. Journal of Neuroscience 26, 13141328425

[12] Jirsa, V. K., Stacey, W. C., Quilichini, P. P., Ivanov, A. I., and Bernard, C. (2014). On the nature of seizure dynamics. Brain 137, 22102230

[13] Rabuffo, G., Fousek, J., Bernard, C., and Jirsa, V. (2021). Neuronal cascades shape whole-brain functional590dynamics at rest.eNeurodoi:10.1523/ENEURO.0283-21.2021

[14] Abi Akar, N., Cumming, B., Karakasis, V., K usters, A., Klijn, W., Peyser, A., et al. (2019). Arbor — A532Morphologically-Detailed Neural Network Simulation Library for Contemporary High-Performance533Computing Architectures. In2019 27th Euromicro International Conference on Parallel, Distributed534and Network-Based Processing (PDP). 274–282. doi:10.1109/EMPDP.2019.8671560

[15] Davison, A. (2013).NineML(New York, NY: Springer New York). 1–2. doi:10.1007/978-1-4614-7320-6547375-2

[16] Montbrió, E., Paź o, D., and Roxin, A. (2015). Macroscopic description for networks of spiking neurons.579Physical Review X5, 1–15. doi:10.1103/PhysRevX.5.021028

[17] Plotnikov, D., Blundell, I., Ippen, T., Eppler, J. M., Morrison, A., and Rumpe, B. (2016). Nestml: a587modeling language for spiking neurons. InModellierung 2016, eds. A. Oberweis and R. Reussner (Bonn:588Gesellschaft f˙ur Informatik e.V.), 93–108

[18] Gleeson P, Crook S, Cannon RC, Hines ML, Billings GO, et al. (2010) NeuroML: A Language for Describing Data Driven Models of Neurons and Networks with a High Degree of Biological Detail. PLOS Computational Biology 6(6): e1000815. https://doi.org/10.1371/journal.pcbi.1000815

Towards fully embedded biologically inspired deep learning on neuromorphic hardware

Ben von Hünerbein[1]*, Ismael Jaras[1,2,3], Laura Kriener[1], Jakob Jordan[1], Walter Senn[1], Mihai A. Petrovici[1,4]

[1]Department of Physiology, University of Bern, Bern, Switzerland
[2]Department of Electrical Engineering, University of Chile, Santiago, Chile
[3]Neurosystems Laboratory, University of Chile, Biomedical Neuroscience Institute, Santiago, Chile
[4]Kirchhoff Institute for Physics, Heidelberg University, Heidelberg, Germany
**ben.vonhuenerbein@unibe.ch*

INTRODUCTION/MOTIVATION

Our brains are able to efficiently process and learn from the vast amount of information our senses provide about our environment. Understanding the computational principles underlying this unparalleled computational capacity is not only important for basic neuroscience research but also for advancing artificial intelligence. Neuromorphic engineering in particular tries to replicate the brain's fundamental principles in new novel hardware to overcome the constraints, for example high energy consumption, present in classical von Neumann architectures. Conversely, error backpropagation [1], the basis of deep learning algorithms, can serve as inspiration to neuroscientific models about how complex tasks may be learned in the brain. However, naive implementations of backpropagation are at odds with neurobiology [2]. Thus, there is an effort in the field of computational neuroscience to devise models that leverage the strength of credit assignment via backpropagation in a biologically plausible way [3,4,5,6]. One approximation of backpropagation which incorporates constraints from biological systems, developed by Sacramento et al. [4], consists of a hierarchical architecture of microcircuits composed of multicompartment inter- and pyramidal neurons. In particular, unlike classical deep learning models, this model does not rely on separate forward and backward phases, avoids the weight transport problem by using random feedback weights, and the learning of synaptic weights relies on a local, plausible plasticity model [7]. In this study we aim to make the model by Sacramento et al. compatible with a range of neuromorphic hardware platforms [8,9,10] by moving from a rate-based to a spike-based implementation. We demonstrate in software simulations that our modified spiking version of the model preserves the functional principles allowing the original rate based model to learn.

METHODS

The original model consists of multiple layers of microcircuits composed of multi-compartment pyramidal cells and interneurons which communicate via rates (Figure 1A). Inputs to the lowest-layer pyramidal neurons propagate through the network to the output layer. An error signal, proportional to the difference between the network output and a desired target, is continuously injected into the apical compartments of the neurons in the output layer. If the output matches the target, the feedback signal from the output layer is cancelled by input from the hidden layer interneurons in the apical compartment of the hidden layer pyramidal neurons. If an error arises in the output layer this will create a mismatch between the top-down feedback and lateral input. This mismatch, representing the error, is reflected in the voltage of the hidden layer apical compartment which modulates the somatic voltage. Synaptic plasticity is driven by the Urbancik Senn learning rule [7], which reduces the error by minimizing the discrepancy between the basal and somatic voltage.

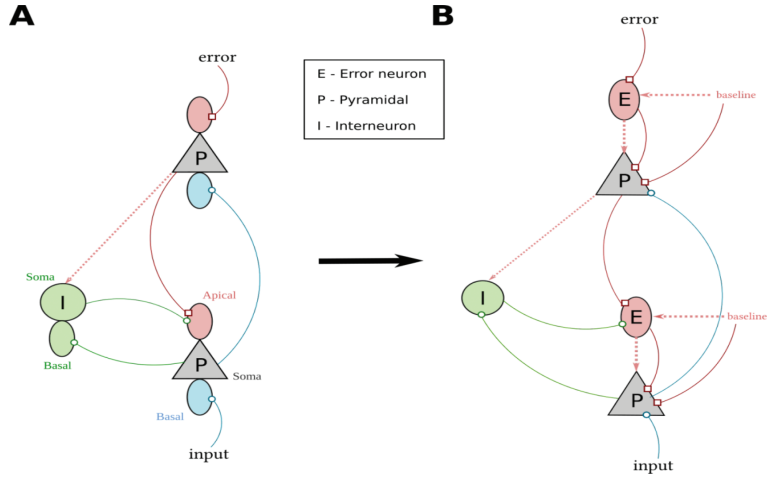

FIGURE 1: (**A**) The dendritic microcircuit described in Sacramento et al., 2018, consisting of an interneuron (green), upper- and lower-layer pyramidal neurons (grey) and their respective apical (red) and basal (blue) dendrites. Synaptic connections are drawn as lines between neurons with a square or circular marker at the end indicating static or plastic synapses respectively. Dashed arrows indicate signals used for synaptic updates. (**B**) The adapted microcircuit. Note that the apical dendrite has been separated from the soma and now serves as an error neuron connected via a synapse to the pyramidal neuron.

We modified the original model to make it suitable for emulation on multiple different neuromorphic substrates. One common ground for most platforms is their ability to emulate Leaky Integrate-and-Fire (LIF) neurons [11]. We replace the apical compartments in the original model with LIF point neurons and combine the somatic and basal compartments into a single LIF neuron (Figure 1B). The error in the apical compartment, which was previously represented as a voltage, is now encoded using spikes. To enable the encoding of negative error values, neurons fire with baseline activities and errors are represented as deviations from this baseline. In the original model, activity was communicated in the form of instantaneous firing rates, a non-linear function of the somatic voltage. Now communication between all neurons is spike-based. As in the original model the plasticity of the synapses is driven by applying the Urbancik Senn learning rule [7] on the neuronal firing rates, computed from the spike counts over the duration of each sample presentation. For the software simulations of the model we chose the PyNN library [12] with NEST [13] as a simulation backend. While the model could have been implemented using other libraries such as Brian [14] or PyNEST [15] or GeNN [16], PyNN was chosen as it can also operate as a frontend for the neuromorphic platforms BrainScaleS 2 [8] and SpiNNaker [9].

RESULTS AND DISCUSSION

To test whether the basic principles of the original model were unchanged by the previously explained modifications, we performed software simulations of a simple nonlinear regression task using a single microcircuit (Figure 1B). The network of LIF neurons was able to learn simple input-output pairs (Figure 2A-D). Furthermore, the errors, represented by the activity of the "apical" error neurons in both the hidden and output layer, drive learning and decay to their respective baselines when the output approaches the target (Figure 2E). Even though our model relies on fundamentally different single-neuron dynamics and employs spike-based communication, we preserved the fundamental principles underlying learning in the original model.

Further work will focus on implementing the modified model on current spiking neuromorphic platforms such as the digital SpiNNaker system [9] and the mixed-signal BrainScales 2 system [8]. By having both learning and inference fully embedded in the same neuromorphic substrate we hope to make full use of the speed and energy efficiency of these brain-inspired architectures.

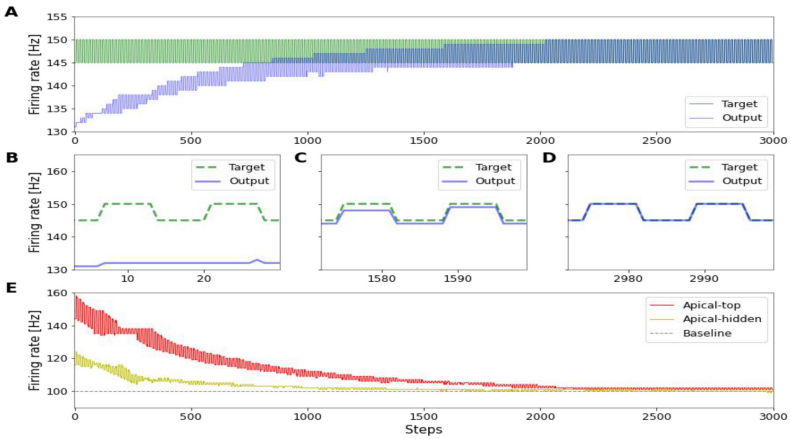

FIGURE 2: The adapted spiking microcircuit learning a simple regression task. (**A**) Comparison of the output activity of the top-layer pyramidal neuron (blue) and the target output throughout training. (B-D) Zoom into the initial (**B**), middle (**C**) and late (**D**) phase of the training. (**E**) The activity of the error neurons in the output and hidden layer converge towards their respective baseline.

ACKNOWLEDGEMENTS

We wish to thank Sebastian Billaudelle and Benjamin Cramer for valuable discussions. We gratefully acknowledge funding from the European Union under grant agreements 604102, 720270, 785907, 945539 (HBP), the Manfred Stärk Foundation, the Agencia Nacional de Investigación y Desarrollo under the grant agreement PFCHA/Doctorado Nacional/2019-21190330 as well as the Intel Corporation within their neuromorphic research community. Additionally, our work has greatly benefitted from access to the Fenix Infrastructure resources, which are partially funded from the European Union's Horizon 2020 research and innovation programme through the ICEI project under the grant agreement No. 800858.

Keywords: learning, neuromorphic hardware, biologically plausible error-backpropagation, synaptic plasticity, spiking neurons

REFERENCES

[1] Rumelhart, D. E., Hinton, G. E., & Williams, R. J. (1986). Learning representations by back-propagating errors. *nature*, *323*(6088), 533-536.

[2] Crick, F. (1989). The recent excitement about neural networks. *Nature*, *337*(6203), 129-132.

[3] Whittington, J. C., & Bogacz, R. (2019). Theories of error back-propagation in the brain. *Trends in cognitive sciences*, *23*(3), 235-250.

[4] Sacramento, J. a., Ponte Costa, R., Bengio, Y. & Senn, W. (2018) Dendritic cortical microcircuits approximate the backpropagation algorithm. *Advances in Neural Information Processing Systems 31*

[5] Scellier, B., & Bengio, Y. (2017). Equilibrium propagation: Bridging the gap between energy-based models and backpropagation. *Frontiers in computational neuroscience*, *11*, 24.

[6] Whittington, J. C., & Bogacz, R. (2017). An approximation of the error backpropagation algorithm in a predictive coding network with local Hebbian synaptic plasticity. *Neural computation*, *29*(5), 1229-1262.

[7] Urbanczik, R., & Senn, W. (2014). Learning by the dendritic prediction of somatic spiking. *Neuron*, *81*(3), 521-528.

[8] Billaudelle, S., Stradmann, Y., Schreiber, K., Cramer, B., Baumbach, A., Dold, D., ... & Meier, K. (2020, October). Versatile emulation of spiking neural networks on an accelerated neuromorphic substrate. In *2020 IEEE International Symposium on Circuits and Systems (ISCAS)* (pp. 1-5). IEEE.

[9] Furber, S. (2016). Large-scale neuromorphic computing systems. *Journal of neural engineering*, *13*(5), 051001.

[10] Davies, M., Srinivasa, N., Lin, T. H., Chinya, G., Cao, Y., Choday, S. H., ... & Wang, H. (2018). Loihi: A neuromorphic manycore processor with on-chip learning. *Ieee Micro*, *38*(1), 82-99.

[11] Dayan, P., & Abbott, L. F. (2001). Theoretical neuroscience: computational and mathematical modeling of neural systems. *Computational Neuroscience Series*.

[12] Davison, A. P., Brüderle, D., Eppler, J. M., Kremkow, J., Muller, E., Pecevski, D., ... & Yger, P. (2009). PyNN: a common interface for neuronal network simulators. *Frontiers in neuroinformatics*, *2*, 11.

[13] Gewaltig, M., & Diesmann, M. (2007). NEST (NEural Simulation Tool). *Scholarpedia, 2*, 1430.

[14] Goodman, D. F., & Brette, R. (2009). The brian simulator. Frontiers in neuroscience, 3, 26.

[15] Eppler, J. M., Helias, M., Muller, E., Diesmann, M., & Gewaltig, M. O. (2009). PyNEST: a convenient interface to the NEST simulator. *Frontiers in neuroinformatics*, *2*, 12.

[16] Yavuz, E., Turner, J., & Nowotny, T. (2016). GeNN: a code generation framework for accelerated brain simulations. Scientific reports, 6(1), 1-14.

III Brain organisation & theoretical neuroscience

Surrogate techniques to evaluate significance of spike patterns

Peter Bouss[1,2]*, Alessandra Stella[1,2]*, Günther Palm[3]*, Sonja Grün[1,2]*

[1]Institute of Neuroscience and Medicine (INM-6), Institute for Advanced Simulation (IAS-6), and JARA Brain Institute I (INM-10), Jülich Research Centre, Jülich, Germany
[2]Theoretical Systems Neurobiology, RWTH Aachen University, Aachen, Germany
[3]Neuroinformatics, University of Ulm, Ulm, Germany
**p.bouss@fz-juelich.de; a.stella@fz-juelich.de; guenther.palm@uni-ulm.de; s.gruen@fz-juelich.de*

INTRODUCTION/MOTIVATION

Surrogate spike train data is used to generate the null hypothesis in the context of the significance analysis of spike train correlations and spatio-temporal spike patterns. In our work, we compare five different surrogate techniques against the classical technique called Uniform Dithering (UD [1]). In particular, we discuss the use of the surrogates to generate the null-hypothesis distribution in the statistical test of the SPADE method (Spike PAttern Detection and Evaluation [2,3]), which detects spatio-temporal spike patterns in parallel spike trains. In SPADE, both spike trains and surrogate realizations are discretized into 0-1 sequences (binarization) before the pattern detection. We discover that binarized surrogates have a lower spike count than the original data, due to the change in the surrogate's inter-spike interval (ISI) distribution caused by the UD algorithm. The spike count mismatch between the original data and the surrogates is predominant in the case of high firing rates, spiking regularity, and presence of a dead time (minimal temporal distance between spikes typically induced by spike sorting). We prove that spike count reduction leads to false positive (FP) detection, motivating us to explore alternative surrogate techniques to UD.

METHODS

Surrogate Techniques (Figure 1)

- Uniform Dithering (UD)[1] displaces each spike individually according to a uniform distribution.
- To account for the dead-time present in experimental data, Uniform Dithering with Dead-Time (UDD) limits the displacement of each spike such that the dead-times are conserved.
- (Joint)-ISI dithering [4] displaces each spike individually preserving the (joint-) ISI distribution.
- Window Shuffling shuffles binarized spike trains inside of short windows.
- Trial Shifting consists in shifting entire segments of a spike train according to a uniform distribution, independently trial by trial, and neuron by neuron [1, 5].

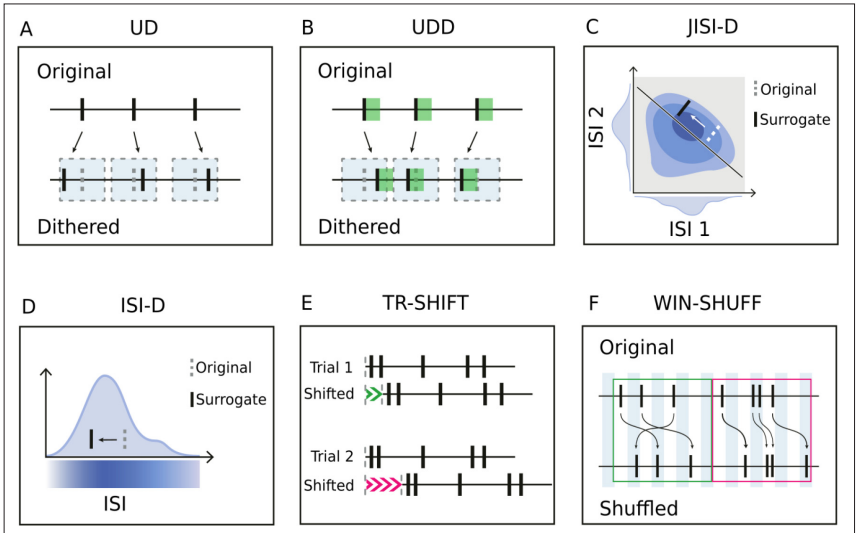

FIGURE 1: Surrogate Techniques. (**A**) Uniform Dithering (UD) displaces each spike according to a uniform distribution centered on the spike. (**B**) Uniform Dithering with dead-time (UDD) is based on uniform dithering, but spikes are constrained not to be closer to each other than a dead-time (**C**) Joint Inter-Spike Interval Dithering (JISI-D) displaces each spike according to the J-ISI distribution of the neuron. (**D**) Inter-Spike Interval Dithering (ISI-D) displaces each spike according to the ISI distribution of the neuron. (**E**) Trial Shifting (TR-SHIFT) shifts each trial according to a uniform distribution. (**F**) Window Shuffling (WIN-SHUFF) shuffles binned spike trains within windows.

SPADE

SPADE detects spike patterns at a millisecond resolution, allowing for temporal delays between the spikes. The spike trains are first discretized and patterns are then mined and counted. To assess the significance of these patterns, the same procedure is performed on multiple realizations of surrogate spike trains, resulting in a p-value spectrum [3]. Significant patterns have p-values lower than the (corrected) significance threshold.

Artificial data generation

In order to evaluate the effect of the different surrogates on SPADE, we create artificial spike trains modeled according to the statistics of experimental data from the pre-/motor cortex of macaque monkeys [6], including non-stationary firing rate profiles. The dead time and regularity of the data are modeled by simulating Poisson processes with dead-time (PPD) and Gamma spike trains, respectively. In particular, using a Gamma process the coefficient of variation can be adjusted explicitly, thus allowing for the generation of regular and bursty processes.

RESULTS AND DISCUSSION

We observe that UD surrogates modify the ISI distribution of PPD and Gamma spike trains (approximately) into an exponential distribution. As a consequence, spike counts are reduced after binarization. By applying SPADE on the artificially generated data, we observe a high number of false positives when employing UD (see Figure 2). Thus, we conclude that UD is not a suitable surrogate technique for spike train data that either contains a dead-time or is regular. The alternative surrogate methods, instead, yield a consistently low number of false-positive patterns; between 8 and 15 FPs in 48 analyzed datasets (except for UDD on Gamma spike trains). In conclusion, since trial shifting is the simplest method among the best-performing ones, we recommend it as the method of choice.

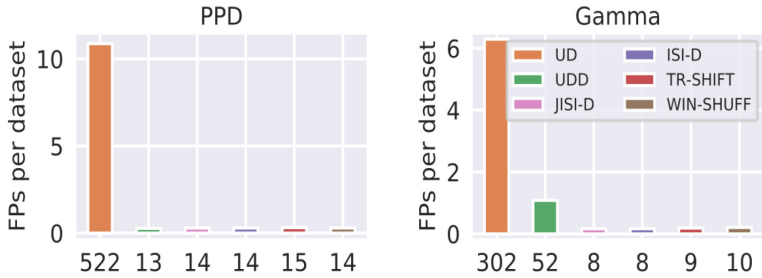

FIGURE 2: False-positive patterns in artificial data. The figure shows the number of false positives (FPs) detected per surrogate techniques (color-coded) normalized over the 48 data sets analyzed (y-axis), left for PPD and right for Gamma process data analyses. Numbers at the x-axis indicate the total number of FPs over all data sets per surrogate technique.

ACKNOWLEDGEMENTS

This project has received funding from the European Union's Horizon 2020 Framework Programme for Research and Innovation under Specific Grant Agreement No. 785907 (Human Brain Project SGA2), No. 945539 (Human Brain Project SGA3), from the Helmholtz Association Initiative and Networking Fund under project number ZT-I-0003, and from the Deutsche Forschungsgemeinschaft (DFG, German Research Foundation) - 368482240/GRK2416. We thank Sebastian Lehmann (SBC) for the help in the design and development of the graphics.

Keywords: spike patterns, surrogate techniques, motor cortex

REFERENCES

[1] Louis S, Borgelt C, Grün S. Generation and Selection of Surrogate Methods for Correlation Analysis. In: Rotter S, Grün S, editors. Analysis of Parallel Spike Trains. Berlin: Springer; 2010. p. 359–382.

[2] Quaglio P, Yegenoglu A, Torre E, Endres DM, Grün S. Detection and evaluation of spatio-temporal spike patterns in massively parallel spike train data with SPADE. Frontiers in computational neuroscience. 2017;11:41.

[3] Stella A, Quaglio P, Torre E, Grün S. 3d-SPADE: Significance evaluation of spatio-temporal patterns of various temporal extents. Biosystems. 2019;185:104022. doi:10.1016/j.biosystems.2019.104022.

[4] Gerstein GL. Searching for significance in spatio-temporal firing patterns. Acta Neurobiol Exp. 2004;64:203–207.

[5] Pipa, G., Wheeler, D. W., Singer, W., and Nikolie, D. (2008). NeuroXidence: reliable and efficient analysis of an excess or deficiency of joint-spike events. *J. Comput. Neurosci.* 25, 64–88. doi: 10.1007/s10827-007-0065-3

[6] Brochier T, Zehl L, Hao Y, Duret M, Sprenger J, Denker M, et al. Massively parallel recordings in macaque motor cortex during an instructed delayed reach-to-grasp task. Scientific Data. 2018;5:180055. doi:10.1038/sdata.2018.55.

Electroencephalographic and behavioural evaluation of visual attention capacity in deaf individuals

Raquel Marques[1]*, Diana Tavares[2,3], António Marques[3], Pedro Monteiro[3], António Correia[3]

[1]Clinical Physiology, School of Health, Polytechnic Institute of Porto, Porto, Portugal
[2]Coordinating Professor, Neurophysiology Scientific Area, School of Health, Polytechnic Institute of Porto, Porto, Portugal
[3]Psychosocial Rehabilitation Laboratory, Center for Rehabilitation Research, School of Health, Polytechnic Institute of Porto, Porto, Portugal
**raquelmarques99@hotmail.com*

INTRODUCTION/MOTIVATION

Hearing loss is a heterogeneous disease that affects about 5% of the world population [1]. Given the central nervous system's plasticity during the maturation period and congenital deaf individuals' visual dependence to interact with the environment, reorganization within intact sensory modalities is expected, especially in vision [2,3]. Compensatory changes resulting from deafness have been reported, particularly the improvement of peripheral visual attention capability [4,5,6]. In terms of behaviour, greater speed and accuracy in detecting peripheral stimuli (visual target) is described, and, in terms of electroencephalography (EEG), a more pronounced desynchronization of the alpha and beta band is associated with attention [7,8,9,10,13,15]. In this sense, we aimed to verify whether there are significant changes in visual attention capability between individuals with congenital or early deafness and individuals with normal hearing.

METHODS

This study was experimental, cross-sectional and descriptive. The participants were divided into the experimental group (congenital or early deafness), constituted by 4 participants, and control group (no auditory deficit), constituted by 7 participants. Each participant completed a selective attention task resorting to the immersive virtual reality equipment HTC vive, with

simultaneous recording of electroencephalographic activity in the parietal and occipital areas using the Biopac System MP36. The selective attention task consisted of a set of objects arranged in a circle. The target object appears in one of the positions of the circle and, inside or outside the circle, appears a second object, the distraction (Figure 1). The levels increase in difficulty when the target and the distraction are incongruent (different objects) and when the fill-in objets are congruent with the target/distraction (same color). The goal of the attention task is to identify which target is present (iogurt or coca-cola). Participants were instructed to ignore the distraction and identify the target as quickly and accurately as possible.

The procedure consisted of a rest period, in which an EEG recording was performed with the participant sitting comfortably, and a study period that corresponded to the EEG recording during the performance of the attention task. The EEG component was analyzed using the AcqKnowledge 5.0 software, in which we used the EEG Frequency Analyzes algorithm to obtain the power of the alpha band frequency. In the behavioral component, reaction time and response (correct or incorrect) were analyzed. Statistical analysis

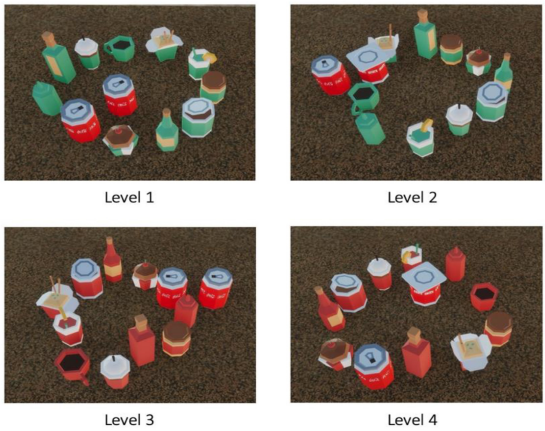

FIGURE 1: Attention Task Levels (image taken from the software of the attention task at the different levels).

was performed using the Statistical Package for Social Sciences (SPSS) 27 and Microsoft Excel 16.52 software.

RESULTS

A decrease in the alpha frequency power between before and during the attention task was observed in the electroencephalographic component. This decrease happened in both groups in the parietal region (experimental p = 0,125; control p = 0,286) and in the occipital region (experimental p = 0,080; control and p = 0,362). When comparing this decrease between both groups there was a statistically significant difference in the occipital region (p = 0,038), more prominent in deaf individuals. Despite not being statistically significant, the remaining electroencephalographic results also suggest a more considerable decrease in the alpha frequency power in the experimental group. In the behavioural component, the same was verified; although there was no statistically significant difference between the experimental and control groups, the results point to greater visual attention in the experimental group. When comparing the reaction time with the peripheral distraction between both groups we obtained a faster response in the experimental group (p = 0,088), the same was verified with the central distraction (p = 0,798).

DISCUSSION

This study was conducted during the COVID-19 pandemic. As a result, one of the most significant limitations we were met with was recruiting volunteers, particularly for the experimental group. Thus, the fact that most of the results found are not statistically significant is most likely due to the sample size, mainly in the experimental group. The electroencephalographic result obtained in the occipital region indicates a higher desynchronization in deaf individuals, which points to a higher visual attention [14,16]. The remaining results, in spite of not being statistically significant, suggest a higher visual attention capacity in deaf individuals as well [11,12]. Therefore, it is essential to carry out new investigations to overcome the limitations in this study, especially the sample size. It should be noted that the investigations focusing on the deaf community are a tool for their inclusion in society as they provide relevant information for the development of new teaching methods and vocational approaches valuing their capabilities, despite their limitations.

Keywords: Early Deafness, EEG, Visual Attention, Virtual Reality

REFERENCES

[1] Sheffield, A. M. & Smith, R. J. H. The epidemiology of deafness. Cold Spring Harb. Perspect. Med. 9, 1–16 (2019).

[2] Sladen, D. P., Tharpe, A. M., Ashmead, D. H., Grantham, D. W. & Chun, M. M. Visual Attention in Deaf and Normal Hearing Adults : Effects of Stimulus Compatibility. 48, 1529–1538 (2005).

[3] Neville, H. J., Schmidt, A. & Kutas, M. Altered visual-evoked potentials in congenitally deaf adults. Brain Res. 266 266, 127–132 (1983).

[4] Dye, M. W. G., Baril, D. E. & Bavelier, D. Which aspects of visual attention are changed by deafness? The case of the Attentional Network Test. *Neuropsychol. 45* 45, 1801–1811 (2007).

[5] Dye, M. W. G. & Bavelier, D. Attentional enhancements and deficits in deaf populations: An integrative review. *Restor. Neurol. Neurosci.* 28, 181–192 (2010).

[6] Bavelier, D., Dye, M. W. G. & Hauser, P. C. Do deaf individuals see better? *Trends Cogn. Sci.* 10, 21–23 (2006).

[7] Bavelier, D. & Hirshorn, E. A. I see where you're hearing: How cross-modal plasticity may exploit homologous brain structures. *Nat. Neurosci.* 13, 1309–1311 (2010).

[8] Neville, H. J. & Lawson, D. Attention to central and peripheral visual space in a movement detection task: an event-related potential and behavioral study. I. Normal hearing adults. *Brain Res.* 405, 253–267 (1987).

[9] Neville, H. J. & Lawson, D. Attention to central and peripheral visual space in a movement detection task: an event-related potential and behavioral study. II. Congenitally deaf adults. *Brain Res.* 405, 268–283 (1987).

[10] Verguts, T. & Notebaert, W. Adaptation by binding: a learning account of cognitive control. *Trends Cogn. Sci.* 13, 252–257 (2009).

[11] Proksch, J. & Bavelier, D. Changes in the spatial distribution of visual attention after early deafness. *J. Cogn. Neurosci.* 14, 687–701 (2002).

[12] Chen, Q., He, G., Chen, K., Jin, Z. & Mo, L. Altered spatial distribution of visual attention in near and far space after early deafness. *Neuropsychologia* 48, 2693–2698 (2010).

[13] Sinke, M. R. T. *et al.* The power of language: Functional brain network topology of deaf and hearing in relation to sign language experience. *Hear. Res.* 373, 32–47 (2019).

[14] Magosso, E., De Crescenzio, F., Ricci, G., Piastra, S. & Ursino, M. EEG alpha power is modulated by attentional changes during cognitive tasks and virtual reality immersion. *Comput. Intell. Neurosci.* 2019, 1–18 (2019).

[15] Marsella, P. *et al.* EEG activity as an objective measure of cognitive load during effortful listening: A study on pediatric subjects with bilateral, asymmetric sensorineural hearing loss. *Int. J. Pediatr. Otorhinolaryngol.* 99, 1–7 (2017).

[16] Quandt, L. C. & Willis, A. S. Earlier and More Robust Sensorimotor Discrimination of ASL Signs in Deaf Signers During Imitation. 1–48 (2020) doi:10.1101/2020.01.31.929208.

[17] Olk, B., Dinu, A., Zielinski, D. J. & Kopper, R. Measuring visual search and distraction in immersive virtual reality. *R. Soc. Open Sci.* 5, (2018).

[18] Eriksen, B. A. & Eriksen, C. W. Effects of noise letters upon the identification of a target letter in a nonsearch task. *Percept. Psychophys.* 16, 143–149 (1974).

Investigation of frontoparietal involvement to working memory functioning by transcranial direct current stimulation

Nikita Otstavnov[1,2]*, Nieto Doval Carlos Murielo[1], Stanislav Otstavnov[2], Matteo Feurra[1]

[1]Institute for Cognitive Neuroscience, High School of Economics, Moscow, Russia
[2]Laboratory of Public Health Indicators Analysis and Health Digitalization, Moscow Institute of Physics and Technology, Dolgoprudny, Russia
**Nikita.otstss@gmail.com*

INTRODUCTION/MOTIVATION

Working memory (WM) is the core cognitive phenomenon, which affects everyday life (Baddeley, 2010). It was shown that WM relies on several brain regions, however, the core areas were proposed to be frontal and parietal (Owen et al., 2005; Chein et al., 2011), which both constitute the frontoparietal network (FPN). The activity of FPN determines working memory capacity (WMC), which serves as a predictor of future academic success (Unsworth, Heitz, Schrock & Engle, 2005) and is usually a target for scientists attempting to increase capacity. One of the most promising tool to enhance WMC is transcranial direct current stimulation (tDCS). A large number of studies were conducted with this neurotechnique, however, their effect on WMC remains contradictory (Hill, Fitzgerald & Hoy, 2016). Moreover, no studies investigate the effect of simultaneous stimulation of both components of the frontoparietal network. Because of the inconsistency of tDCS results and lack of data about the effect of simultaneous stimulation of both frontal and parietal areas during working memory functioning, we conducted a study, where we compared the performance of working memory task for the groups with no stimulation, stimulation of one FPC component and both.

METHODS

We used tDCS to influence the performance during the operation span task. Forty-five participants were equally split into three stimulation groups: with simultaneous anodal stimulation of P3 and F3 brain areas (double stimulation

group) according to the 10/20 EEG system (Lagerlund et al., 1993), with anodal stimulation of only F3 area (single group) and with sham stimulation. We calculated with power analysis that 45 participants will be enough for the between-group design. The stimulation lasted fifteen minutes. After it, participants performed an operation span – complex working memory task, where respondents have to memorize a set of letters while simultaneously verifying mathematical equations (Turner & Engle, 1989). This task was shown to reveal good validity and reliability rates (Klein & Fiss, 1999) and allows precise measurement of domain-general WMC. We analyzed the effect of stimulation type on memory performance measured traditionally with mathematical accuracy inside it (Conway et al, 2005), to memory and mathematics separately, and to response time (time of calculation and time of recall). We considered separate results of memory and math in order to reveal a potential attentional bias to one of the tasks due to stimulation. Memory performance was calculated as partial credit scoring (PCS – the average ratio of correctly recalled items) and partial credit load scoring (PCLS – the average number of correctly recalled items). We applied one-way (between-group factor – stimulation type) and two-way (between-group factors – stimulation type and span size) ANOVA to reveal any possible effects. We hypothesized that stimulation of only one component of FPN will increase WMC in comparison to sham stimulation. The stimulation of the second component will increase WMC significantly higher in comparison to both single and sham groups, which will indicate that the two components of FPN are functioning as separate units.

RESULTS

There was no difference in mathematical accuracy (Fig. 1) and time of calculation among the three groups (Fig. 2). Memory performance was impaired in the single stimulation group compared to both sham and double groups only if we consider no mathematics inside memory measurements (Fig. 1) for both one-way ANOVA (p-value_PCS = 0.0041, p-value_PCLS = 0.0137) and two-way ANOVA (p-value_PCS = 5.64e-07, p-value_PCLS = 2.8e-05). A significant effect of tDCS was observed for memory performance without math in span sizes "four" and "six". The time of recall showed a trend for a decrease in the single stimulation group in comparison to others (Fig. 2) according to one-way ANOVA (p-value_t_recall = 0.0738) and was significant for spans "five" and "six" in two-way ANOVA (p-value_t_recall = 0.000986). The difference between other measurements remains not significant.

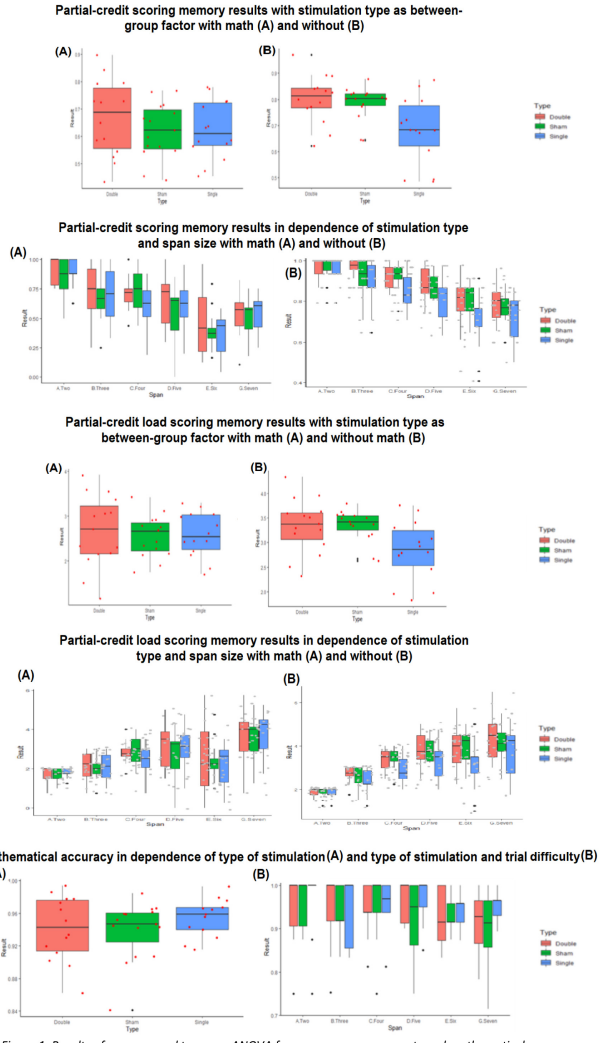

FIGURE 1: Results of one-way and two-way ANOVA for memory measurements and mathematical accuracy.

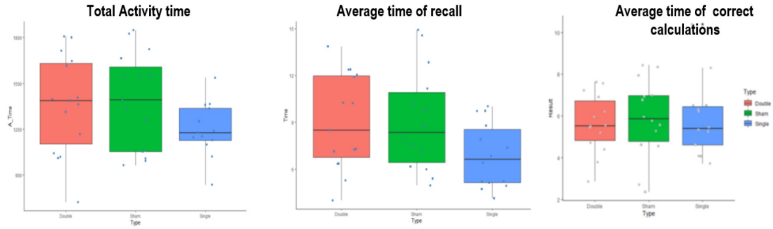

FIGURE 2: Results of one-way ANOVA for the time of performing the experiment.

DISCUSSION

The results go beyond our initial hypothesis that stimulation will improve WMC. In the experiment, memory results without math were impaired only after a single stimulation, but not double. We assume that such effect was observed due to desynchronization of the components of the FPN, which was restored in case we apply the same stimulation protocol to the second component (P3). Thus, the results indicate that the frontoparietal network functions as not a single cognitive unit, but as two separate and highly interconnected neuronal units. By modulating the synchrony of the components of the FPN by tDCS, we were able to modulate working memory capacity during the operation span task. This explanation goes in line with several investigations, where the synchronization between brain areas, which are responsible for particular cognitive function, was important for task success (Hill, Rogasch, Fitzgerald & Hoy, 2018; Luria, 1966). We suggest that frontoparietal desynchronization manifests itself on a cognitive level by an attentional shift towards easier tasks (math) or impaired inhibition of irrelevant thoughts, which impair memory performance. Both explanations allow understanding the presence of tDCS effect to memory, but not mathematics.

ACKNOWLEDGEMENTS

This study has been carried out using HSE unique equipment (Reg. num 354937). Supported by the RF Government grant ag. No 075-15-2021-673

Keywords: transcranial direct current stimulation, working memory, frontoparietal network, operation span, working memory capacity, multicomponent model, ANOVA, high-definition transcranial direct current stimulation

REFERENCES

[1] Baddeley, A. (2010). Working memory. Current Biology, 20(4), R136-R140. http://dx.doi.org/10.1016/j.cub.2009.12.014

[2] Chein, J. M., Moore, A. B., & Conway, A. R. A. (2011). NeuroImage domain-general mechanisms of complex working memory span. Neuroimage 54, 550–559. http://dx.doi.org/10.1016/j.neuroimage.2010.07.067

[3] Conway, A., Kane, M., Bunting, M., Hambrick, D., Wilhelm, O., & Engle, R. (2005). Working memory span tasks: A methodological review and user's guide. Psychonomic Bulletin & Review, 12(5), 769-786. http://dx.doi.org/10.3758/bf03196772

[4] Hill, A., Fitzgerald, P., & Hoy, K. (2016). Effects of Anodal Transcranial Direct Current Stimulation on Working Memory: A Systematic Review and Meta-Analysis of Findings from Healthy and Neuropsychiatric Populations. Brain Stimulation, 9(2), 197-208. http://dx.doi.org/10.1016/j.brs.2015.10.006

[5] Hill A., Rogasch N., Fitzgerald P., & Hoy K. (2018). Effects of single versus dual-site High-Definition transcranial direct current stimulation (HD-tDCS) on cortical activity and working memory performance in healthy subjects. Brain Stimulation, 11(5), 1033-1043. http://dx.doi.org/10.1016/j.brs.2018.06.005

[6] Klein, K., & Fiss, W. H. (1999). The reliability and stability of the Turner and Engle working memory task. Behavior Research Methods, Instruments & Computers, 31(3), 429–432. https://doi.org/10.3758/BF03200722

[7] Lagerlund, T., Sharbrough, F., Jack, C., Erickson, B., Strelow, D., Cicora, K., & Busacker, N. (1993). Determination of 10–20 system electrode locations using magnetic resonance image scanning with markers. Electroencephalography And Clinical Neurophysiology, 86(1), 7-14. http://dx.doi.org/10.1016/0013-4694(93)90062-z

[8] Luria, A. (1966). Higher cortical functions in man. New York: Basic Books.

[9] Owen, A. M., McMillan, K. M., Laird, A. R., & Bullmore, E. (2005). N-back working memory paradigm: a meta-analysis of normative functional neuroimaging studies. Hum. Brain Mapp. 25, 46–59. http://dx.doi.org/10.1002/hbm.20131

[10] Turner, M. L., & Engle, R. W. (1989). Is working memory capacity task dependent? Journal of Memory and Language, 28(2), 127–154. https://doi.org/10.1016/0749-596X(89)90040-5

[11] Unsworth, N., Heitz, R. P., Schrock, J. C., & Engle, R. W. (2005). An automated version of the operation span task. Behavior Research Methods, 37(3), 498–505. http://dx.doi.org/10.3758/BF03192720

Focused Ion Bean/Scanning electron microscopy on the study of the human entorhinal cortex

Sergio Plaza-Alonso[1,2,3]*, Nicolás Cano-Astorga[1,2,3], Javier DeFelipe[1,2,3], Lidia Alonso-Nanclares[1,2,3]

[1]Laboratorio Cajal de Circuitos Corticales, Centro de Tecnología Biomédica, Universidad Politécnica de Madrid, Madrid, Spain
[2]Instituto Cajal, Consejo Superior de Investigaciones Científicas (CSIC), Madrid, Spain
[3]Centro de Investigación Biomédica en Red sobre Enfermedades Neurodegenerativas (CIBERNED), Instituto de Salud Carlos III, Madrid, Spain
**serplalo@cajal.csic.es*

INTRODUCTION/MOTIVATION

Over the last century, neuroscience has struggled to understand how synaptic organization contributes to the functional organization of the brain. Traditionally, most of the studies regarding the synaptology of human brain have been performed using conventional electron microscopy and stereological methods on single, two-dimensional tissue sections. However, these methods carry several major issues, since the identification and classification of synapses often represent a difficult task, which led to an erroneous characterization of the synaptic organization (1) Furthermore, previous electron microscope studies have reported differences in the synaptic organization in different cortical regions and layers (2–8). In the present study, we have focused on the synaptology of layer V of the human entorhinal cortex (EC), a crucial region located in the medial temporal lobe, essential for memory functions and spatial navigation (9). To this end, we have used Focused Ion Bean / Scanning Electron Microscopy (FIB/SEM). This methodology provides a large number of serial sections of the neuropil at an ultraestructural resolution, allowing 3D reconstruction of synapses, in which the synaptic organization could be accurately performed (10).

METHODS

Human brain tissue was obtained from autopsies from 2 males and 1 female subjects (supplied by Unidad Asociada Neuromax, Laboratorio de

Neuroanatomía Humana, Facultad de Medicina, Universidad de Castilla-La Mancha, Albacete, Spain), and processed for electron microscopy as detailed elsewhere (3,5). The 3D study of the samples was carried out using a dual-beam microscope (Crossbeam® 540 electron microscope, Carl Zeiss NTS GmbH, Oberkochen, Germany), which combines a high-resolution field-emission SEM column with a focused gallium ion beam (FIB). This allows the removal of thin layers of material from the sample surface on a nanometer scale. After removal, the exposed surface of the sample is imaged by the SEM. The sequential automated use of FIB milling and SEM imaging allowed us to obtain long series of photographs of a 3D sample on selected regions (10). A total of 9 stacks of FIB/SEM images of the EC layer V neuropil were obtained and analyzed using EspINA software (Figure 1) (11). Synapses were fully 3D reconstructed and classified as asymmetric (AS or type I) or symmetric (SS or type II), based on the thickness of the post-synaptic density (12,13). In addition,

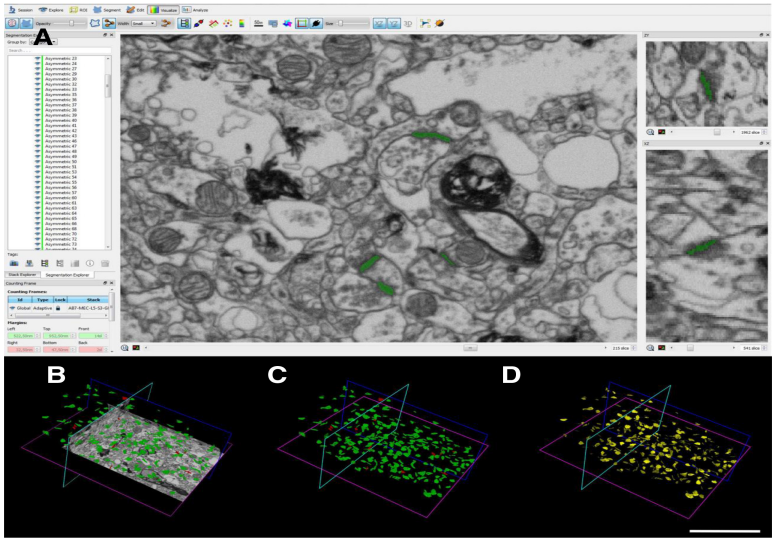

FIGURE 1: Screenshots of the EspINA software user interface. (**A**) In the main window, sections are viewed through the xy plane. Orthogonal planes (yz and xz) are also shown in the adjacent windows (right). (**B**) Three orthogonal planes and the 3D reconstruction of asymmetric (in green) and symmetric (in red) segmented synapses. (**C-D**) 3D-segmented synapses (C), and their computed SAS (D, in yellow). Scale bar (B-D): 6μm.

geometrical features (size and shape) of the synapses were determined using EspINA software, which extracts the Synaptic Apposition Surface (SAS) and provides its morphological measurements (Figure 1) (14). Finally, postsynaptic elements of the synapses were also studied with EspINA software.

RESULTS AND DISCUSSION

The present study constitutes a detailed description of the synaptology of human EC layer V. Data are based on the study of a large number of synapses (1334), fully reconstructed in 3D at the ultraestructural level. In those synapses, we analyzed the following parameters:

-Synaptic Density and Proportion of Excitatory and Inhibitory Synapses: Synaptic density values were obtained by dividing the total number of synapses identified and included within a stereological counting frame (CF) by the total volume of the CF. The average synaptic density of the EC layer V was 0.39 synapses/μm^3 and he proportion of AS:SS was 95:5.

-Synaptic Size: The study of the synaptic size was performed analyzing the area of the SAS of each synapse reconstructed. In layer V, the average of the SAS for the AS was 122 071 nm^2, and 73 713 nm^2 in the case of SS. Thus, the SAS of AS were significantly larger than SS (Mann Whitney, <0.0001).

-Synaptic Shape: Synapses were classified into four categories: macular, perforated, horseshoe-shaped or fragmented (detailed in (7). 80.2% of the synapses presented a macular morphology, followed by 16.4% perforated, 2% horseshoe-shaped and 1.4% fragmented (Figure 2). Since the vast majority of synapses presented a macular shape, we determined the proportions of AS and SS for that particular morphology, revealing that, of the total macular synapses, 96% were AS and 4% were SS.

-Postsynaptic Elements: Postsynaptic targets were identified and classified as spines and dendritic shafts. When the postsynaptic element was a spine, we distinguished the location of the synapse on the neck or on the head of this spine. When the postsynaptic element was identified as a dendritic shaft, it was classified as spiny or non-spiny, according to the presence or

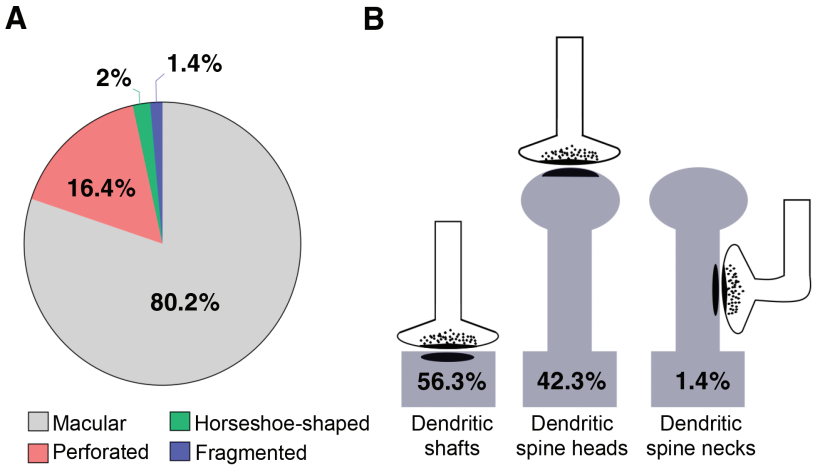

FIGURE 2: Analysis of synaptic shape and postsynaptic elements in Human EC layer V. (**A**) Proportion of the different synaptic shapes. Most of the synapses (80%) show a macular morphology. (**B**) Schematic representation of the distribution of all synapses on different postsynaptic targets: on dendritic shafts (including both spiny and non-spiny shafts), dendritic spine heads and dendritic spine necks.

not of spines (3). Most synapses were established on dendritic shafts (56.3%, 27.1% on spiny shafts and 29.2% on non-spiny shafts), followed by a 42.3% established on spine heads and a 1.4% on spine necks (Figure 2).

Further analyses are currently ongoing, which will both complete the synaptic study of layer V and include new layers, in order to provide a detailed description of the synaptology of the human EC. In any case, these results highlight the importance of the methodological approach presented here, which guarantees a precise characterization of the synaptic structure, avoiding most of the problems associated with traditional methods (1,10). The characterization of synaptic structure is crucial for a better understanding of synaptic function. For instance, differences in the excitatory/inhibitory balance are influenced by changes in the proportions of AS and SS synapses (15). Likewise, synaptic size and shape correlate with synaptic strength and

plasticity (16,17). Therefore, the use of this experimental approach is essential to fully understand the microcircuits that shape human brain and its functional organization, both in health and disease.

Keywords: Enthorinal Cortex, electron microscopy, FIB-SEM, neuropil, synaptology

REFERENCES

[1] DeFelipe J, Marco P, Busturia I, Merchán-Pérez A. Estimation of the number of synapses in the cerebral cortex: methodological considerations. Cereb Cortex. 1999;9(7):722–32.

[2] Montero-Crespo M, Domínguez-Álvaro M, Alonso-Nanclares L, DeFelipe J, Blazquez-Llorca L. Three-dimensional analysis of synaptic organization in the hippocampal CA1 field in Alzheimer's disease. Brain. 2021 Mar;144(2):553–73.

[3] Domínguez-Álvaro M, Montero-Crespo M, Blazquez-Llorca L, DeFelipe J, Alonso-Nanclares L. 3D Ultrastructural Study of Synapses in the Human Entorhinal Cortex. Cereb Cortex. 2021 Jan;31(1):410–25.

[4] Domínguez-álvaro M, Montero-Crespo M, Blazquez-Llorca L, Plaza-Alonso S, Cano-Astorga N, Defelipe J, et al. 3D Analysis of the Synaptic Organization in the Entorhinal Cortex in Alzheimer'S Disease. eNeuro. 2021 Jan 1;8(3):2020.10.19.345025.

[5] Montero-Crespo M, Dominguez-Alvaro M, Rondon-Carrillo P, Alonso-Nanclares L, DeFelipe J, Blazquez-Llorca L. Three-dimensional synaptic organization of the human hippocampal CA1 field. Elife. 2020 Jul;9.

[6] Domínguez-Álvaro M, Montero-Crespo M, Blazquez-Llorca L, Insausti R, DeFelipe J, Alonso-Nanclares L. Three-dimensional analysis of synapses in the transentorhinal cortex of Alzheimer's disease patients. Acta Neuropathol Commun. 2018;6(1):20.

[7] Dominguez-Alvaro M, Montero-Crespo M, Blazquez-Llorca L, DeFelipe J, Alonso-Nanclares L. 3D Electron Microscopy Study of Synaptic Organization of the Normal Human Transentorhinal Cortex and Its Possible Alterations in Alzheimer's Disease. eNeuro. 2019;6(4).

[8] Cano-Astorga N, DeFelipe J, Alonso-Nanclares L. Three-Dimensional Synaptic Organization of Layer III of the Human Temporal Neocortex. Cereb Cortex. 2021 May;

[9] Schultz H, Sommer T, Peters J. The Role of the Human Entorhinal Cortex in a Representational Account of Memory. Front Hum Neurosci. 2015;9:628.

[10] Merchan-Perez A, Rodriguez J-R, Alonso-Nanclares L, Schertel A, Defelipe J. Counting Synapses Using FIB/SEM Microscopy: A True Revolution for Ultrastructural Volume Reconstruction. Front Neuroanat. 2009;3:18.

[11] Morales J, Alonso-Nanclares L, Rodríguez J-R, Defelipe J, Rodríguez A, Merchán-Pérez A. Espina: a tool for the automated segmentation and counting of synapses in large stacks of electron microscopy images. Front Neuroanat. 2011 Mar 18;5:18.

[12] GRAY EG. Axo-somatic and axo-dendritic synapses of the cerebral cortex: an electron microscope study. J Anat. 1959 Oct;93(Pt 4):420–33.

[13] Peters A, Palay SL. The morphology of synapses. J Neurocytol. 1996 Dec;25(12):687–700.

[14] Morales J, Rodríguez A, Rodríguez J-R, Defelipe J, Merchán-Pérez A. Characterization and extraction of the synaptic apposition surface for synaptic geometry analysis. Front Neuroanat. 2013;7:20.

[15] Froemke RC. Plasticity of cortical excitatory-inhibitory balance. Annu Rev Neurosci. 2015 Jul;38:195–219.

[16] Ganeshina O, Berry RW, Petralia RS, Nicholson DA, Geinisman Y. Differences in the expression of AMPA and NMDA receptors between axospinous perforated and nonperforated synapses are related to the configuration and size of postsynaptic densities. J Comp Neurol. 2004 Jan 1;468(1):86–95.

[17] Biederer T, Kaeser PS, Blanpied TA. Transcellular Nanoalignment of Synaptic Function. Neuron. 2017;96(3):680–96.

Does backpropagation yield the underlying solution used by the brain?

Meghana Gayatri Potta*, Pau Vilimelis Aceituno, Benjamin F. Grewe

Institute of Neuroinformatics, University of Zürich and ETH Zürich, Zürich, Switzerland
**mpotta@ini.uzh.ch*

INTRODUCTION/MOTIVATION

Artificial Recurrent Neural Networks (RNNs) are increasingly used in neuroscience research to explain neurobiological phenomena while considering the architectural and computational constraints of biological networks. Such an approach aims to train an RNN using machine learning tools and then compare it to the network dynamics observed in the brain [1]. Credit assignment in RNNs is classically performed using backpropagation-through-time (BPTT), the temporal analog of the standard backpropagation-of-error algorithm [2]. However, it remains unclear if BPTT learns solutions to dynamic problems similar to those employed by the brain, particularly because deep learning algorithms are often considered black boxes [3]. In this work, we aim to address this fundamental algorithmic question for learning dynamic time series by exploring the spectral structure of RNNs trained via BPTT on temporal tasks. Specifically, we take single-variable time-series processing tasks and compare the solutions found by BPTT against solutions based on feedback loops. Since feedback loops are widely used in control theory [4], are known to be efficient in time-series processing [5], and are also very prominent in neuroscience [8-11], particularly cortical circuits [12], they are ideal candidates for this comparison.

METHODS

Teacher forcing is a technique that is frequently used in dynamical supervised learning tasks where the model (student) receives the ground truth output d(t) (teacher) as input in the subsequent computation of the behaviour of the network [13]. In a biological context, this learning paradigm corresponds to an agent that tries to imitate the responses of another agent by observing its

inputs and outputs. In our context, this framework allows us to design tasks that we understand perfectly, and since the teacher and student are both neural networks with the same activation function, we also know that the student is, in principle, capable of imitating the teacher flawlessly. We employ such a teacher-student model where a teacher network is generated and given Gaussian noise as input, and the student network is trained via the BPTT algorithm to apply the same function as the teacher. In our case, we consider linear systems that process input time-series through feedback loops.

In linear and linearizable networks, a system with feedback loops is fully characterized by its poles, which can be realized as the eigenvalues of the weight matrix of a linear neural network (see Fig. 1). As multiple weight matrices can implement the same dynamics by having identical eigenvalues, we compare teacher and student networks not by their network structure but by their eigenvalues representing their primary modes of activity. We find that BPTT rarely finds the same eigenvalues for the student network as the teacher, implying that the networks are fundamentally different despite implementing a similar function. Interestingly, only when network resources are increased, i.e., the number of neurons is much larger than the number of poles, can BPTT find the right solution. Additionally, the eigenvalues found by BPTT tend to be real even if the teacher has complex eigenvalues.

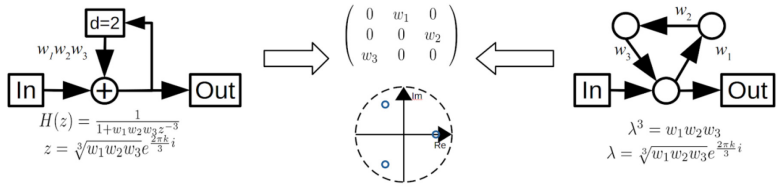

FIGURE 1: Simple example of the relationship between poles and eigenvalues: A feedback loop system with a delay of two and feedback weight w1 w2 w3 with its corresponding transfer function H(z) (left) can be implemented as a cycle of length 3 with weights w1 w2 w3 characterized by its eigenvalues $\boldsymbol{\lambda}$ (right) and the poles of the transfer function are given by the eigenvalues of the adjacency matrix (center). The plot in the complex plane thus represents the poles (or eigenvalues) of this system.

RESULTS AND DISCUSSION

Our first results illustrate that BPTT finds solutions that can obtain good performances in different temporal tasks, but it does so via network structures that do not always align with the feedback loop architecture (Fig. 2). This is especially true for tasks where the order of the underlying filter is high (see Fig. 2c), implying that BPTT might not be ideally suited to model temporally very complex systems as often observed in the real world. Thus, our results add to the evidence [14] that the brain does not use backpropagation-through-time for time-series learning. Moreover, since the identified analytical solutions are known to be efficient both in theory and in practice, and we also know that biology uses feedback loops for control [6-9], we should be careful when using BPTT to understand recurrent biological networks.

Lastly, our results also generalize the limitations of BPTT to other domains. For instance, to enable good learning performance, the size of an RNN needs to increase very fast with the order of the system to be imitated. This makes it generally difficult for small embedded applications and neural systems based on small RNNs. Furthermore, since the design of stable systems requires understanding the poles and eigenvalues of constituent systems [4], our work might help design RNNs for fields with critical failures to ensure the stability of performance guarantees. In future work, we plan to extend RNN training to more complex tasks, like forecasting chaotic time-series, and then

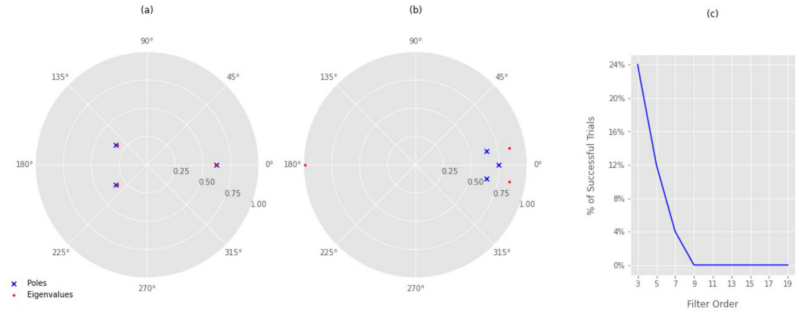

FIGURE 2: (**a**) and (**b**) show two examples of RNNs trained with BPTT (red dots) and compared with the original teacher (blue crosses). In (a), the network has eigenvalues matching the teacher poles, thus can implement the exact function. In (b), the eigenvalues do not align; thus, the network differs. Finally, in (**c**), we show the number of successful trials where BPTT finds the analytical solution structure (from 25 trials where the number of poles equals the number of neurons).

use our results to improve artificial RNNs by adding the required feedback structure, a known method to improve RNN performance [15] without BPTT.

Keywords: Recurrent Neural Networks, Backpropagation-through-time, Time Series Prediction, Feedback Loops, Cybernetics

REFERENCES

[1] Mante, V., Sussillo, D., Shenoy, K. V. and Newsome, W. T. (2013). Context-dependent computation by recurrent dynamics in prefrontal cortex. Nature, 503(7474):78–84.

[2] Pascanu, R., Mikolov, T. and Bengio, Y. (2013). On the difficulty of training recurrent neural networks. In ICML, III–1310–III–1318.

[3] Castelvecchi, Davide. "Can we open the black box of AI?." Nature News 538.7623 (2016): 20.

[4] Doyle, John C., Bruce A. Francis, and Allen R. Tannenbaum. Feedback control theory. Courier Corporation, 2013

[5] Rabiner, Lawrence R., and Bernard Gold. "Theory and application of digital signal processing." Englewood Cliffs: Prentice-Hall (1975).

[6] Callaway, Edward M. "Feedforward, feedback and inhibitory connections in primate visual cortex." Neural Networks 17.5-6 (2004): 625-632.

[7] Douglas RJ, Koch C, Mahowald M, Martin K, Suarez H (1995) Recurrent excitation in neocortical circuits. Science 269: 981–985.

[8] Shao, Zhengwei, and Andreas Burkhalter. "Different balance of excitation and inhibition in forward and feedback circuits of rat visual cortex." Journal of Neuroscience 16.22 (1996): 7353-7365.

[9] Wiener, Norbert, and Johannes Petrus Schade. Cybernetics of the nervous system. Elsevier, 1965.

[10] Maass, Wolfgang, Prashant Joshi, and Eduardo D. Sontag. "Computational aspects of feedback in neural circuits." PLoS computational biology 3.1 (2007): e165.

[13] R. J. Williams and D. Zipser, "A Learning Algorithm for Continually Running Fully Recurrent Neural Networks," in Neural Computation, vol. 1, no. 2, pp. 270-280, June 1989, doi: 10.1162/neco.1989.1.2.270.

[14] Lillicrap, Timothy P., et al. "Backpropagation and the brain." Nature Reviews Neuroscience 21.6 (2020): 335-346.

[15] Aceituno, Pau Vilimelis, Gang Yan, and Yang-Yu Liu. "Tailoring Echo State Networks for Optimal Learning." iScience 23.9 (2020).

Deep phenotyping to build inter-subject alignments using optimal transport

Alexis Thual[1,2,3,*], Bertrand Thirion[3], Stanislas Dehaene[1,2]

[1]Neurospin, CEA, Gif-sur-Yvette, France
[2]Inserm, Collège de France, Paris, France
[3]Mind, Inria Paris-Saclay, Palaiseau, France
**alexis.thual@cea.fr*

INTRODUCTION/MOTIVATION

Between-subject brain variability in shape and function is a major challenge to the definition of accurate brain models [1, 2]. It also obscures the comparison between species. Recently, precision mapping has started to provide data to ground the definition of accurate brain models [3]. Yet technology has been missing to identify correspondences between brains. Leveraging Optimal Transport (OT) methods [5, 6], we derive an algorithm, denoted as Fused Unbalanced Gromov Wasserstein (FUGW), to compute whole-brain mappings between subjects with minimal anatomical priors, and provide a fast GPU-based Python implementation. We apply it to the Individual Brain Charting (IBC) dataset - a collection of more than 200 maps of functional activations (contrasts) acquired in each of the 12 human subjects [4]. We also provide a web-based tool to explore IBC as well as derived mappings. This is ongoing work and we intend to later on (a) run these methods on other MRI datasets, including resting state and naturalistic stimuli and (b) to assess the existence of cortical reorganisations between species, pushing forward recent efforts made in cross-species comparisons [8, 9, 10].

METHODS

In short, a contrast map for a given subject represents the activity of each part of the cortex after the subject has been exposed to a specific stimulus (for instance seeing an image of a familiar human face, hearing a complex sentence, or hearing mathematical assertions). As illustrated in Figure 1, anatomies from one human subject to another vary greatly, as well as the activation maps elicited by similar stimulus. Alignment aims at alleviating these differences. Like other methods, FUGW focuses on building mappings for surface-sampled contrasts, which we obtain by projecting volume-based fMRI

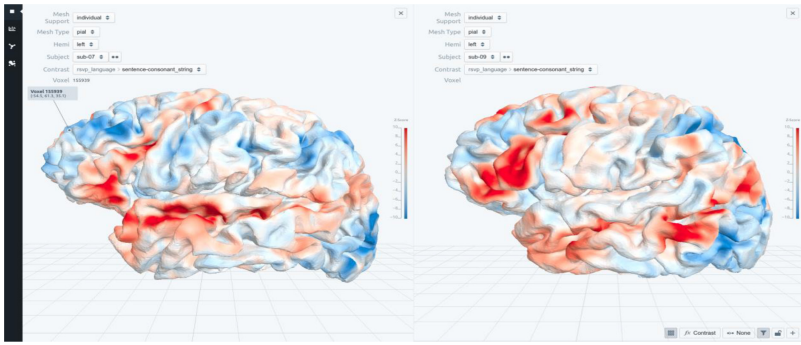

FIGURE 1: Brain-cockpit, a web-based visualisation tool to explore the training dataset as well as derived mappings Contrast maps elicited by listening to complex sentences are shown for 2 subjects of the IBC dataset. Parts in red (blue) are activated (deactivated) compared to the rest of the brain. Contrast maps are measured in z-score.

data using Freesurfer [11]. We compare several methods to build mappings between cortical surfaces. We identify three main categories of methods:

1. topologically-loose methods such as point-wise nearest neighbours, which map source and target cortical areas based on functional information only (contrast map) without taking anatomical information into account
2. well known diffeomorphic methods such as Procrustes [12], Multimodal Surface Matching (MSM) [7] or spherical daemon [13], which align source and target subjects based on function information while enforcing derived mapping to be continuous between surfaces
3. FUGW, which we advocate is a combination of the two previous categories, as it doesn't enforce diffeomorphicity between source and target surfaces but only fosters it

In order to compare them, we systematically evaluate the relevance of derived mappings by (a) quantitatively assessing how well they transfer unseen contrasts and (b) qualitatively looking at the cortical reorganisation they induce between subjects through a dedicated web-based interactive visualisation tool. Our process is the same for all methods: one derives a mapping function for every pair of source and target subject of IBC using a set of training contrasts (see Figure 2.A). This function can then be used to map test contrasts

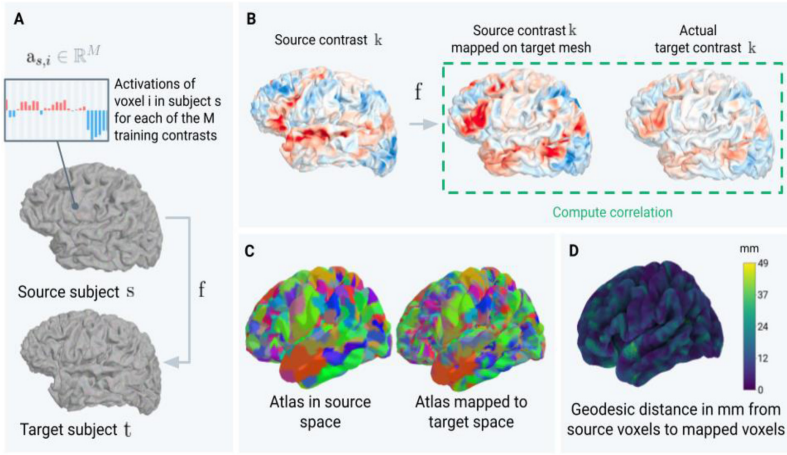

FIGURE 2: Aligning individuals using large functional datasets with OT (**A**) UFGW derives an invertible function f mapping a source mesh to a target mesh (respectively of size Vs and Vt) which tries to maximize the correspondence between activation patterns ai observed in each voxel while preserving the topology of both meshes. (**B**) Applying f to unseen contrasts and comparing the result with actual contrasts allows to assess the relevance of f. (**C**) f can be used to transport atlases between subjects, which qualitatively shows that the global topology of the cortex is preserved between human subjects. (**D**) When source and target meshes are the same (here, fsaverage5 [11]), computing geodesic distance between source and mapped voxels shows which parts of the cortex show higher anatomical variability.

from the source anatomy to the target anatomy. Computing correlation between these mapped contrasts and the actual target contrast allows us to derive a metric to compare these methods (see Figure 2.B). Manually exploring derived mappings also helps assessing their anatomical relevance: one can map atlases from source to target (see Figure 2.C), measure distance on the cortex between mapped points in some specific case (see Figure 2.D), or explore them in our viewer.

RESULTS AND DISCUSSION

Topologically-loose methods correctly align primary areas of the cortex between subjects, but fail to correctly map areas involved in more complex tasks. Classical OT methods (simple Wasserstein distance) with no anatomical

priors yield similar results. These can be greatly improved by adding little topological constraints on the derived mappings (which is what FUGW does). Contrast maps transferred from source subjects to target subjects using these functions show high correlation with contrast maps acquired for these target subjects. On top of being computationally very efficient and easy to deploy, FUGW outperforms other alternatives. It makes it possible to capture subtle changes between individuals, such as the size and shape of functional areas or their position relative to other areas. Our visualisation tool facilitates exploring these changes. Moreover, as our method is not based on anatomical landmarks, it is particularly suited for cross-species comparisons (e.g. human vs. macaques).

Keywords: fmri, subject alignment, optimal transport, inter-subject variability, surface-based analysis

REFERENCES

[1] Fedorenko et al. 2011 doi.org/c29hx7
[2] Glasser et al. 2016 doi.org/f8z3gb
[3] Naselaris et al. 2021 doi.org/ghvf8c
[4] Pinho et al. 2018 doi.org/gdp4q2
[5] Séjourné et al. 2021 arxiv.org/abs/2009.04266
[6] Vayer et al. 2020 doi.org/g6kw
[7] Robinson et al. 2014 doi.org/gc96pn
[8] Mantini et al. 2012 doi.org/gf4q53
[9] Xu et al. 2019 doi.org/gg3xn4
[10] Eichert et al. 2020 doi.org/gg3xqr
[11] Fischl 2012 doi.org/fzcbq3
[12] Haxby et al. 2020 doi.org/ggx5j2
[13] Yeo et al. 2010 doi.org/bnxjvx

Finding order in thousands of fully reconstructed long-range projection neurons in the mouse brain

Nestor Timonidis[1]*, Rembrandt Bakker[1,2]*, Maria Carla Piastra[3], Maria Garcia-Amado[4], Mario Rubio[4], Francisco Clasca[4], Paul Tiesinga[1]

[1]Department of Neuroinformatics, Radboud University Nijmegen, Donders Institute for Brain, Cognition and Behaviour, Nijmegen, The Netherlands
[2]Inst. of Neuroscience and Medicine (INM-6) and Inst. for Advanced Simulation (IAS-6) and JARA BRAIN Inst. I, Jülich, Germany
[3]Department of Clinical Neurophysiology, University of Twente, Institute for Technical Medicine, Technical Medical Centre, Enschede, The Netherlands
[4]Department of Anatomy and Neuroscience, Autónoma de Madrid University, School of Medicine, Madrid, Spain
**nestor.timonidis@donders.ru.nl (*) equal contribution*

INTRODUCTION/MOTIVATION

The past decade has seen a tremendous development of connectomics approaches [1], but most of them cannot bridge the gap between the micro-scale level of single-cell resolution and the meso-scale level of whole-brain bulk axonal projections. Electron microscopy [2] and direct synaptic labeling [3] cannot scale up to the whole brain level, while anatomical tract-tracing [4] and diffusion tensor imaging [5] cover the whole brain but lack single-cell resolution. One way to bridge the gap could be given by automated tissue-to-volume reconstructions of single-neurons based on fluorescence micro-optical sectioning tomography (fMOST) [6] or light-sheet fluorescence microscopy [7]. However, fully automated techniques are inadequate to precisely identify the brain areas, cortical layers and subcortical nuclei of the axonal tree terminals, when compared to manually traced neuronal reconstructions. The reason is that automated techniques do not allow experimenters to place a reconstructed neuron in a reference atlas, curate the position of each soma, dendrites or axonal terminals, and compare the final outcome with the original experimental tissue. Moreover, tens of thousands of neuronal reconstructions are needed to reach a whole-brain coverage similar to [4]. As a consequence, we have developed a tool for searching similar neurons across databases, based on their axonal morphology and registration coordinates, and correcting the cortical layer distribution patterns. As a use-case, we compare neurons from high-throughput databases with a small repository of manually traced and precisely placed neurons from a recently developed pipeline.

This pipeline labels single-neurons according to [10], followed by manual reconstruction using Neurolucida [11] and registration to the volumetric space of the Allen Common Coordinate Framework v. 3.0 [12]. Finally, the neuron is shifted towards or away from the cortical surface to bring the manually annotated layer borders as close as possible to those of the atlas.

METHODS

We compared two sources of reconstructed neurons from the large online repositories of MouseLight [8]. and Braintell [9] (labeled as high throughput neurons), with a smaller one produced by an in-house pipeline that is currently under development (labeled as 'reference' neurons). We first load each reference neuron as a 4D point cloud, with the first three dimensions representing the spatial coordinates and the fourth one representing the distance from the soma. We then use an API to download all high throughput neurons whose soma distance from the reference neuron is lower than a given threshold. We then apply the Coherent Point Drift (CPD) method [13] to compare all neuronal pairs through a two-step registration process. Initially, CPD finds the missing correspondences between the two neurons by minimizing the negative log-likelihood that the reference neuron's point cloud was sampled from the distribution of the high throughput one, as modelled by a Gaussian Mixture Model. Subsequently, CPD applies a rigid transformation of the high throughput point-cloud to the reference one (Fig. 1). We thus select the high

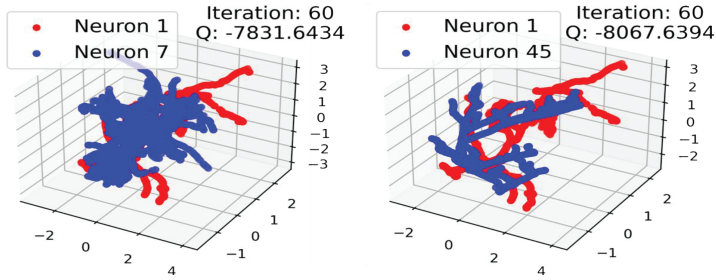

FIGURE 1: Two examples of rigid registration using the Coherent Point Drift (CPD) algorithm [13], specifically of high throughput Neurons 7 (a) and 45 (b) to reference Neuron 1. After 60 rounds of iteration, the minimum negative log-likelihood that Neuron 1 has been sampled from the distribution of Neuron 7 or of Neuron 45 is –7079 or –8067, respectively. Blue color: axonal branches of Neurons 7 (a) and 45 (b). Red color: axonal branches of Neuron 1 (both panels). All three axonal reconstructions have been retrieved from the Mouselight repository [8].

throughput neuron with the minimum negative log-likelihood as the neuronal match. Lastly, we load the SBA composer [14] tool to visually compare all selected pairs in 3D.

RESULTS AND DISCUSSION

Our approach represents a significant extension to existing tools, since the extent of the full axonal tree, instead of only regions of interest, is taken into account. Moreover, it is applicable to neurons reconstructed in smaller laboratories and allows for integration with other similarly registered datasets. The pipeline is expected to be updated before the end of the year with one-to-one matches of reconstructed neurons between our repository and the Mouselight and Braintell ones. In addition, we intend to compare the matches in terms of coverage in brain areas, cortical layers and subcortical nuclei. With the integration of neuronal reconstructions from multiple datasets, we will proceed to a number of future steps. We intend to translate the reconstructed axonal morphologies into a statistical model for the underlying axonal projections similarly to [15], characterize the overlap between axonal arbors and replicate the axonal trees to densely fill the volumetric space. Lastly, the tools, pipeline and models will become part of EBRAINS infrastructure.

ACKNOWLEDGEMENTS

This work was supported by the FLAG-ERA grant NeuronsReunited, by NWO (680-91-318), by Spains MICINN-AEI (PCI2019-111900-2), and by EU H2020 Research and Innovation Programme under grant agreement 945539 (HBP SGA3).

Keywords: connectomics, neuronal reconstruction, morphology comparison, alignment & registration, coherent point drift, scalable brain composer, allen reference atlas

REFERENCES

[1] Cazemier, J.L., Clasca, F. & Tiesinga, P.H. (2016) Connectomic Analysis of Brain Networks: Novel Techniques and Future Directions. Frontiers in neuroanatomy, 10, 110.

[2] Kasthuri, N., et al (2015) Saturated Reconstruction of a Volume of Neocortex. Cell, 162, 648-661.

[3] Druckmann, S., et al (2014) Structured synaptic connectivity between hippocampal regions. Neuron, 81, 629-640.

[4] Oh, S.W., et al (2014) A mesoscale connectome of the mouse brain. Nature, 508:207–214.

[5] Calabrese, E. et al (2015) A Diffusion MRI Tractography Connectome of the Mouse Brain and Comparison with Neuronal Tracer Data. Cerebral cortex.

[6] Li, A., et al (2010) Micro-optical sectioning tomography to obtain a high-resolution atlas of the mouse brain. Science, 330, 1404-1408.

[7] Economo, M.N., et al (2016) A platform for brain-wide imaging and reconstruction of individual neurons. Elife, **5**, e10566.

[8] Winnubst, J. et al. (2019). Reconstruction of 1,000 projection neurons reveals new cell types and organization of long-range connectivity in the mouse brain. Cell, 179(1):268 281.e13.

[9] Peng, H. et al. (2021). Morphological diversity of single neurons in molecularly defined cell types. Nature, 598(7879):174181.

[10] Porrero, C., Rodríguez-Moreno, J., Quetglas, J. I., Smerdou, C., Furuta, T., and Clasca, F. (2016). A simple and efficient in vivo non-viral rna transfection method for labeling the whole axonal tree of individual adult long-range projection neurons. Frontiers in Neuroanatomy, 10:27.

[11] Glaser, J. R. and Glaser, E. M. (1990). Neuron imaging with neurolucida — a pc-based system for image combining microscopy. Computerized Medical Imaging and Graphics, 14(5):307–317.

[12] Q. Wang et al. (2020). The allen mouse brain common coordinate framework: A 3d reference atlas, Cell 181 (4):936 – 953.e20.

[13] Myronenko, A. and Song, X. (2010). Point set registration: Coherent point drift. IEEE Transactions on Pattern Analysis and Machine Intelligence, 32(12):22622275.

[14] Bakker, R., Tiesinga, P., and Kötter, R. (2015). The scalable brain atlas: Instant web-based access to public brain atlases and related content. Neuroinformatics, 13(3):353:366.

[15] Han, Y., et al (2018) The logic of single-cell projections from visual cortex. Nature, 556, 51-56.

IV Systems & cognitive neuroscience

Reality monitoring in native and foreign language

Aleksandra Dolgoarshinnaia*, Beatriz Martín-Luengo*

Centre for Cognition and Decision making, National Research University Higher School of Economics Institute for Cognitive Neuroscience, , Moscow, Russian Federation
**adolgoarshinnaya@hse.ru; bmartinluengo@hse.ru*

INTRODUCTION/MOTIVATION

Reality monitoring (RM) is a type of source monitoring for which individuals have to distinguish between internally and externally generated memories [1]. Discrimination between external and internal sources of memory is suggested to rely on specific perceptual and cognitive characteristics that are intrinsic to these sources and serve as cues for memory monitoring [1] [3]. For instance, greater cognitive operations are typically linked to self- or internally-generated information, whereas greater sensory and contextual content is related to externally-generated information [1][3]. These different cues usually result in higher proportions of correct attributions to the self-generated information than for the externally-generated one [1][4][5]. In previous research we found that in bilinguals source monitoring processes might differ depending on the language in which information was presented [2]. Therefore, we designed a new cross-linguistic experiment to further test this, expecting that participants would remember better the words said or read aloud by themselves compared to the words pronounced by another person. As for incorrect attributions, there is a particular effect observed in the studies – externalization bias which suggests that participants more often misattribute the foil not presented items to the external source than to the internal one [3][4][5][6].

To date, RM was not specifically tested in a cross-linguistic experiment using self- or other-generated paradigm. Yet, results of studies implementing Deese–Roediger–McDermott paradigm suggest that in bilinguals false recognition is typically higher in the more proficient or dominant language [7]. Therefore, overall, we expected more incorrect answers to be found for the Russian language.

METHODS

Fifty-six Russian-native participants (38 females, mean age = 25.3 *SD* = 5.77) who scored minimum of 16 points (*M* = 20.8, SD =3.1) on English proficiency test (https://www.cambridgeenglish.org) completed the online experiment ("Gorilla"[8]). We used a 2 (language: Russian, English) x 2 (modality: heard, said) within subject design. Our stimuli comprised 40 high frequency common nouns in Russian and English cross-translated resulting in 40 pairs of words as well as 20 pairs of foil not presented words. The language and modality of the presentation were fully counterbalanced. Participants either read aoud or listened to words presented on the screen either in Russian, or English. Then, they performed a recognition test, followed by reality monitoring (modality) and source monitoring (language) tasks.

RESULTS

Regarding general recognition, the 2x2 ANOVA with proportion of correct responses showed the main effect of the modality reflected in higher proportions for said modality (*M* = .82, *SD* = .23) over heard modality (*M* = .75, *SD* = .23), *p* = .02, as well the main effect of the language as the proportion of correct answers for English words (*M* = .87, *SD* = .23) was higher than for Russian words (M = .69, *SD* = .16), *p* <.001. The interaction between the language and modality, however, was borderline not significant, *p* = .055. Regarding analysis on reality monitoring, the said modality (*M* = .52, *SD* = .19) demonstrated the lowest rate of correct attributions among the three conditions, *p* <.001. Further analysis for incorrect modality attributions (see Figure 1) showed that in both, said and not presented conditions, misattributions to the heard modality (said-to-heard: *M* = .32, *SD* = .16; np-to-heard: *M* = .16, *SD* = .13) were significantly higher than to respective alternatives, p < .001. Finally, analysis on source monitoring (see Figure 2) showed that correct attributions to the English (*M* = .82, *SD* = .15) and not presented (*M* = .82, *SD* = .15) sources were higher than for the Russian source (*M* = .60, *SD* = .22), *p* < .001. Regarding incorrect source attributions, analysis for the Russian and not presented sources showed that incorrect attributions to the English source (Russian-to-English: *M* = .10, *SD* = .12; np-to-English: *M* = .07, *SD* = .58) were lower than for the not presented and Russian (Russian-to-np: *M* = .15, *SD* = .09 ; np-to-Russian: *M* = .10, *SD* = .10), respectively, *p* < 0.5. At the same time, for the English source analysis showed no significant difference in misattributions to the Russian or not presented sources, *p* = .723.

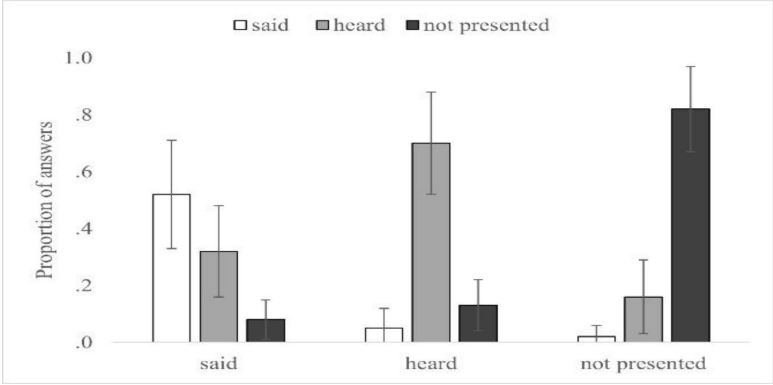

FIGURE 1: Proportion of answers for each correct and incorrect modalities. Error bars indicate standard deviation.

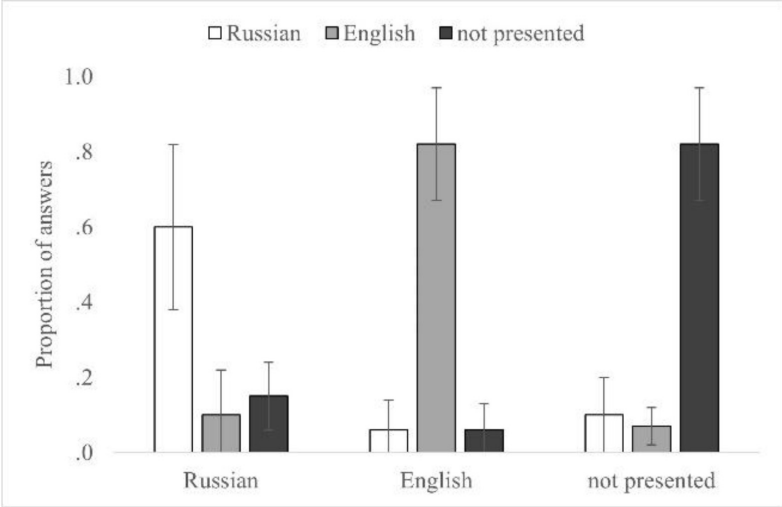

FIGURE 2: Proportion of answers for each correct and incorrect sources. Error bars indicate standard deviation.

DISCUSSION

Firstly, the expected interaction between the language and the modality of the words was not found. Secondly, while previous studies on RM report overall better accuracy for self-generated information, our explicit test showed that correct attributions to the said modality were the lowest. One explanation to such results can be the presence of the externalization bias as reflected by higher proportion of misattributions of not only not presented items to the external source, but of the internally generated items as well. Overall, this suggests that words said by the participants possessed enough cues or "weight" to be recognized as presented on the recognition test, however, not enough to indicate whether the word was self- or other generated. Finally, results on source monitoring suggest that processing information in English required more cognitive effort and therefore contained more characteristics related to internal cognitive processes that usually allow for successful monitoring.

To our knowledge, this is the first bilingual RM paradigm that manipulated not only the language of presented information, but the modality of its presentation. Although no direct interaction between the modality and the language was detected, there might still be differences in information processing and memory functioning when information is presented in the second language versus is the first language. To conclude, these results, specifically results on source monitoring, support the idea that monitoring information in the second language can differ from monitoring information in the first language. Nevertheless, further examination of these differences as well as the mechanisms of different types of monitoring processes is required.

ACKNOWLEDGEMENTS

This study was funded by the Russian Science Foundation (RSF 19-18-00534)

Keywords: reality monitoring, source memory, bilingualism

REFERENCES

[1] Raye CL, Johnson MK. Reality monitoring vs. discriminating between external sources of memories. *Bull Psychon Soc.* 1980; 15(6):405–408.

[2] Dolgoarshinnaia A, Martin-Luengo B. False Memories in Native and Foreign Languages. *Front Psychol.* 2021; 12:716336.

[3] Garrison JR, Bond R, Gibbard E, Johnson MK, Simons JS. Monitoring what is real: The effects of modality and action on accuracy and type of reality monitoring error. *Cortex.* 2017; 87:108-117.

[4] Leynes PA, Cairns A, Crawford JT. Event-related potentials indicate that reality monitoring differs from external source monitoring. *Am J Psychol.* 2005; 118(4):497–524.

[5] Mondino M, Poulet E, Suaud-Chagny MF, Brunelin J. Anodal tDCS targeting the left temporo-parietal junction disrupts verbal reality-monitoring. *Neuropsychologia.* 2016; 89:478–484.

[6] Johnson MK, Raye CL, Foley HJ, Foley MA. Cognitive Operations and Decision Bias in Reality Monitoring. *Am J Psychol.* 1981; 94(1):37-64.

[7] Suarez M, Beato MS. The Role of Language Proficiency in False Memory: A Mini Review. *Front Psychol.* 2021; 12; 659434.

[8] Anwyl-Irvine AL, Massonnié J, Flitton A, Kirkham N, Evershed JK. Gorilla in our midst: An online behavioral experiment builder. *Behav Res Methods.* 2019; 52(1):388–407.

Diachronic changes in oscillatory activity and its cortical generators in non-pathological development measured by MEG

Sandra Doval[1,2]*, Pablo Cuesta[2,3], Ricardo Bruña[2,3,4], Lucía Torres Simón[1,2], Brenda Chino[2,6], Inés Abalo Rodríguez[1,2] Fernando Maestú[1,2,5], David López-Sanz[2,7]

[1]Departamento de Psicología Experimental, Procesos Básicos y Logopedia, UCM, Facultad de Psicología, Pozuelo de Alarcón, Madrid, Spain
[2]Laboratorio de Neurociencia Cognitiva y Computacional, Centro de Tecnología Biomédica, UPM-UCM, Pozuelo de Alarcón, Madrid, Spain
[3]Departamento de Radiología, Rehabilitación y Fisioterapia, UCM, Facultad de Medicina, Madrid, Spain
[4]Departamento de Ingeniería Eléctrica, Universidad de La Laguna, Tenerife, Spain
[5]Centro de Investigación Biomédica en Red en Bioingeniería, Biomateriales y Nanomedicina (CIBER-BBN), Madrid, Spain
[6]Instituto de Neurociencia, Universidad Autónoma de Barcelona, Barcelona, Spain
[7]Departamento de Psicobiología y Metodología de las Ciencias del Comportamiento, UCM, Facultad de Educación, Madrid, Spain
**sdoval@ucm.es*

INTRODUCTION/MOTIVATION

Multiple evidences prove how brain oscillations at different frequencies underlie several processes of key relevance for human behavior, such as, long-distance brain coordination, cognitive and perceptual processes, or plasticity and brain maintenance through life [3][4][6][10]. Nowadays, numerous studies power estimates of the different bands of the frequency spectrum as potential biomarkers for different pathologies. However, little is known about the typical diachronic development of these markers during development and aging in life, which should be an important pre-requisite for its use under pathological conditions. Classically, power changes throughout life have been described using simplistic models based on linear fittings;due to restricted sample sizes or limitations in methodological approach. This classical conceptualization assumes, therefore, a monotonic and constant change that may not adjust to the developmental complexity. Moreover, previous literature is not consistent regarding these changes´ direction; reporting both increases and decreases for specific frequency bands depending on the study [1][2][7][8][12][13]. A complementary topic when studying ongoing oscillatory brain activity

is the study of natural frequencies distribution through the cortex. Different brain regions show a *natural tendency* to synchronize its neuronal activity at different frequencies, the so-called "natural frequencies". However, there are also few studies regarding topographic distribution of natural frequencies and its evolution during development and aging. The motivation of this study was to properly describe how brain activity changes due to the healthy maturational process. For that reason, our main objective was to characterize in detail, the profile of electrophysiological evolution in healthy development and particularly, unveil whether brain activity changes during aging could be related with cognitive performance to assess whether these changes can be interpreted as a scaffolding compensatory mechanism or rather as a sign of brain tissue and activity deterioration during normal aging.

METHODS

For this study, brain activity of 792 healthy participants (13-80y/o) have been characterized using Magnetoencephalography.

Firstly, signal was filtered (using temporal-Signal-Space-Separation), then artefacts were removed, and Independent-Component-Analysis was applied (to discard Electrooculogram and Electrocardiogram components). After signal was pre-processed, the activity of each subject in each of the 1202 cortical sources was reconstructed and their relative power was calculated using Beamformer Linearly-Constrained-Minimum-Variance.

Regression models-power and age: Power in each frequency band and age adjustment was evaluated considering three possible fitting models (linear, quadratic, and cubic) by using multiple regression analysis, and Likelihood-ratio-test to evaluate the best model (corrected p-values by FDR, q= 0.05).

Natural frequencies: The natural sources that generate each brain rhythm, as well as its modification through the life continuum were studied by conducting Pearson's correlations between relative source contribution (z-value; standardized value of each source´s power value compared to the other sources in each band) and age (. Rho values obtained representhow sources change its relative contribution throughout maturation.

Cognition: Performance in different cognitive test domains were studied; to reduce dimensionality Principal Component Analysis (PCA) was conducted; so finally, we had five main cognitive domains: Declarative Memory, Working Memory; Processing Speed; Visuospatial Memory and Verbal Fluency. To analyse the potential relation between cognitive domain scores and power in each band, partial correlations were applied between performance in each cognitive domain and power in each source and band (corrected by age due to its relevant role in cognitive performance and power trajectory), estimating the potential correlation (rho-values) between each band power and cognitive performance in each domain.

RESULTS AND DISCUSSION

Results showed a specific topographic distribution of the generators for each band, which was modified through life. Likewise, power change patterns were observed in each band through life following different statistical adjustments depending on the frequency band and cortical region analysed (Fig1) .

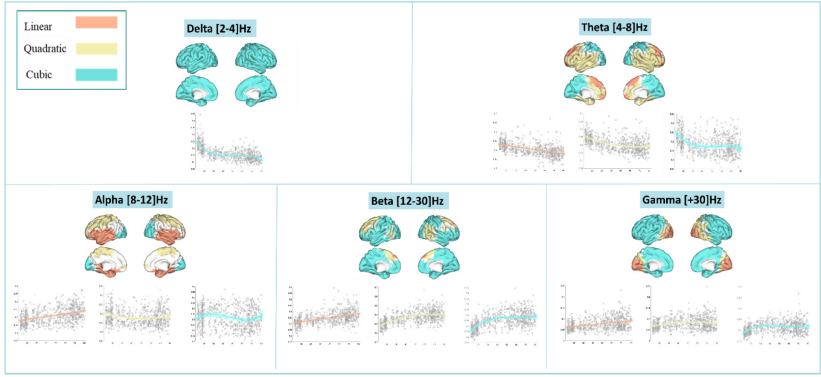

FIGURE 1

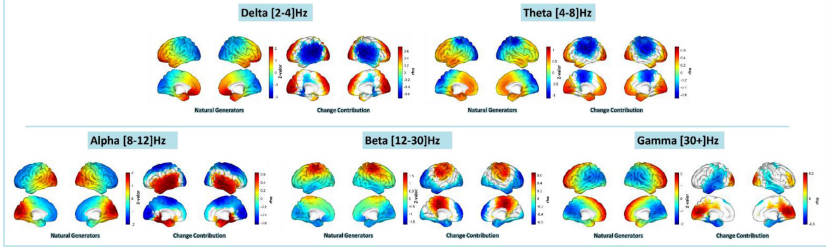

FIGURE 2

Although there were regions in which a linear model could give a better explanation of the changes across the life continuum, mainly, complex adjustments gave a significantly better explanation of the diachronic changes. In addition, natural generators, despite being relatively stable, modify their topography on the cortical surface through life (Fig2).

The main conclusions of this research were: Firstly, there was a relation between age and the different cerebral rhythms, and this relation is not strictly linear. Also, that evolution depends on the topographical region as well as the band. It was also interesting the fact that the more pronounced changes in electrophysiology for all classical bands were found during the first decades of life (13-30y/o) matching with youth maturation [14] and in the last ones [11] (60-80 y/o), the typical age range associated with the aging process. Interestingly, most fitting models showed a steady plateau during middle age, in which rhythms tended to be more stable. Secondly, regarding natural frequencies distribution, there were topographical changes for each band (Fig2). For slow waves (< 8Hz) their main generators increase their importance with age; alpha's main generator, located in the occipital lobe, decreased its relevance in the life continuum increasing towards more anterior-temporal regions, and for gamma, its main generator also decreased its importance during life [5][9]. Regarding the relationship between power-cognitive performance during aging, we found a negative relation between beta power in occipital areas, and gamma in sensorimotor areas and working memory performance. For processing speed performance, there was a positive relationship between slow waves power, in somatosensory and sensorimotor areas, and a positive relation in beta in occipital lobe. Similar tendency was observed for visual memory, also showing a negative relation between slow

waves (delta in somatosensorial, and theta in occipital areas) and a positive relation for beta in occipital areas regarding the performance in this specific domain. No statistically significant correlations were found for the other cognitive domains. Remarkably, when closely interpreting the relationship observed between power in the aging portion of our sample and cognition, we observed that a more intense slow wave activity (i.e. delta and theta) and a less pronounced fast wave activity (beta and gamma) were associated to overall cognitive performance. This supports the notion that the changes we described in the resting-state power spectrum during normal aging represent a sign of brain activity deterioration rather than a compensatory attempt as they are accompanied by cognitive decline in all cognitive domains.

Keywords: Healthy aging, Magnetoencephalography, Electrophysiology, Cognition, Spectral Analysis

REFERENCES

[1] Babiloni, C.et al. Sources of cortical rhythms in adults during physiological aging: a multicentric EEG study. *Hum Brain Mapp* 27, 162–172 (2006)).

[2] Barry, R.J., De Blasio, F.M., 2017. EEG differences between eyes-closed and eyes-open resting remain in healthy ageing. *Biol. Psychol*. 129, 293–304.

[3] Breslau, J., Starr, A., Sicotte, N., Higa, J. B. M. S., & Buchsbaum, M. S. (1989). Topographic EEG changes with normal aging and SDAT. *Electroencephalography and clinical neurophysiology*, 72(4), 281-289.

[4] Caplan, J.B., Bottomley, M., Kang, P., Dixon, R.A., 2015. Distinguishing rhythmic from non-rhythmic brain activity during rest in healthy neurocognitive aging. *Neuroimage* 112, 341–352.

[5] Edden, R.A.E., Muthukumaraswamy, S.D., Freeman, T.C.A., Singh, K.D., 2009.Orientation discrimination performance is predicted by GABA concentration and gamma oscillation frequency in human primary visual cortex. *J. Neurosci*. 29,15721–15726.

[6] Jennekens-Schinkel, A. (1987*). A textbook of clinical neurophysiology*: By AM Halliday, SR Butler and R. Paul (eds.), John Wiley & Sons, Chichester, New York, Brisbane, Toronto, Singapore, 1987, ISBN 0-471-90969-6.

[7] Klimesch, W. (1999). EEG alpha and theta oscillations reflect cognitive and memory performance: A review & analysis. *Brain Research Reviews*, 29, 169–195.

[8] Murty, D. V., Manikandan, K., Kumar, W. S., Ramesh, R. G., Purokayastha, S., Javali, M., ... & Ray, S. (2020). Gamma oscillations weaken with age in healthy elderly in human EEG. *Neuroimage*, 215, 116826.

[9] Pinto, J.G.A., Hornby, K.R., Jones, D.G., Murphy, K.M., 2010. Developmental changes inGABAergic mechanisms in human visual cortex across the lifespan. *Front. Cell.Neurosci*. 4.

[10] Scally, B., Burke, M.R., Bunce, D., Delvenne, J.F., 2018. Resting-state EEG power and connectivity are associated with alpha peak frequency slowing in healthy aging. *Neurobiol. Aging* 71, 149–155

[11] Schlee, W., Leirer, V., Kolassa, S., Thurm, F., Elbert, T., & Kolassa, I. T. (2012). Development of large-scale functional networks over the lifespan. *Neurobiology of Aging*, 33(10), 2411–2421. https://doi.org/10.1016/j.neurobiolaging.2011.11.031.

[12] Stacey, J. E., Crook-Rumsey, M., Sumich, A., Howard, C. J., Crawford, T., Livne, K., ... & Badham, S. (2021). Age differences in resting state EEG and their relation to eye movements and cognitive performance. *Neuropsychologia*, 157, 107887.

[13] Vlahou, Eleni L.; Thurm, Franka; Kolassa, Iris-Tatjana; Schlee, Winfried (2014). Resting-state slow wave power, healthy aging and cognitive performance. *Scientific Reports*, 4(), –. doi:10.1038/srep05101

[14] Whitford, T. J., Rennie, C. J., Grieve, S. M., Clark, C. R., Gordon, E., & Williams, L. M. (2007). Brain maturation in adolescence: Concurrent changes in neuroanatomy and neurophysiology. *Human Brain Mapping*, 28(3), 228–237. https://doi.org/10.1002/ hbm.20273

Emotional prosody processing in trans women

Claudia Sigrid Hofmann[1,2]*, Sonja Rossi[2]

[1]Department of Psychology, University of Innsbruck, Innsbruck, Austria
[2]Department for Hearing, Medical University of Innsbruck, ICONE - Innsbruck Cognitive Neuroscience, Speech, and Voice Disorders, Innsbruck, Austria
**claudia.hofmann@student.uibk.ac.at*

INTRODUCTION/MOTIVATION

So far, neurocognitive studies with trans individuals (i.e. people whose gender identity differs from their sex assigned at birth) have primarily focused on the question of whether their cognitive functions were more akin to their gender identity or their sex assigned at birth (see [1] for an overview). While this research did have its merits, it is barely of any relevance to trans individuals themselves [1]. The current project aims to leave this older path and instead puts trans individuals and trans issues in the focus of attention. Emotional and social processing is often considered a dividing factor between (cis) men and (cis) women, hence multiple studies used tasks relating to these processes to assess the masculinization/femininization of trans individual's brains [2][3]. Contrary to their intended outset, these studies found no differences between their cis gender groups, however they did detect a difference between their trans groups compared to both cis gender groups prior to the start of gender-affirming hormone therapy (GAHT). A difference that was no longer detectable after a few months of GAHT [2][3]. Interestingly, hormone levels alone were not enough to explain these changes [2][4]. These results make it evident that emotional processing changes over the transitioning process, but why or how this occurs has not yet been researched. This project consequently aims to start filling this gap by assessing emotional prosody processing (EPP) in trans women at multiple time points in their first year of transitioning, as well as by assessing long-term changes in EPP in trans women who have been using GAHT for over 2 years and correlating these findings with outcomes on a variety of psychological factors.

METHODS

The project consists of two experiments:

1. A longitudinal study consisting of trans women at the beginning of the transitioning process. They participate in the experiment at three different time points: T1 (before the start of GAHT and voice therapy), T2 (after 6 months of GAHT, which coincides with the end of voice therapy) and T3 (after 12 months of GAHT). The aim of this study is to evaluate changes in EPP over the course of the first year of transitioning.
2. A cross-sectional study, consisting of trans women after at least 24 months of GAHT and a control group of cis gender women and men, who lack a transitioning experience. This study aims to evaluate potential long-term influences of GAHT on emotional processing. The decision to include cis men in the control group has been made because cis women are more likely than cis men to take hormones for non-transitioning purposes, e.g. as contraceptive measures, which might influence findings.

Both studies use the same experimental setting. EPP is measured using two non-invasive instruments simultaneously: electroencephalography (EEG), which assesses the temporal component and functional near-infrared spectroscopy (fNIRS) which assesses the spatial component of EPP in the cortex. The experimental stimuli consist of a total of 180 pseudo sentences spoken in three different emotional valences (positive, neutral, negative) by two speakers (female and male sounding voice). For a more holistic approach, additional factors are assessed via questionnaires: physical and mental well-being, quality of life, body image, sense of belonging and autism spectrum traits.

RESULTS AND DISCUSSION

The project is still in an early stage, however, preliminary data from the control group has already been collected and a detailed statistical analysis will be available at the time of the conference. To our knowledge, this study will be the first to assess changes in EPP during the transitioning process. Based on studies on neural correlates of reductions in emotional processing capacity in various other groups, such as people with major depression (e.g. [5][6][7][8][9]), autism spectrum condition (for a meta-analysis see: [10]), parkinson's disease (e.g. [12][13][14]) or schizophrenia (for meta-analyses see: [15] and [16]), we propose the following hypothesis: We expect to see changes in the P200 and LPP (late positive potential) components of the EEG [17] and in the activation in areas relating to the STS/G (Superior temporal sulcus / gyrus) and

the IFG (inferior frontal gyrus) in the fNIRS [17][18]. These changes will point toward an increased capacity for emotional prosody processing. Furthermore, we expect more favourable outcomes on the questionnaires to correlate to more efficient EPP. In detail, for study 1, we expect the amplitude of the P200 in relation to emotional stimuli to decrease over the course of one year, indicating a more efficient emotional salience detection. Similarly, we expect the LPP to increase and to differentiate better between the different emotional valences with a maximum for positive valence over the course of one year. We also expect increased activation in the areas of the STS/G and the IFG. To our knowledge, so far no studies have attempted to capture long-term effects of transitioning on emotional processing, so potential outcomes for study 2 are harder to define. However, we expect similar results when comparing trans women to cis gender individuals, indicating a lasting effect of the transitioning process on EPP.

ACKNOWLEDGEMENT

I would like to thank my supervisor, Sonja Rossi, for her time and expertise, and for giving me the opportunity to work on a project I am truly passionate about. I would also like to thank Katharina Feil and Barbara Moser for their insights into transgender care and for their recruitment work. Furthermore, I would like to thank the University of Innsbruck, Vizerektorat für Forschung for the financial support of the project via a Doktoratsstipendium aus der Nachwuchsförderung der Universität Innsbruck, as well as the Department for Hearing, Speech, and Voice Disorders of the Medical University of Innsbruck for providing the equipment and room needed for the realization of the project.

Keywords: transgender, transitioning, emotional prosody, emotion processing, EEG, fNIRS

REFERENCES

[1] Nguyen, H. B., Loughead, J., Lipner, E., Hantsoo, L., Kornfield, S. L., & Epperson, C. N. (2019). What has sex got to do with it? The role of hormones in the transgender brain. Neuropsychopharmacology, 44(1), 22–37. https://doi.org/10.1038/s41386-018-0140-7

[2] Spies, M., Hahn, A., Kranz, G. S., Sladky, R., Kaufmann, U., Hummer, A., ... Lanzenberger, R. (2016). Gender transition affects neural correlates of empathy: A resting state functional connectivity study with ultra high-field 7T MR imaging. NeuroImage, 138, 257–265. https://doi.org/10.1016/j.neuroimage.2016.05.060

[3] Beking, T., Burke, S. M., Geuze, R. H., Staphorsius, A. S., Bakker, J., Groothuis, A. G. G., & Kreukels, B. P. C. (2020). Testosterone effects on functional amygdala lateralization: A study in adolescent transgender boys and cisgender boys and girls. Psychoneuroendocrinology, 111, 104461. https://doi.org/10.1016/j.psyneuen.2019.104461

[4] Soleman, R. S., Staphorsius, A. S., Cohen-Kettenis, P. T., Lambalk, C. B., Veltman, D. J., van Trotsenburg, M. A. A., Hompes, P. G. A., Drent, M. L., de Ronde, W. P., & Kreukels, B. P. C. (2014). Oestrogens are Not Related to Emotional Processing: A Study of Regional Brain Activity in Female-to-Male Transsexuals Under Gonadal Suppression. Cerebral Cortex, bhu201. https://doi.org/10.1093/cercor/bhu201

[5] Hill, K. E., South, S. C., Egan, R. P., & Foti, D. (2019). Abnormal emotional reactivity in depression: Contrasting theoretical models using neurophysiological data. Biological Psychology, 141, 35–43. https://doi.org/10.1016/j.biopsycho.2018.12.011

[6] Koch, K., Stegmaier, S., Schwarz, L., Erb, M., Reinl, M., Scheffler, K., … Ethofer, T. (2018). Neural correlates of processing emotional prosody in unipolar depression. Human Brain Mapping, 39(8), 3419–3427. https://doi.org/10.1002/hbm.24185

[7] MacNamara, A., Kotov, R., & Hajcak, G. (2016). Diagnostic and Symptom-Based Predictors of Emotional Processing in Generalized Anxiety Disorder and Major Depressive Disorder: An Event-Related Potential Study. Cognitive Therapy and Research, 40(3), 275–289. https://doi.org/10.1007/s10608-015-9717-1

[8] Péron, J., El Tamer, S., Grandjean, D., Leray, E., Travers, D., Drapier, D., … Millet, B. (2011). Major depressive disorder skews the recognition of emotional prosody. Progress in Neuro-Psychopharmacology and Biological Psychiatry, 35(4), 987–996. https://doi.org/10.1016/j.pnpbp.2011.01.019

[9] Uekermann, J., Abdel-Hamid, M., Lehmkämper, C., Vollmoeller, W., & Daum, I. (2008). Perception of affective prosody in major depression: A link to executive functions? Journal of the International Neuropsychological Society, 14(4), 552–561. https://doi.org/10.1017/S1355617708080740

[10] Zhang, M., Xu, S., Chen, Y., Lin, Y., Ding, H., & Zhang, Y. (2021). Recognition of affective prosody in autism spectrum conditions: A systematic review and meta-analysis. Autism, 136236132199572. https://doi.org/10.1177/1362361321995725

[11] Garrido-Vásquez, P., Pell, M. D., Paulmann, S., Strecker, K., Schwarz, J., & Kotz, S. A. (2013). An ERP study of vocal emotion processing in asymmetric Parkinson's disease. Social Cognitive and Affective Neuroscience, 8(8), 918–927. https://doi.org/10.1093/scan/nss094

[12] Hill, K. E., South, S. C., Egan, R. P., & Foti, D. (2019). Abnormal emotional reactivity in depression: Contrasting theoretical models using neurophysiological data. Biological Psychology, 141, 35–43. https://doi.org/10.1016/j.biopsycho.2018.12.011

[13] Dietz, J., Bradley, M. M., Jones, J., Okun, M. S., Perlstein, W. M., & Bowers, D. (2013). The late positive potential, emotion and apathy in Parkinson's disease. Neuropsychologia, 51(5), 960–966. https://doi.org/10.1016/j.neuropsychologia.2013.01.001

[14] Copland, D. A. (2019). Depression symptomatology correlates with event-related potentials in Parkinson's disease: An affective priming study. Journal of Affective Disorders, 245, 897–904. https://doi.org/10.1016/j.jad.2018.11.094

[15] Castro, M. K., Bailey, D. H., Zinger, J. F., & Martin, E. A. (2019). Late electrophysiological potentials and emotion in schizophrenia: A meta-analytic review. Schizophrenia Research, 211, 21–31. https://doi.org/10.1016/j.schres.2019.07.013

[16] Lin, Y., Ding, H., & Zhang, Y. (2018). Emotional Prosody Processing in Schizophrenic Patients: A Selective Review and Meta-Analysis. Journal of Clinical Medicine, 7(10), 363. https://doi.org/10.3390/jcm7100363

[17] Kotz, S. A., & Paulmann, S. (2011). Emotion, Language, and the Brain: Emotional Speech and Language Comprehension. Language and Linguistics Compass, 5(3), 108–125. https://doi.org/10.1111/j.1749-818X.2010.00267.x

[18] Witteman, J., Van Heuven, V. J. P., & Schiller, N. O. (2012). Hearing feelings: A quantitative meta-analysis on the neuroimaging literature of emotional prosody perception. Neuropsychologia, 50(12), 2752–2763. https://doi.org/10.1016/j.neuropsychologia.2012.07.026

Prospective metamemory monitoring: Source vs item

Elizaveta Ivanova*, Beatriz Martín-Luengo

Centre for Cognition & Decision Making, Institute for Cognitive Neuroscience, National Research University – Higher School of Economics, Moscow, Russia
**elizaveta.ivanova.w@gmail.com*

INTRODUCTION/MOTIVATION

Prospective metamemory is a subfield of metacognition, which refers to an individual's ability to predict and regulate one's own memory during encoding [1,2]. A real-life example of prospective metamemory can look like students assessing if the material they are learning at the moment is easy to remember when the test comes. Prospective metamemory can be studied from the perspective of how we make judgements regarding the source of the information (metamemory source monitoring) and judgements regarding the information itself (metamemory item monitoring). It is not clear yet whether source and item metamemory monitoring share similar mechanisms or not. On the one hand, early studies agree on the item- and source-monitoring similarity: whether item-source pairs were varied by emotional intensity or modality (source seen or imagined), participants' judgement about sources was positively correlated with their judgement about items [3-5]. On the other hand, a new study of Schaper et al. [6] showed that recognition rates were higher for incongruent pairs source-wise, and for congruent pairs item-wise. However, unlike early studies, Schaper et al. [6] used a between-subject design, which could potentially distort data analysis – due to lack of control of individual sensitivity toward metamemory judgements. Therefore, the main aim of this study was to disentangle whether source and item metamemory monitoring rely on the same monitoring mechanisms. To do so, we used 2 tasks: Judgement of Learning (JOL) to assess confidence in future remembering of an item and Judgement of Source (JOS) - a twin task of JOL for source metamemory monitoring [3,7]. To control for subjectivity, we used congruence between source-item as a varying factor, and to control for individual sensitivity, we chose a within subject design. We set three hypotheses: JOL and JOS will have a high similarity; congruent source-item pairs will have higher confidence ratings than incongruent pairs; and lastly,

recognition accuracy, despite differences in confidence ratings, will be similar for congruent and incongruent source-item pairs.

METHODS

First, we conducted an online normative study to select the stimuli for the main experiment. Final lists had 36 Source A-only-related items, 36 Source B-only-related items and 34 filler items related to both sources. For the main experiment, forty participants completed an encoding, a distractor task, and a memory test phases. The encoding phase contained two blocks: block-JOS (in which participants assessed their confidence about memorizing the source) and block-JOL (in which participants assessed their confidence about memorizing the item) (see Figure 1). Each block contained 36 items: 18 items were presented with a congruent source and 18 items with an incongruent source. Participants made either JOL or JOS (depending on the block) and rated their confidence of future remembering from 0 to 100%. Between JOL and JOS stages, participants had a short distractor task to unload short-term memory. During memory test, all items from the encoding phase including a similar amount of filler items were presented. Participants' task was to indicate whether a presented item was before and rate their confidence from 0 to 100%. If participants said the item was presented before, they were asked to name the source with which that item was shown and rate their confidence from 50 to 100%. The experiment was conducted online and build via Gorilla software [8].

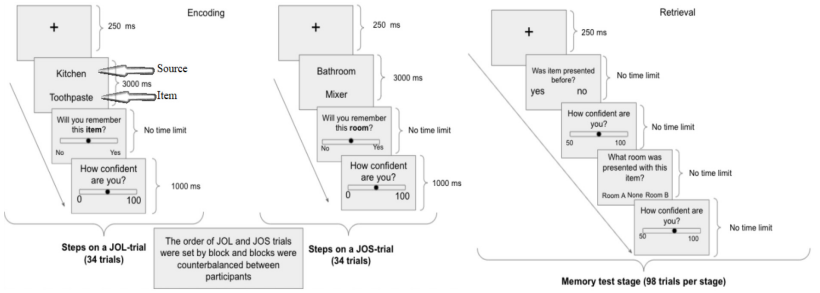

FIGURE 1: Procedure of the main experiment.

RESULTS

The analysis of confidence during encoding showed an interaction effect of Congruence and Object (Item vs Source) (p = .009). Student t-tests showed differences in Congruent Source vs Incongruent Source (p = <.001), Congruent Source to Congruent Item (p < .001), Congruent Item to Incongruent Item (p = <.001), Incongruent Item to Congruent Source (p = <.001), but not in Incongruent Source to Incongruent Item (p = .59). Next, we tested confidence and accuracy during memory test (Figure 2). For confidence, we found a significant main effect of Congruence (p = .018) and Object (p < .001). Analysis also showed a tendency towards significant interaction between Object and Task (p = .022). These main effects were qualified by their interaction: we found significant differences in every condition comparison except Item in JOS task vs Item in JOL task (p = .72). For accuracy rates, we found a significant main effect of Congruency (p = .038) and Object (p < .001). Analysis also showed a tendency towards significant interaction between Object and Task (p = .058). The post-hoc tests confirmed significant differences in every condition comparison except Item in JOS task vs Item in JOL task.

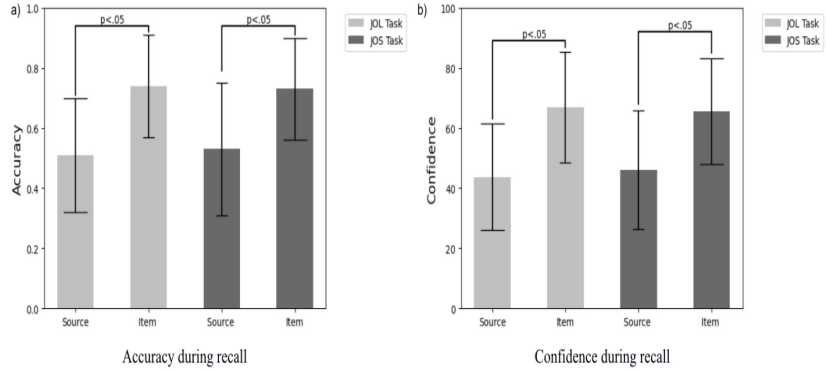

FIGURE 2: (**a**) Interaction effects between congruence and object in accuracy during recall (**b**) interaction effects between congruence and object in accuracy during recall.

DISCUSSION

In this study we examined whether source and item metamemory monitoring are similar to one another and whether they are influenced by congruence. We found that JOL and JOS did not differ across measures of accuracy and pre- and post- learning confidence, that is, our participants had similar accuracy and confidence levels when focused on either source or item. The results are in line with previous studies that found strong positive correlation between JOL and JOS [3-5]. They also contradict previous results of Schaper et al. [6] study, which showed a stronger influence of congruence on JOS. In our analysis, congruence was shown to significantly influence both source and item, that is, the results of our participants were formed mostly by congruence factor. Taking together both results in JOL vs JOS comparison and congruence influence, we can suggest that mechanisms of source and item metamemory monitoring are similar. Moreover, we can conclude that item-source congruence positively influences both confidence and accuracy and is more important than choosing to focus on source or item. In future, the neural underpinnings of prospective metamemory monitoring (both source and item) can be explored.

ACKNOWLEDGEMENTS

This research was supported by the Russian Science Foundation grant RSF 19 18 00534.

Keywords: metamemory, JOL, JOS, memory monitoring, congruence

REFERENCES

[1] Flavell, J. H., & Wellman, H. M. (1975). Metamemory. *Perspectives on the development of memory and cognition.*

[2] Joslyn, S., Loftus, E., Mcnoughton, A., & Powers, J. (2001). Memory for memory. *Memory & Cognition, 29(6),* 789–797. https://doi.org/10.3758/bf03196408

[3] Carroll, M., Mazzoni, G., Andrews, S., & Pocock, P. (1999). Monitoring the future: Object and source memory for real and imagined events. *Applied Cognitive Psychology: The Official Journal of the Society for Applied Research in Memory and Cognition*, *13*(4), 373-390. https://doi.org/10.1002/(SICI)1099-0720(199908)13:4<373::AID-ACP605>3.0.CO;2-F

[4] Dutton, A., & Carroll, M. (2001). Eyewitness testimony: Effects of source of arousal on memory, source monitoring, and metamemory judgments. *Australian Journal of Psychology*, *53*(2), 83-91. https://doi.org/10.1080/00049530108255128

[5] Kelly, A., Carroll, M., & Mazzoni, G. (2002). Metamemory and reality monitoring. *Applied Cognitive Psychology: The Official Journal of the Society for Applied Research in Memory and Cognition*, *16*(4), 407-428. https://doi.org/10.1002/acp.803

[6] Schaper, M. L., Kuhlmann, B. G., & Bayen, U. J. (2019). Metamemory expectancy illusion and schema-consistent guessing in source monitoring. *Journal of Experimental Psychology: Learning, Memory, and Cognition*, *45*(3), 470. https://doi.org/10.1037/xlm0000602

[7] Arbuckle, T. Y., & Cuddy, L. L. (1969). Discrimination of item strength at time of presentation. *Journal of experimental psychology*, *81*(1), 126. https://doi.org/10.1037/h0027455

[8] Anwyl-Irvine, A. L., Massonnié, J., Flitton, A., Kirkham, N., & Evershed, J. K. (2020). Gorilla in our midst: An online behavioral experiment builder. *Behavior research methods*, *52*(1), 388-407. https://doi.org/10.3758/s13428-019-01237-x

At-risk alcohol users have disrupted valence discrimination during reward anticipation

Mica Komarnyckyj[1]*, Chris Retzler[1], Zhipeng Cao[2, 3], Giorgio Ganis[4], Anna Murphy[1], Robert Whelan[2^], Elsa Fouragnan[4*^]

[1]Centre for Cognition and Neuroscience, University of Huddersfield, Huddersfield, UK
[2]School of Psychology, Trinity College Dublin, Dublin, Ireland
[3]Department of Psychiatry, University of Vermont College of Medicine, Burlington, USA
[4]School of Psychology, University of Plymouth, Plymouth, UK
**mica.komarnyckyj@hud.ac.uk, elsa.fouragnan@plymouth.ac.uk*
^Authors equally contributed to this work

INTRODUCTION/MOTIVATION

Alcohol dependency (AD) is characterised by disrupted reward processing, underpinned by dysfunctional cortico-striatal reward pathways.[1] Functional magnetic resonance imaging (fMRI) studies with AD subjects have generally shown reward processing brain regions are hypoactive (i.e., blunted) during reward anticipation [2–4]. and hyperactive during reward outcome.[1,5]. However, little is known about the biology reward processing in populations at-risk of AD, which could facilitate more targeted prevention and intervention strategies.

METHODS

Here, we used an electroencephalography (EEG) version of the monetary incentive delay task[6] (Fig. 1b) to examine if young adults with hazardous alcohol use have disrupted reward anticipation (e.g., hyper/hypoactive relative to controls). This task involved responding to a target stimulus following reward incentive cues to win, or avoid losing, the cued outcome while brain activity was recorded under 64-channel EEG. Participants were recruited via university campuses and the Alcohol Use Disorders Identification Test (AUDIT) (i.e., alcohol harm screening tool developed by the World Health Organisation) was used to split participants into high audit (HA) (i.e., hazardous at-risk drinkers) (n = 22, mean AUDIT score: 13.82) and low audit (LA) (i.e., low risk for AD) (n = 22, mean AUDIT score: 5.77) groups. Trial averaged event related potential (ERP) and single trial machine learning (ML) discriminant analyses

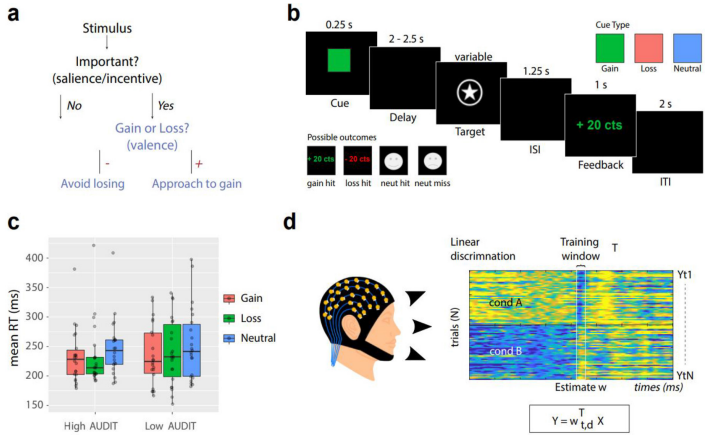

FIGURE 1: experimental design, rt analysis and single-trial discriminant component maps. (**a**) Flowchart representation of stimulus type, illustrating the difference between valence and salience. (**b**) Schematic representation of the experimental paradigm. On each trial, one of three cue symbols was presented for 0.25 s indicating if participants could win or lose 20cents, or if the trial would have no impact on earnings (i.e., neutral). Following a jittered delay of 2 – 2.5 s a square target was presented. A staircase algorithm adapted the target duration attempting to fix accuracy at ~66% within each trial type. Following a delay of 1.25 s feedback was shown for 1 s. (**c**) Reaction time results for both groups are presented together and are visualised using box and whisker plots, including the median, two hinges and two whiskers. (d) Example of a discriminant component map resulting from our single-trial linear discrimination analysis. The panels represent the discriminator amplitudes for the valence component for monetary loss (top) and loss cue (bottom) trials, using the training window (fixed length of δ = 60 ms, increasing in 10-ms increments) shown by the vertical bars labelled training window.

was applied to the EEG data[7] (Fig. 1d). ML discriminator performance was quantified by calculating the area under a receiver operating characteristic (ROC) curve (termed Az value) using a leave-one-out trial (LOO) cross validation approach. Az significance was assessed using the LOO procedure after randomizing the labels associated with each trial. Group averaged Az values were compared using one-dimensional Statistical Parametric Mapping (SPM1d), a method which corrects for multiple comparisons using random field theory to account for covariance between timepoints.[8]

RESULTS AND DISCUSSION

For the LA group, we observed a wide temporal window of significant valence discrimination (i.e., gain vs loss trials, Fig. 1a) during reward anticipation, with Az values exceeding the threshold p<0.05 between 333 and 512 ms after cue onset (Fig. 2c). In contrast, the HA group was insensitive to valence at all time points between cue and target onset (Fig 2d). Az values were significantly larger in the LA group compared to the HA group from 480 – 550 ms (SPM1d *p*cluster = 0.017) (Fig. 2e-f). Notably, the LA group but not the HA group, demonstrated a significant negative relationship between single-trial variability in valence component and reaction times for gain and loss trials

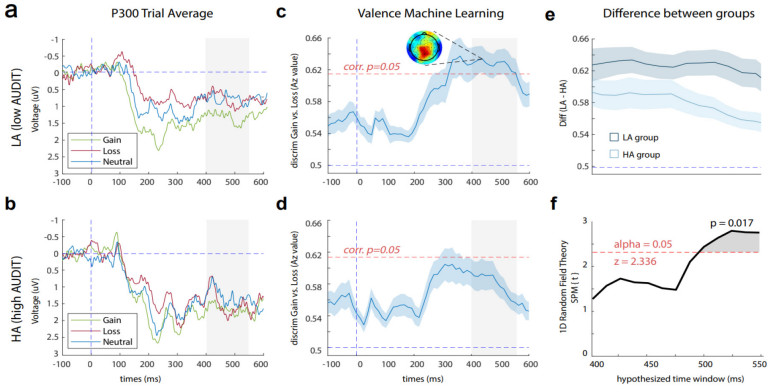

FIGURE 2: cue-locked valence erps and discrimination results. (**a**) Average ERP components for the LA group, computed at Pz. For the valence comparisons, red, blue and green traces represent Loss, Neutral and Gain trials respectively. Note that ERPs are plotted with the negative y-axis pointing up. (**b**) Average ERP components for the HA group, computed at Pz. For the valence comparisons, red, blue and green traces represent Loss, Neutral and Gain trials respectively. (**c**) Single-trial discriminator performance (Az) between Gain and Losses as a function of cue-locked time for the LA group. Results are averaged over all participants (mean line in blue +- se across participants, represented by the shaded blue area). The dotted red line represents the Az leading to a significance level of p=0.05. (**d**) Single-trial discriminator performance (Az) between Gain and Losses as a function of cue-locked time for the HA group. (**e**) Comparison of mean HA-Az and LA-Az across the window of interest (400-550 ms). (**f**) Results of SPM1d analysis, illustrating the magnitude of LA-Az to HA-Az differences (i.e., SPM{t}) across time window of interest (400-550). Grey shaded region indicates where there is a significant difference between HA-Az and LA-Az values i.e., where the critical threshold (2.336) has been crossed by the SPM{t}.

(estimated regression coefficients were significantly different than zero t(21) = -2.14, p = 0.044). There were no significant between-group differences in reaction time (Fig. 1c), ERP cue-P3 values (Fig. 2a-b) or salience discrimination (i.e., incentive vs neutral trials, Fig. 1a).

Young adults with at-risk drinking exhibited disrupted hypoactive valence processing, compared to those with low-risk drinking. Absence of EEG valence sensitivity in the at-risk group may reflect pre-existing blunted motivational mechanisms for non-drug rewards. Our single trial ML approach preserved variance among trials, thus improving signal to noise ratio compared with conventional ERP analyses. The single trial method allowed us to investigate the changing cognitive states of individual participants across the task and the relationship between their brain and behaviour. These benefits have clinical relevance as they could support patient diagnosis and stratification, where subtle individual differences in neural processing may be informative of predisposing vulnerability to addiction and potential treatment response.

Keywords: addiction, reward, machine learning, electroencephalography

REFERENCES

[1] Luijten, M., Schellekens, A. F., Kühn, S., Machielse, M. W. J. & Sescousse, G. Disruption of Reward Processing in Addiction. JAMA Psychiatry 74, 387 (2017).

[2] Beck, A. et al. Ventral Striatal Activation During Reward Anticipation Correlates with Impulsivity in Alcoholics. Biol. Psychiatry 66, 734–742 (2009).

[3] Nestor, L. J. et al. Acute naltrexone does not remediate fronto-striatal disturbances in alcoholic and alcoholic polysubstance-dependent populations during a monetary incentive delay task. Addict. Biol. 22, 1576–1589 (2017).

[4] Wrase, J. et al. Dysfunction of reward processing correlates with alcohol craving in detoxified alcoholics. Neuroimage 35, 787–794 (2007).

[5] Bjork, J. M., Smith, A. R. & Hommer, D. W. Striatal sensitivity to reward deliveries and omissions in substance dependent patients. Neuroimage 42, 1609–1621 (2008).

[6] Knutson, B., Westdorp, A., Kaiser, E. & Hommer, D. FMRI Visualization of Brain Activity during a Monetary Incentive Delay Task. Neuroimage 12, 20–27 (2000).

[7] Fouragnan, E., Retzler, C., Mullinger, K. & Philiastides, M. G. Two spatiotemporally distinct value systems shape reward-based learning in the human brain. Nat. Commun. 6, 8107 (2015).

[8] Pataky, T. C., Vanrenterghem, J. & Robinson, M. Statistical Parametric Mapping (SPM): Theory, Software and Future Directions. www.spm1d.org (2017).

Effect of stimulus category on fast perceptual learning evidenced with ERP and behavioural responses

Valentina Pergher[1,2]*, Marc M. Van Hulle[2]

[1]Department of Psychology, Harvard University, Laboratory of Cognitive Neuropsychology, Cambridge, US
[2]Department of Neurosciences, KU Leuven - University of Leuven, Laboratory for Neuro- & Psychophysiology, Leuven, Belgium
**valentinapergher@fas.harvard.edu*

INTRODUCTION/MOTIVATION

Perceptual learning (PL) refers to lasting improved perception skills after participating in targeted single or repeated training sessions. It has been shown that repetition of a certain cognitive task that involves PL can improve implicit memory and attention processes (Maniglia & Seitz, 2018). The application of PL can be categorized as fast when leading to improvements after a few sessions only (Leclercq, et al., 2014; Poggio et al., 1992) or slow when involving several training sessions (Seitz et al., 2005). Several EEG-ERPs studies on visual PL were able to shed light on the neural mechanisms underlying visual perception, for both fast and slow learning conditions (Mishra, et al., 2015; Song et al., 2008). However, no studies on fast PL distinguished between different visual stimulus categories (objects, animals, etc.). For instance, the study of Shahin et al. (2005) reported an enhancement of the P2 ERP component in response to musical sounds as a function of training and likewise in response to complex auditory patterns comprising sequences of individual frequencies (Atienza et al., 2002). Furthermore, Ji et al. (1998) showed a larger posterior N1 component for images of animals compared to images of vegetables and fruit. In particular, the N1 amplitude reflects visual discrimination processes, and its latency was affected by processing effort by showing a lower amplitude and larger latency for stimuli that are more difficult to discriminate. Although learning effects on ERPs components have been already studied, especially N1 and P2, the cognitive processes behind learning gains are still unclear. Previous ERP studies suggested that these changes might depend on several factors, such as improvements in processing of perceptual features (Hamamé, et al., 2011), access to perceptual representations (Sagi,

2011), and inhibition of irrelevant stimuli (Sheehan et al., 2005). One issue with these studies is the lack of information about how fast PL depends on stimulus category and what are the changes in ERP components when different stimuli are used.

METHODS

To address this, we recruited 16 participants and were administered a single session of a visual working memory task, called N-Back, that included three different stimulus categories. Our goal was to investigate the relationship between stimulus category (objects, animals, and fruit), and the P1, N1, P2, N2, P3 and N4 ERP components, and to better understand to what extent stimulus category impacts on learning-associated cognitive processes.

RESULTS AND DISCUSSION

Our results revealed that stimulus category affects both behavioural (Figure 1) and neurophysiological responses, and that fast PL is paralleled by changes in amplitude and latency of several ERP components: P1, N1, P2, N2, P3 and N4

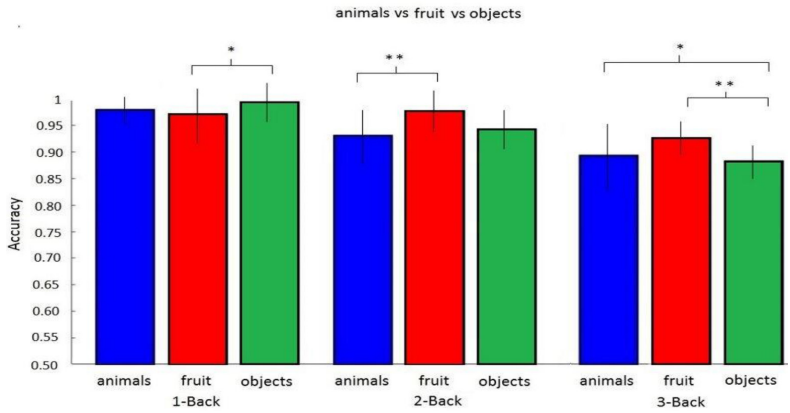

FIGURE 1: Comparison of response accuracies of the three stimulus categories (animals vs. fruit vs. objects), for different N-Back levels. Significance level *p<0.05, **<0.01.

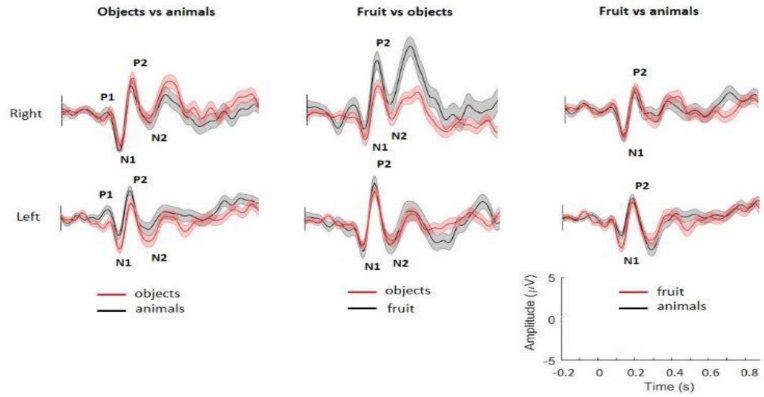

FIGURE 2: Range and mean ERPs of trials plotted per hemisphere and stimulus category (animals vs. fruits vs. objects) across N-Back levels. Trials were rejected prior to including them in the plots when their amplitudes were higher than 30 μV. The labeled ERP components are those that were significant for $p<0.05$ or <0.01.

(Figure 2). In addition to the well-established N1 and P2 amplitude changes, our observations provide evidence of the impact of stimulus category on fast PL in terms of amplitudes and latencies of other ERP components. In line with the study of Proverbio et al. (2008), we did not observe any significant correlation between ERP components and behavioural responses. In conclusion, our outcomes highlight that both behavioural and neurophysiological responses, in particular ERP components, reflect the impact of fast PL even when performing a single N-Back training session. Differing from existing literature, we considered several visual stimulus categories (objects, animals, etc.) and showed significant latency variations in different ERP components. Finally, the variety in used training lengths and stimulus repetitions (e.g., Song et al., 2008; Mishra, et al., 2015) led to changes in different ERP components, which we hypothesize to reflect fast or slow PL effects.

Keywords: Perceptual learning (PL), Event-Related Potential (ERP), Fast learning, N-Back task, stimulus category

REFERENCES

[1] Maniglia, M., & Seitz, A. R. (2018). Towards a whole brain model of Perceptual Learning. Current Opinion in Behavioral Sciences, 20, 47-55.

[2] Leclercq, V., Le Dantec, C. C., & Seitz, A. R. (2014). Encoding of episodic information through fast task-irrelevant perceptual learning. Vision research, 99, 5-11.

[3] Poggio, T., Fahle, M., & Edelman, S. (1992). Fast perceptual learning in visual hyperacuity. Science, 256(5059), 1018-1021.

[4] Seitz, A., & Watanabe, T. (2005). A unified model for perceptual learning. Trends in cognitive sciences, 9(7), 329-334.

[5] Mishra, J., Rolle, C., & Gazzaley, A. (2015). Neural plasticity underlying visual perceptual learning in aging. Brain research, 1612, 140-151.

[6] Song, J. H., Skoe, E., Wong, P. C., Kraus, N. (2008). Plasticity in the adult human auditory brainstem following short-term linguistic training. Journal of Cognitive Neuroscience, 10, 1892-1902.

[7] Shahin, A., Roberts, L. E., Pantev, C., Trainor, L. J., & Ross, B. (2005). Modulation of P2 auditory-evoked responses by the spectral complexity of musical sounds. Neuroreport, 16(16), 1781-1785.

[8] Atienza, M., Cantero, J. L., & Dominguez-Marin, E. (2002). The time course of neural changes underlying auditory perceptual learning. Learning & Memory, 9(3), 138-150.

[9] Hamamé, C. M., Cosmelli, D., Henriquez, R., & Aboitiz, F. (2011). Neural mechanisms of human perceptual learning: electrophysiological evidence for a two-stage process. PLoS One, 6(4), e19221.

[10] Sagi, D. (2011). Perceptual learning in vision research. Vision research, 51(13), 1552-1566.

[11] Sheehan, K. A., McArthur, G. M., & Bishop, D. V. (2005). Is discrimination training necessary to cause changes in the P2 auditory event-related brain potential to speech sounds?. Cognitive Brain Research, 25(2), 547-553.

M1 muscarinic acetylcholine receptor improves the memory in D-galactose induced ageing mice model

Ashrafur Rahman[1]*, Mahadi Hassan Fahim[2], Shakil Ahmed[2], Mehedi Hasan Apu[2], Arif Anzum Shuvo[2], Rehnuma Tabassum Jhalak[2], Kazi Nishat Tasnim[2], Khadiza Sharmin Lopa[2]

[1]Department of Pharmacology and Neuroscience, Texas Tech University and Health Science Center, Amarillo, USA

[2]Department of Pharmaceutical Sciences, North South University, Dhaka, Bangladesh

**rahman.ashrafur@northsouth.edu*

INTRODUCTION/MOTIVATION

Aging-induced memory impairment results in loss of muscarinic receptors (mAChRs) (1). This causes massive oxidative damage by generating uncontrolled oxidative biomarkers (MDA, GSH and SOD) in the brain, commonly found in Alzheimer's disease (AD) (2). Studies have shown that mAChRs play a vital role in different learning, like spatial learning, contextual fear conditioning, and trace eyeblink conditioning, and serial feature positive discrimination tasks (3). Other studies showed that among the five subtypes of mAChRs, the M1 receptors are closely associated with learning (4). Several behavioral studies showed that the m1mAChR plays a vital role in attention and is a promising target for memory functions (4). Another study showed that m1mAChR controlled oxidative stress in the brain (5). Therefore, the m1mAChRs could be a promising target to improve memory in aging-induced AD (6). VU0357017 is a highly selective and potent m1 allosteric agonist having a substantial effect on hippocampal-dependent learning in rodents (7). Several studies showed that VU0357017 exhibits antioxidant properties by stimulating b-Arrestin pathway (7,8). However, no studies have investigated the beneficiary role of VU0357017 in aging-induced memory impairment and their associated biomarkers. Our study aims to find an effective treatment approach for AD using selective m1mAChR agonist VU0357017 by (i) establishing its cholinergic activity in mice via two commonly used behavioral tasks and (ii) identifying its regulatory activity in AD-associated oxidative stress biomarkers via a bioassay technique.

METHODS

A. Passive Avoidance (PA): On the first day, mice were free to roam in the testing chamber, considered habituation. Then they were subjected to a

mild foot shock (US) every day for seven days. Days 8-11 were devoted to the examination (testing period) (9). We computed the latency needed to pass through the gate that separates the two compartments (Diagram 1) (10).

B. Contextual Fear Conditioning (CFC): CFC includes keeping the animal in a novel environment, delivering an unconditioned stimulus (US: from the shocking device) associated with a conditioned stimulus (tone: CS), and then getting rid of it (day 1: conditioning session). When the animal was kept in

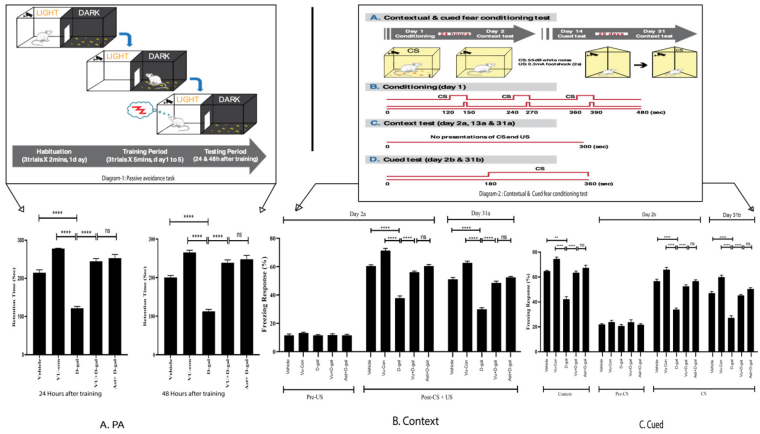

FIGURE 1: Effects of VU0357017 on (**A**) PA and (**B**), (**C**) CFC. Data were analyzed by one-way ANOVA followed by post-hoc tukey test and expressed as mean ± standard error of the mean. ns = not significant and p<0.05 is considered as significant (10).

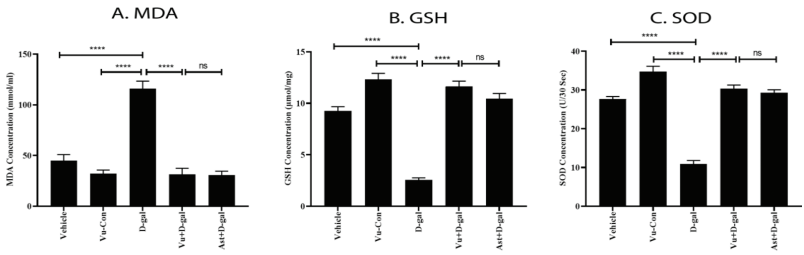

FIGURE 2: Effects of VU0357017 on oxidative stress biomarkers (**A**) MDA (**B**) GSH and (**C**) SOD. Data were analyzed by one-way ANOVA followed by post-hoc tukey test and expressed as mean ± standard error of the mean. ns = not significant, and p<0.05 is considered as significant.

the same environment again, it showed a freezing response if it could recall (day 2a & 31a: context) (11). The responses were analyzed by changing the shape of the chamber (day 2b & 31b: cued session) (Diagram 2).

C. Bioassay: Oxidative biomarkers (MDA, GSH, and SOD) were measured from the hippocampus.

D. Animals: We divided forty mice into the following five groups: Group 1: Saline 1ml (n=8) (Intrapertonial; i.p) Group 2: D-gal (n=8): D-gal 100 mg/kg (12) (i.p) Group 3: VU0357017 (VU) (positive control; n=8): VU 0.15mg/kg (i.p) (13) (i.p) Group 4: VU0357017 (VU) + D-gal (n=8): VU 0.15 mg/kg (13) (i.p) and D-gal 100 mg/kg (12) (i.p) Group 5: Astaxanthin (Ast) (Standard Antioxidant) + D-gal (n=8): Ast 20 mg/kg (14) (oral) and D-gal 100 mg/kg (12) (i.p); After ten weeks of treatment, firstly, all groups were exposed to the passive avoidance (PA) task. After seven days of completion of PA the same group of mice has experienced the Contextual Fear Conditioning followed by collecting brain tissues to assay oxidative stress biomarkers.

RESULTS

Effects of VU0357017 on PA and CFC: After 24 and 48 hours of training, the RT value was decreased to 116.43 $\pm$ 2.62 s and 105.87 $\pm$ 3.58 s, respectively in mice that received D-gal injection. Contrarily, the RT was prominently elevated to 255.62 $\pm$ 14.11 s after 24 hours and 246.81 $\pm$ 14.38 s in case of 48 hours of training after administration of VU0357017 in D-gal mice. In the conditioning session, day 2A and 31A, the FR value was decreased to 42.5 $\pm$ 3.60 % and 35 $\pm$ 2.45 %, respectively after administration of D-gal. Intriguingly, FR increased to 67.60 $\pm$ 2.62 % (day 2A) and 62.18 $\pm$ 6.57 (day 31A) after treatment with VU0357017. In context and cued test, similar results were observed.

Effects of VU0357017 on oxidative stress biomarkers: The level of oxidative stress biomarkers was changed in D-gal mice. The MDA level was remarkably increased (115.9 $\pm$ 7.49 nmol/ml) whereas GSH and SOD level was significantly decreased (2.54 $\pm$ 0.23 µmol/mg and 10.85 $\pm$ 0.94 U/30s; respectively; P <0.0001). However, the GSH and SOD levels were increased (11.62 $\pm$ 0.53 µmol/mg and 30.89 $\pm$ 0.89 U/30s; respectively) whereas MDA was significantly decreased (31.34 $\pm$ 6.11) nmol/ml after administration of VU0357017 (P<0.0001).

DISCUSSION

In this study, the D-gal mice exhibited a low level of learning, whereas an improvement of learning was detected in mice treated with VU0357017. These results suggested that VU0357017 can potentially affect learning and memory-impaired by D-gal (Fig.1). The biochemical study revealed significant changes in oxidative biomarkers in D-gal treated mice, whereas the expressions of biomarkers were regulated after using VU0357017 (Fig.2), suggesting VU0357107 has the potential antioxidant properties. Other studies showed that M1mAChRs have antioxidant activity (15). Therefore, it could be stated that VU0357017 improves memory by increasing the amount of m1mAChRs via modulating the oxidative biomarkers in the brain. The probable underlying antioxidant mechanism is due to the stimulation of b-arrestin pathway (7,8) by inhibiting NADPH oxidase 4 (7), a key generator of ROS in the brain (16). A study on human cell line have shown an outstanding selectivity of VU0357017 towards the m1mAChR and is regarded as a novel approach for AD (7). However, there is a lack of evidence to find the advantages and propitious effects of VU0357017 on AD. Therefore, the results obtained from animal studies might be transformed in human cases in the treatment of AD.

REFERENCES

[1] Schliebs R, Arendt T. The cholinergic system in aging and neuronal degeneration. Behavioral Brain Research. 2011 Aug;221(2):555–63.

[2] Kandlur A, Satyamoorthy K, Gangadharan G. Oxidative Stress in Cognitive and Epigenetic Aging: A Retrospective Glance. Front Mol Neurosci. 2020 Mar 18;13:41.

[3] Rahman MdA, Tanaka N, Usui K, Kawahara S. Role of Muscarinic Acetylcholine Receptors in Serial Feature-Positive Discrimination Task during Eyeblink Conditioning in Mice. Sakakibara M, editor. PLoS ONE. 2016 Jan 25;11(1):e0147572.

[4] Rahman MA, Tanaka N, Nuruzzaman Md, Debnath S, Kawahara S. Blockade of the M1 muscarinic acetylcholine receptors impairs eyeblink serial feature-positive discrimination learning in mice. Sakakibara M, editor. PLoS ONE. 2020 Aug 13;15(8):e0237451.

[5] Frinchi M, Nuzzo D, Scaduto P, Di Carlo M, Massenti MF, Belluardo N, et al. Anti-inflammatory and antioxidant effects of muscarinic acetylcholine receptor (mAChR) activation in the rat hippocampus. Sci Rep. 2019 Dec;9(1):14233.

[6] Fisher A, Pittel Z, Haring R, Bar-Ner N, Kliger-Spatz M, Natan N, et al. M_1 Muscarinic Agonists Can Modulate Some of the Hallmarks in Alzheimer's Disease: Implications in Future Therapy. JMN. 2003;20(3):349–56.

[7] Digby GJ, Noetzel MJ, Bubser M, Utley TJ, Walker AG, Byun NE, et al. Novel Allosteric Agonists of M1 Muscarinic Acetylcholine Receptors Induce Brain Region-Specific Responses That

Correspond with Behavioral Effects in Animal Models. Journal of Neuroscience. 2012 Jun 20;32(25):8532–44.

[8] van Gastel J, Hendrickx JO, Leysen H, Santos-Otte P, Luttrell LM, Martin B, et al. β-Arrestin Based Receptor Signaling Paradigms: Potential Therapeutic Targets for Complex Age-Related Disorders. Front Pharmacol. 2018 Nov 28;9:1369.

[9] Tabrizian K, Yaghoobi NS, Iranshahi M, Shahraki J, Rezaee R, Hashemzaei M. Auraptene consolidates memory, reverses scopolamine-disrupted memory in passive avoidance task, and ameliorates retention deficits in mice. Iran J Basic Med Sci. 2015 Oct;18(10):1014–9.

[10] Sweatt JD. Rodent Behavioral Learning and Memory Models. In: Mechanisms of Memory [Internet]. Elsevier; 2010 [cited 2021 Nov 26]. p. 76–103. Available from: https://linkinghub.elsevier.com/retrieve/pii/B9780123749512000044

[11] Shoji H, Takao K, Hattori S, Miyakawa T. Contextual and Cued Fear Conditioning Test Using a Video Analyzing System in Mice. JoVE. 2014 Mar 1;(85):50871.

[12] Zhang X, Wang J, Xing Y, Gong L, Li H, Wu Z, et al. Effects of ginsenoside Rg1 or 17β-estradiol on a cognitively impaired, ovariectomized rat model of Alzheimer's disease. Neuroscience. 2012 Sep;220:191–200.

[13] Cieślik P, Radulska A, Burnat G, Kalinowski L, Wierońska JM. Serotonergic–Muscarinic Interaction within the Prefrontal Cortex as a Novel Target to Reverse Schizophrenia-Related Cognitive Symptoms. IJMS. 2021 Aug 10;22(16):8612.

[14] Pei L, Dong F, Hui B. [Effects of Astaxanthin on the damage of osteoblast induced by H2O2]. Zhongguo Gu Shang. 2008 Mar;21(3):187–9.

[15] adeja RN, Urrunaga NH, Ahmad D, Khurana S. Data regarding M1 muscarinic receptor-mediated modulation of hepatic catalase activity in response to oxidative stress. Data in Brief. 2016 Mar;6:405–9.

[16] Kuroda J, Ago T, Nishimura A, Nakamura K, Matsuo R, Wakisaka Y, et al. Nox4 Is a Major Source of Superoxide Production in Human Brain Pericytes. J Vasc Res. 2014;51(6):429–38.

The effect of tDCS on the rSTS on reading speed of social sentences is modulated by personality traits

Cristian Reyes[1]*, Iván Padrón[3,4], Sara Nila Yagual[5], Hipólito Marrero[2,4]

[1]Department of Psychology, Carl von Ossietzky University Experimental Psychology Lab, Oldenburg, Germany.
[2]Departamento de Psicología Cognitiva, Universidad de La Laguna, Social y Organizacional, San Cristóbal de La Laguna, Spain
[3]Departamento de Psicología Evolutiva y de la Educación, Universidad de La Laguna, San Cristóbal de La Laguna, Spain
[4]Instituto Universitario de Neurociencia, Universidad de La Laguna, San Cristóbal de La Laguna, Spain
[5]Facultad de Ciencias Sociales y de la Salud, Universidad Estatal La Libertad, Ecuador
**cristian.reyes.moreno@uni-oldenburg.de*

INTRODUCTION/MOTIVATION

Intentionality is a basic component of understanding the minds and behaviors of others. In this regard, the temporal lobe (anterior temporal lobe, superior temporal sulcus, middle and superior temporal gyrus) and the precuneus and temporo-parietal junction constitute a "mentalizing" network [1,2] that encodes intentionality. Within this network, the Superior Temporal Sulcus (STS) and regions surrounding it have been related to being especially involved in processing communicative intention for interactions by means of gaze (direct vs. averted) in social perception [3-7]. Approach intentionality has been linked with greater activation of posterior right Superior Temporal Sulcus (rSTS) than avoidance [8]. STS could be an area required for processing intentionality for social interactions. Regarding transcranial direct current stimulation (tDCS) effects on the STS and relationship-actions processing, Marrero et al. [9] found a greater improvement in discriminability of approach sentences in a memorization task after applying anodal tDCS on the rSTS, compared to either sham or cathodal stimulation. However, the question whether the advantage of approach contents could start before memorization (as during sentence reading) remains open. The goal of this study has been to see whether improvement in information encoding could start during the reading process. Based on Marrero et al. [9], we hypothesized anodal tDCS would produce a greater improvement for approach sentences. Moreover, we explored whether an effect of tDCS on reading speed could be moderated by behavioral activation system (BAS, approach trait) and behavioral inhibition system (BIS, avoid-

ance trait) [10]. Low approach [11,12] has been found as benefitting from anodal stimulation, but high avoidance trait has been shown to disturb attentional allocation [13] in previous research. Hence, we would expect participant with high BAS and high BIS traits to be less capable of taking advantage of extra processing resources probably provided by anodal tDCS for the reading task. Therefore, we predicted a poorer reading improvement in approach as well as in avoidance sentences in high compared to low-BAS and BIS participants.

METHODS

62 healthy right-handed students (54 females M= 19,95, SD = 2,33) voluntarily participated in the experiment. All participants provided informed consent. Inclusion criteria included: being right-handed according to the Edinburgh Handedness Inventory [14]. Exclusion criteria were suffering from epilepsy (or having close relatives affected), migraine, brain damage, cardiac, neurological or psychiatric disease. 31 participants were assigned to the anodal condition and 31 to the sham condition. The behavioral inhibition system (BIS) and behavioral activation system (BAS) scales were measured by the scales of Carver & White [15]. The difference between anodal and sham groups relied on stimulation duration: anodal-tDCS participants received stimulation for 20 minutes at 2 mA plus 15 s for fade in and 15 s for fade out, as the sham group did for only 15 s plus 15 s for fade in and 15 s for fade out as well. Participants were given one list before receiving tDCS (pre-test) and the other list after tDCS (post-test). Participants were randomly assigned to one of the four sets of sentences resulting from the counterbalance. Sentences were randomly presented to the participants in each of the counterbalanced sets. At the start of the experiment, participants were given seven sentences to practice. Then, they were given 60 sentences, 20 for each direction (Approach, Avoidance, Neutral). Sentences presentation was segmented (see Table 1). Each segment was displayed till the participant pressed the corresponding button. After 750 ms a new sentence appeared. Sixteen sentences were followed by a yes-no question on the content just read. Feedback on correctness and time required for it was given. These questions were aimed at keeping the attention of participants on reading comprehension.

Table 1: Examples of sentences with questions

Sentence	Direction	Question Example	Correct Answer
Pedro/aceptó a Rosa/en Whatshapp (Pedro/accepted Rosa/in Whatsapp)	Approach	¿Dice que Pedro aceptó a Rosa en Whatshapp? (Is it stated that Pedro accepted Rosa in Whatshapp?)	Yes
Pedro/bloqueó a Rosa/en Whatshapp (Pedro/blocked Rosa/in Whatshapp	Avoidance	¿Dice que Pedro aceptó a Rosa en Whatshapp? (Is it stated that Pedro accepted Rosa in Whatshapp?)	No
Verónica/dedujo el precio/del abrigo (Verónica/deduced the price/of the coat)	Neutral	¿Dice que Verónica dedujo el precio del abrigo? (Is it stated that Verónica deduced the price of the coat?)	Yes

RESULTS AND DISCUSSION

Two 3 X 2 mixed Two-Way ANOVAs were performed with Direction (Approach, Avoidance, Neutral) as a within-subjects and Stimulation (anodal, sham) as a between-subjects factor. The dependent variable (d) was the difference between time required to read both the second and third segments before and after the Stimulation condition (anodal or sham). Latency to answer questions after neutral sentences was considered as covariate. Anodal tDCS was able to enhance reading speed for all the three types of sentences ($F(1, 58) = 4.174$, $p < .05$, $\eta p^2 = .068$). No interaction effect between Stimulation and Direction was found.

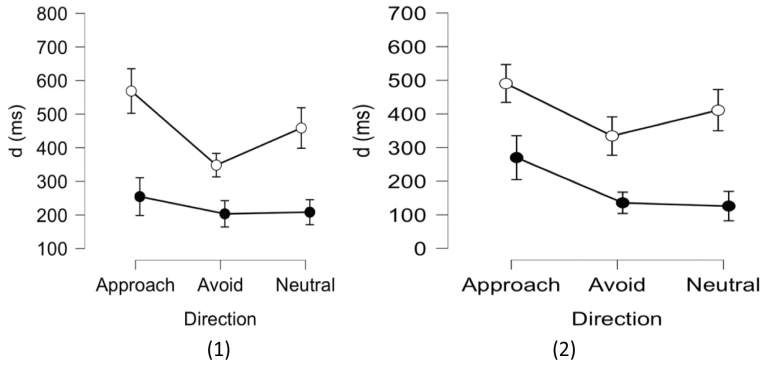

FIGURE 1: Reading speed improvement (d) in the second set of sentences for low-BIS (**1**) and low-BAS (**2**) participants.

Significant effect of anodal tDCS was found in low-BIS (avoidance/anxiety, F (1,19) = 8.502, $p < .01$, $\eta p^2 = .321$) participants and in low-BAS (approach/impulsivity, Stimulation, F (1, 19) = 6.53, p = .02, $\eta p^2 = .205$). Anodal tDCS enhance reading speed more for approach than avoidance sentences in low-BIS participants, F (2,19) = 3.181, p = .067, ηp2 = .272, (Figure 1).

In conclusion, anodal tDCS had no effect on reading approach content as we predicted but an overall effect on reading speed. However, affective traits have emerged as a modulator for tDCS effects. As we hypothesized, high levels in BIS/BAS traits predicted a poorer benefit from anodal tDCS. In contrast, low level BIS/BAS traits see, to be benefited from tDCS. More gender-balanced and older groups are needed. This may be interpreted as interference of personality traits as in previous research [17,18]. Since the reading task was somewhat passive, a recognition task after reading is suggested to find tDCS improvement in information encoding.

ACKNOWLEDGEMENTS

This study was supported by the Spanish Ministry of Economy, Industry and Competitiveness (Grant PSI2017-84527-P). We also thank the Canarian Agency

of Research, Innovation and Knowledge Society (NEUROCOG project), the Education Department of Cabildo Insular de Tenerife, The Colegio Oficial de la Psicología de Las Palmas, and the European Regional Development Funds

Keywords: Approach/avoidance intentionality, relationship action-sentences, tDCS, Reading Speed, Superior Temporal Sulcus, STS

REFERENCES

[1] Dodell-Feder, D.; Koster-Hale, J; Bedny; Saxe, R. fMRI item analysis in a theory of mind task. Neuroimage 2011, 55, 705-712.

[2] Kennedy, D.P.; Adolphs, R. The social brain in psychiatric and neurological disorders. Trends Cogn. Sci. 2012, 16, 559–572.

[3] Johnson, M.H.; Senju, A.; Tomalski, P. The two-process theory of face processing: Modifications based on two decades of data from infants and adults. Neurosci. Biobehav. Rev. 2015, 50C, 169–179.

[4] Pelphrey, K.A.; Morris, J.P. Brain mechanisms for interpreting the actions of others from biological motion cues. Curr. Dir. Psychol. Sci. 2006, 15, 136–140.

[5] Pelphrey, K.A.; Carter, E.J. Brain mechanisms for social perception: Lessons from autism and typical development. Ann. N. Y. Acad. Sci. 2008, 1145, 283–299.

[6] Saitovitch, A.; Bargiacchi, A.; Chabane, N.; Brunelle, F.; Samson, Y.; Boddaert, N.; Zilbovicius, M. Social cognition and the superior temporal sulcus: Implications in autism. Rev. Neurol. 2012, 168, 762–770.

[7] Yang, D.Y.; Rosenblau, G.; Keifer, C.; Pelphrey, K.A. An integrative neural model of social perception, action observation, and theory of mind. Neurosci. Biobehav. Rev. 2015, 51, 263–275.

[8] Pelphrey, K.A.; Viola, R.J.; McCarthy, G. When strangers pass. Psychol. Sci. 2004, 15, 598–603.

[9] Marrero, H.; Sara N. Y.; García-Marco, E.; Gámez, E.; Beltrán, D.; Díaz, J. M. and Urrutia, M. 2020. "Enhancing Memory for Relationship Actions by Transcranial Direct Current Stimulation of the Superior Temporal Sulcus." *Brain Sciences* 10 (8): 1–16.

[10] Gray, J.A.A. A critique of Eysenck's theory of personality. In A Model for Personality; Eysenck, H.J., Ed.; Springer: Berlin/Heidelberg, Germany, 1981; pp. 246–276.

[11] Metuki, N.; Sela, T.; Lavidor, M. Enhancing cognitive control components of insight problem solving by anodal tDCS of the left dorsolateral prefrontal cortex. Brain Stimul. 2012, 5, 110–115.

[12] Sela, T.; Ivry, R.B.; Lavidor, M. Prefrontal control during a semantic decision task that involves idiom comprehension: A transcranial direct current stimulation study. Neuropsychologia 2012, 50, 2271–2280.

[13] Eysenck, M.W.; Derakshan, N.; Santos, R.; Calvo, M.G. Anxiety and cognitive performance: Attentional control theory. Emotion 2007, 7, 336–353.

[14] Oldfield, R.C. The assessment and analysis of handedness: The Edinburgh inventory. Neuropsychology 1971, 9, 97–113.

[15] Carver, C.S.; White, T.L. Behavioral inhibition, behavioral activation, and affective responses to impending reward and punishment: The BIS/BAS scales. J. Personal. Soc. Psychol. 1994, 67, 319–333.

In silico brain-inspired meta-learning framework for task-specific action suppression

Federica Robertazzi[1,2]*, Matteo Vissani[1,2], Guido Schillaci[1,2], Egidio Falotico[1,2]

[1]The BioRobotics Institute, Sant'Anna School of Advanced Studies, Pisa, Italy
[2]Department of Excellence in Robotics & AI, Sant'Anna School of Advanced Studies, Pisa, Italy
**federica.robertazzi@santannapisa.it*

INTRODUCTION/MOTIVATION

Modern artificial agents demonstrate well-established performance in terms of accuracy, speed, and reliability in operating on single task instances after the exposure of a long stationary learning. However, they might exhibit worse performance in non-deterministic environments, i.e., human real-case applications characterized by sources of uncertainty and variability such as unpredictable cues and constraints [1], [2]. Meta-learning, also known as "learning-to-learn", applied to reinforcement learning may empower the design of flexible control algorithms, where an outer learning system progressively adjusts the operation of an inner learning system [3]–[5]. This approach could lead to practical learning optimization benefits, such as the reducing of the explicit hand-tuning of the hyperparameters of the learning schema and the generalization error [6], [7].

METHODS

Our work inherits the meta-learning principles in the neuromodulation theory proposed by Doya [8]–[10] and the neural architecture developed by Khamassi and colleagues [11], [12] for agent-environment interaction. The neuromodulation theory propounds a direct equivalence between the dynamics of the four major neurotransmitters (e.g., acetylcholine, serotonin, dopamine, and noradrenaline) and the computational role of the hyperparameters which shape the meta-learning processes.

In this brain-inspired meta-learning framework for inhibition cognitive control we included meta-learner representations of the distributed learning

systems in the human brain ,e.g., cortical areas such as the prefrontal cortex (e.g., Posterior Parietal Cortex (PPC), Anterior Cingulate Cortex (ACC), Ventral Tegmental Area (VTA), Lateral Prefrontal Cortex (LPFC), Premotor Cortex (PMC)) and subcortical regions such as basal ganglia circuitry (e.g., Striatum, Substantia Nigra reticulata (SNr), Thalamus, Substantia Nigra compacta (SNc)) (Figure 1). Each layer is composed of three firing rate neurons (the output of the differential equation of each neuron is mapped from 0 to 1 with a sigmoid activation function) that topographically codify different space regions [13]; we used two neurons to encode two different opposite directions, e.g., left and right, and one neuron to encode the action inhibition [14]–[16]. The connection between neurons is only inter-layers (i.e., no intra-layer recurrent connections) mediated by one-to-one excitatory or inhibitory synapses [17] The visual perception and the external reward modules regulate how

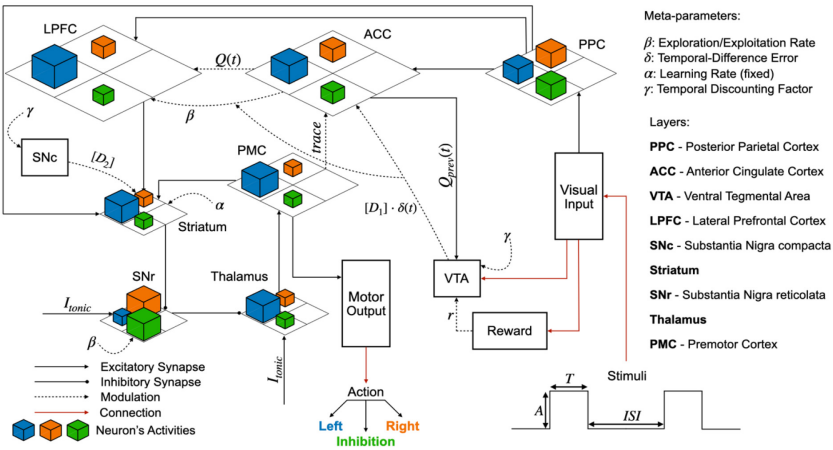

FIGURE 1: The model architecture inspired by [11], [12] and the meta-learning mechanism based on principles of Doya's neuromodulation theory [8]–[10] are illustrated. The volume of the cubes displays the intensity of the neuron's activity, topographically associated with the two directions (Left (blue), Right (orange)) and action inhibition (Inhibition (Green)). Excitatory (black arrow) and inhibitory (black circle arrow) neural synapses, reinforcement learning, meta-learning mechanisms (e.g., action values , dopamine , serotonin , noradrenaline , etc.) (black dashed arrows), and input/output connections (red line) are displayed. Stimuli are fed in the model by simulating a square wave ((amplitude) = 1 [a.u.], (duration) = 100 [samples], (inter-stimuli interval) = 200 [samples]) for neurons codifying Left or Right movement.

the agent interacts with the environment and the output module delivers the corresponded motor commands of the selected action. We formalized brain-inspired meta-learning hyperparameters optimization rules, mimicking explicitly the dynamics and mutual interaction of the major neurotransmitters in the brain. Briefly, (i) dopamine receptors D_1 modulate the noradrenergic system (i.e. exploration/exploitation rate) with an inverse linear function that relates dopamine to the entropy of the probability distribution of the actions [18], (ii) dopamine receptors D_2 tune the striatum neuron's excitability [19], and (iii) serotonin regulates the overall dopamine release and the reward temporal scale [20], [21]. The artificial agent was tested in two different well-described in literature conflictual tasks that involve different types of action inhibition [22], [23]: action restraint in NoGo Paradigm and action cancellation in Stop-Signal Paradigm. In the former, we evaluated the ability to withdraw a not-yet-initiated action from responding by the appearance of a hold signal before the movement execution. In the latter, we investigated the ability to cancel an initiated response triggering an unpredictable hold signal after a range of delays from the action onset.

RESULTS AND DISCUSSION

The artificial agent, after the training session, learned how to adjust successfully its hyperparameters (e.g., driving the system towards exploitation regimes) in response to the appearance of the hold signal in both paradigms, and hence, showing a proper encoding of the action inhibition command (Figure 2). In particular, both right inhibition and global accuracy increased significantly during the test phase in NoGo Paradigm (accuracy, training: 53.10 ± 15.43% vs test: 86.74 ± 3.68%, t-test, p-value < 0.001; right inhibition, training: 0% vs test: 73.48 ± 7.86%, t-test, p-value < 0.001) and in Stop-Signal Paradigm (accuracy, training: 51.32 ± 14.78% vs test: 75.78 ± 5.38%, t-test, p-value <0.001; right inhibition: training: 0% vs test: 51.06 ± 12.22%, t-test, p-value <0.001). Finally, considering the Stop-Signal Paradigm, high serotoninergic concentration acting on the dopamine release led to behavioral effects as such it shifted of the agent's behavior towards non-impulsive regimes, e.g., shorter reaction time and higher right inhibition as well as a reduction in the Stop Signal Reaction time, i.e., the latency of the cancellation process.

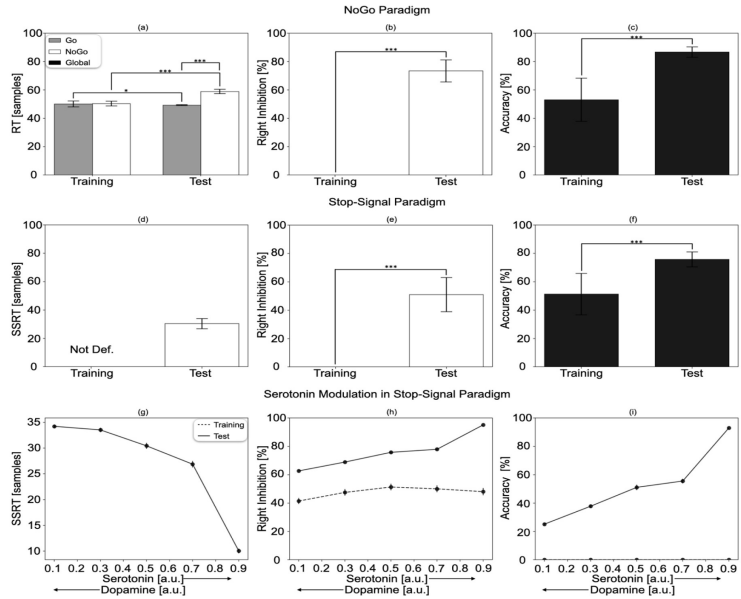

FIGURE 2: Performance of the simulated agent in NoGo and Stop-Signal Paradigms. Results are averaged across 40 simulations of 1000 stimuli during the training and test phases in NoGo Paradigm (**a-c**) and Stop-Signal Paradigm (**d-i**). Reaction time (RT) (**a**), Right Inhibition (**b**) and Accuracy (**c**) are displayed for both training and test phases in NoGo Paradigm. The color of the bar indicates the type of trials used to compute the metrics: Go trials (gray), NoGo trials (white) and all trials (black). Stop Signal Reaction time (SSRT) (**d**), Right Inhibition (**e**) and Accuracy (**f**) are displayed for both training and test phases in Stop-Signal Paradigm. The color of the bar indicates the type of trials used to compute the metrics: Go trials (gray), Stop-Signal trials (white) and all trials (black). SSRT is not defined during the training phase as the right inhibition is 0%. In (**a-f**) results are expressed as Mean $\pm$ SD and asterisks indicate the statistical significance (<0.05*, <0.01** and <0.001***). Parameters ((**g**) Right Inhibition, (**h**) Accuracy and (**i**) SSRT) are plotted against the serotonin concentration $[\gamma] \in \{0.1, 0.3, 0.5, 0.7, 0.9\}$ and they are obtained averaging across all the stimuli presentation in each simulation during the hold trials (both NoGo and Stop-Signal trials) in training (dashed black line) and test (black line) phases (except for SSRT for which in training is not defined). In (**g-i**) results are expressed as Mean $\pm$ SEM.

In previous works Khamassi and colleagues [11], [12] implemented a brain-inspired meta-learning hyperparameter optimization framework for reinforcement learning by linking the exploration/exploitation meta-parameter with the activity of two types of neurons [24], [25] (i.e., correct and error neurons) that react to positive and negative temporal difference error , respectively. The model was tested both in silico and in a humanoid

robot (i-Cub) in two problem solving tasks where environmental uncertainties are included either changing the cue or by cheating.

In the framework of the Cyber Rodent project [26], Doya e Uchibe used genetic algorithms to investigate the underlying mechanisms of self-reproduction, self-preservation as well as foraging in artificial agents [26]–[28] This evolutionary approach was adopted to co-evolve the meta-parameters (e.g., exploitation/exploration rate, learning rate and temporal discounting factor) in synergy with shaping reward, accelerating significantly the learning curve in foraging [29] and mating [30]. Lowe & Ziemke [31] used genetic algorithms to investigate meta-learned exploration and planning in a multi-episode two-armed bandit navigation problem under different representations (e.g., absence/presence) of external rewards and punishments.

We demonstrated that brain-inspired meta-learning rules may pave the way of the design of cognitive control architectures for artificial agents that achieve more flexible and accurate behavior when conflictual inhibitory signals are present in the non-deterministic environment.

ACKNOWLEDGEMENTS

F.R. & E.F. have received funding from the European Union's Horizon 2020 Framework Programme for Research and Innovation under the Specific Grant Agreement No. 945539 (Human Brain Project SGA3). G.S. has received funding from the European Union's 2020 Framework Programme for Research and Innovation under the Marie Skłodowska-Curie grant agreement No. 838861 ("Predictive Robots"). M.V. has received internal fundings from Sant'Anna School of Advanced Studies.

Keywords: Meta-learning, Brain-inspired Modeling, Inhibition Cognitive Control, Basal Ganglia, Prefrontal Cortex

REFERENCES

[1] R. Pfeifer, M. Lungarella, e F. Iida, «Self-Organization, Embodiment, and Biologically Inspired Robotics», *Science*, vol. 318, n. 5853, pagg. 1088–1093, nov. 2007, doi: 10.1126/science.1145803.

[2] E. S. Spelke e K. D. Kinzler, «Core knowledge», *Developmental Science*, vol. 10, n. 1, pagg. 89–96, gen. 2007, doi: 10.1111/j.1467-7687.2007.00569.x.

[3] J. Baxter, «Theoretical Models of Learning to Learn», in *Learning to Learn*, S. Thrun e L. Pratt, A c. di Boston, MA: Springer US, 1998, pagg. 71–94. doi: 10.1007/978-1-4615-5529-2_4.

[4] S. Thrun e L. Pratt, «Learning to Learn: Introduction and Overview», in *Learning to Learn*, S. Thrun e L. Pratt, A c. di Boston, MA: Springer US, 1998, pagg. 3–17. doi: 10.1007/978-1-4615-5529-2_1.

[5] J. Schmidhuber, J. Zhao, e M. Wiering, «Simple Principles Of Metalearning», 1999.

[6] Z. Xu, H. van Hasselt, e D. Silver, «Meta-Gradient Reinforcement Learning», *arXiv:1805.09801 [cs, stat]*, mag. 2018, Consultato: mag. 22, 2021. [Online]. Disponibile su: http://arxiv.org/abs/1805.09801

[7] Z. Xu, H. van Hasselt, M. Hessel, J. Oh, S. Singh, e D. Silver, «Meta-Gradient Reinforcement Learning with an Objective Discovered Online», *arXiv:2007.08433 [cs, stat]*, lug. 2020, Consultato: mag. 22, 2021. [Online]. Disponibile su: http://arxiv.org/abs/2007.08433

[8] K. Doya, «Metalearning and neuromodulation», *Neural Netw*, vol. 15, n. 4–6, pagg. 495–506, lug. 2002, doi: 10.1016/s0893-6080(02)00044-8.

[9] N. Schweighofer e K. Doya, «Meta-learning in Reinforcement Learning», *Neural Networks*, vol. 16, n. 1, pagg. 5–9, gen. 2003, doi: 10.1016/S0893-6080(02)00228-9.

[10] K. Doya, «Reinforcement learning: Computational theory and biological mechanisms», *HFSP Journal*, vol. 1, n. 1, pagg. 30–40, mag. 2007, doi: 10.2976/1.2732246/10.2976/1.

[11] M. Khamassi, S. Lallée, P. Enel, E. Procyk, e P. F. Dominey, «Robot Cognitive Control with a Neurophysiologically Inspired Reinforcement Learning Model», *Front. Neurorobot.*, vol. 5, 2011, doi: 10.3389/fnbot.2011.00001.

[12] M. Khamassi, P. Enel, P. F. Dominey, e E. Procyk, «Medial prefrontal cortex and the adaptive regulation of reinforcement learning parameters», in *Progress in Brain Research*, vol. 202, Elsevier, 2013, pagg. 441–464. doi: 10.1016/B978-0-444-62604-2.00022-8.

[13] F. Middleton e P. Strick, «Anatomical evidence for cerebellar and basal ganglia involvement in higher cognitive function», *Science*, vol. 266, n. 5184, pagg. 458–461, ott. 1994, doi: 10.1126/science.7939688.

[14] B. Pasquereau e R. S. Turner, «A selective role for ventromedial subthalamic nucleus in inhibitory control», *eLife*, vol. 6, pag. e31627, dic. 2017, doi: 10.7554/eLife.31627.

[15] F. Verbruggen *et al.*, «A consensus guide to capturing the ability to inhibit actions and impulsive behaviors in the stop-signal task», *eLife*, vol. 8, pag. e46323, apr. 2019, doi: 10.7554/eLife.46323.

[16] C. P. Mosher, A. N. Mamelak, M. Malekmohammadi, N. Pouratian, e U. Rutishauser, «Distinct roles of dorsal and ventral subthalamic neurons in action selection and cancellation», *Neuron*, vol. 109, n. 5, pagg. 869-881.e6, mar. 2021, doi: 10.1016/j.neuron.2020.12.025.

[17] K. I. Nagel e R. I. Wilson, «Mechanisms Underlying Population Response Dynamics in Inhibitory Interneurons of the Drosophila Antennal Lobe», *J Neurosci*, vol. 36, n. 15, pagg. 4325–4338, apr. 2016, doi: 10.1523/JNEUROSCI.3887-15.2016.

[18] M. Humphries, «Dopaminergic control of the exploration-exploitation trade-off via the basal ganglia», *Front. Neurosci.*, vol. 6, 2012, doi: 10.3389/fnins.2012.00009.

[19] S. C. Tanaka, K. Doya, G. Okada, K. Ueda, Y. Okamoto, e S. Yamawaki, «Prediction of immediate and future rewards differentially recruits cortico-basal ganglia loops», *Nat Neurosci*, vol. 7, n. 8, pagg. 887–893, ago. 2004, doi: 10.1038/nn1279.

[20] S. C. Tanaka *et al.*, «Serotonin Differentially Regulates Short- and Long-Term Prediction of Rewards in the Ventral and Dorsal Striatum», *PLoS ONE*, vol. 2, n. 12, pag. e1333, dic. 2007, doi: 10.1371/journal.pone.0001333.

[21] N. Schweighofer, S. C. Tanaka, e K. Doya, «Serotonin and the Evaluation of Future Rewards: Theory, Experiments, and Possible Neural Mechanisms», *Annals of the New York Academy of Sciences*, vol. 1104, n. 1, pagg. 289–300, apr. 2007, doi: 10.1196/annals.1390.011.

[22] D. M. Eagle, C. Baunez, D. M. Hutcheson, O. Lehmann, A. P. Shah, e T. W. Robbins, «Stop-Signal Reaction-Time Task Performance: Role of Prefrontal Cortex and Subthalamic Nucleus», *Cerebral Cortex*, vol. 18, n. 1, pagg. 178–188, gen. 2008, doi: 10.1093/cercor/bhm044.

[23] J. D. Schall, T. J. Palmeri, e G. D. Logan, «Models of inhibitory control», *Phil. Trans. R. Soc. B*, vol. 372, n. 1718, pag. 20160193, apr. 2017, doi: 10.1098/rstb.2016.0193.

[24] S. Dehaene, M. Kerszberg, e J.-P. Changeux, «A neuronal model of a global workspace in effortful cognitive tasks», *Proceedings of the National Academy of Sciences*, vol. 95, n. 24, pagg. 14529–14534, nov. 1998, doi: 10.1073/pnas.95.24.14529.

[25] C. B. Holroyd e M. G. H. Coles, «The neural basis of human error processing: Reinforcement learning, dopamine, and the error-related negativity.», *Psychological Review*, vol. 109, n. 4, pagg. 679–709, ott. 2002, doi: 10.1037/0033-295X.109.4.679.

[26] K. Doya e E. Uchibe, «The Cyber Rodent Project: Exploration of Adaptive Mechanisms for Self-Preservation and Self-Reproduction», *Adaptive Behavior*, vol. 13, n. 2, pagg. 149–160, giu. 2005, doi: 10.1177/105971230501300206.

[27] G. Capi e K. Doya, «Evolution of Neural Architecture Fitting Environmental Dynamics», *Adaptive Behavior*, vol. 13, n. 1, pagg. 53–66, mar. 2005, doi: 10.1177/105971230501300103.

[28] A. Eriksson, G. Capi, e K. Doya, «Evolution of meta-parameters in reinforcement learning algorithm», in *Proceedings 2003 IEEE/RSJ International Conference on Intelligent Robots and Systems (IROS 2003) (Cat. No.03CH37453)*, Las Vegas, Nevada, USA, 2003, vol. 1, pagg. 412–417. doi: 10.1109/IROS.2003.1250664.

[29] S. Elfwing, E. Uchibe, K. Doya, e H. I. Christensen, «Co-evolution of Shaping Rewards and Meta-Parameters in Reinforcement Learning», *Adaptive Behavior*, vol. 16, n. 6, pagg. 400–412, dic. 2008, doi: 10.1177/1059712308092835.

[30] S. Elfwing, E. Uchibe, e K. Doya, «Emergence of Different Mating Strategies in Artificial Embodied Evolution», in *Neural Information Processing*, vol. 5864, C. S. Leung, M. Lee, e J. H. Chan, A c. di Berlin, Heidelberg: Springer Berlin Heidelberg, 2009, pagg. 638–647. doi: 10.1007/978-3-642-10684-2_71.

[31] R. Lowe e T. Ziemke, «The Feeling of Action Tendencies: On the Emotional Regulation of Goal-Directed Behavior», *Front. Psychology*, vol. 2, 2011, doi: 10.3389/fpsyg.2011.00346.

V Other

The Scientific Liaison Unit of EBRAINS - Our support for you!

Claudia Bachmann*, Marissa Pier Diaz[+], Wouter Klijn[++]

Jülich Supercomputer Centre (JSC), Institute for Advance Simulation (IAS), Jülich Research Centre, Jülich, Germany

**c.bachmann@fz-juelich.de, [+]m.diaz.pier@fz-juelich.de,[++]w.klijn@fz-juelich.de*

INTRODUCTION/MOTIVATION

EBRAINS [1] comprises more than 130 European research organizations, each with a large number of scientists, programmers, and technical coordinators. Developing, operating, and using an immense infrastructure such as EBRAINS is a complex task that bears the risk of an individual scientist getting lost in details. The Scientific Liaison Unit (SLU) was founded to provide a helping hand in navigating the complexity of EBRAINS services [2] and science [3]. This work details the structured methodology the SLU uses to guide its activities. The method creates a shared understanding of the research plans of the scientists and the associated technical requirements for the engineers. Secondly, it facilitates the identification of major scientific needs, which serve as a precious source for defining the future direction of tool and service development in EBRAINS.

METHODS

Here we present the process we followed to develop a technique that describes scientific research as standardized requirements that conduces to a workflow compatible with EBRAINS infrastructure.

Also, here is clarified how this process of gathering requirements, can be applied to different types of research, and how it can help in similar cases to transform the actual state of research into compatible description workflows able to be integrated as a part of EBRAINS and how we designed tools to

optimize this process. *To exemplify we present showcases models and how the evolution of the used tools in their research.*

As a key tool, we introduce a descriptive template [4,5] that guides the scientist through a couple of steps: from a scientific description of her/his science case at the beginning, followed by a progressively technical presentation of it. The technical representation also includes a diagram with symbols organized according to specific rules that allow us to identify commonalities between different scientific cases and infer major scientific needs.

RESULTS AND DISCUSSION

Based on an example of the hyper-parameter optimization framework ([6], L2L in Fig.1) we demonstrate how the structure of the document leads the reader from a scientific description into technical requirement analysis. In this particular case, the technical requirement analysis focuses on different types of data transfer needed for this workflow e.g. data needs to be transferred from the super-compute site (ICEI site) in which the hyper-parameter optimization

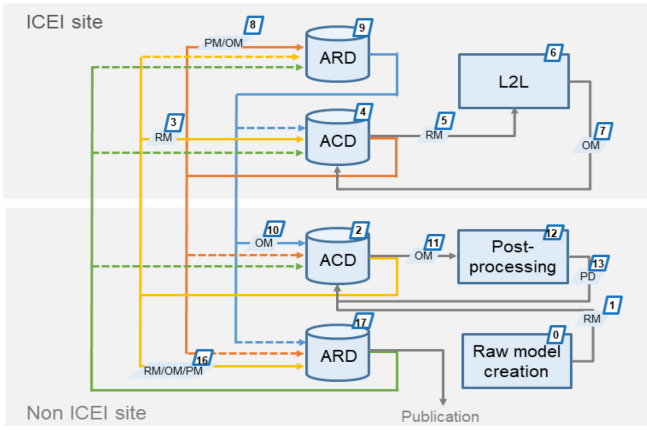

FIGURE1: Diagram description of the hyperparameter optimizaion framework. Lines indicate data transfer between storages (cylinder) and processing sites (rectangles). Solid lines indicate data transfer taking place in the actual use case. Dashed lines show alternative routes. ARD: Archival data storage, ACD: Active data storage. RM: raw data model, OM: optimized model, PM: Post processing results, L2L: learning to learn framework.

takes place, to another site (e.g. your computer) in which the analysis of the result is carried out. Based on such a requirement analysis, potential project challenges, as well as opportunities for extensions and interaction, are identified early on.

This work gives an overview of the different areas of responsibility that the SLU has. In particular, it explains our strategies for identifying and prioritizing the needs of the scientific community and their formulation into technical requirements based on scientific cases in a systematic and standardized way.

ACKNOWLEDGEMENTS

This research was supported by the EBRAINS research infrastructure, funded from the European Union's Horizon 2020 Framework Program for Research and Innovation under the Specific Grant Agreement No. 945539 (Human Brain Project SGA3)

Keywords: workflow description, science communication, requirement analysis, hyper-parameter optimization, data transfer, HPC

REFERENCES

[1] https://ebrains.eu/

[2] https://ebrains.eu/services

[3] https://www.humanbrainproject.eu/en/science/overview/

[4] https://drive.ebrains.eu/f/2d30a9a6284f4cc0b8c9/

[5] https://fenix-ri.eu/sites/default/files/public/file-uploads/ICEI-D3.6-v3.1_clean.pdf
(Examples of scientific cases applying a precursor version of the template)

[6] https://meta-optimization.github.io/L2L/

Advantages of publishing in Frontiers

OPEN ACCESS
Articles are free to read for greatest visibility and readership

FAST PUBLICATION
Around 90 days from submission to decision

HIGH QUALITY PEER-REVIEW
Rigorous, collaborative, and constructive peer-review

TRANSPARENT PEER-REVIEW
Editors and reviewers acknowledged by name on published articles

Frontiers
Avenue du Tribunal-Fédéral 34
1005 Lausanne | Switzerland

Visit us: www.frontiersin.org
Contact us: info@frontiersin.org | +41 21 510 17 00

REPRODUCIBILITY OF RESEARCH
Support open data and methods to enhance research reproducibility

DIGITAL PUBLISHING
Articles designed for optimal readership across devices

FOLLOW US
@frontiersin

IMPACT METRICS
Advanced article metrics track visibility across digital media

EXTENSIVE PROMOTION
Marketing and promotion of impactful research

LOOP RESEARCH NETWORK
Our network increases your article's readership